Linking satellite and point micrometeorological data to estimate vegetation water use: Distributed evapotranspiration modelling based on MODIS LAI, Penman-Monteith and Functional Convergence Theory

Craig I. Weideman
B.Sc. Hons. (Environmental Science)
Rhodes University

Submitted in partial fulfilment of the requirements for the degree of

MASTER OF SCIENCE
Environmental Science Discipline
Department of Environmental Science
Faculty of Science
Rhodes University
Grahamstown
South Africa

2013

Declaration

I hereby declare that the research work reported in this thesis is the result of my own original investigations except where acknowledged.

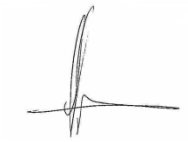

Signed_____

Craig I. Weideman

Signed_____

Principle Supervisor: W. N. Ellery
Professor of Environmental Science

Signed_____

Co-Supervisor: A. R. Palmer
Senior Scientist: Agricultural Research Council

Acknowledgements

This thesis is dedicated to my mother and my brother. Also, to Dr. Tony Palmer, who, I hope, never lost faith.

About the Data Used in this Study

Most data sets used in the development and testing of models developed in this study were collected by other researchers. In all cases these data, where they are not already in the public domain, have been used with permission of the authors, project leaders or principle investigators. Where data are available in the public domain, sources have been indicated, and include the WRC for flux data used at the Groenkop and Bellevue sites, SAFARI for flux data at the Skukuza site, and ARC-ISCW for automatic weather station data. Where data have been acquired from published sources, these studies are cited comprehensively. In order to achieve a flow to the thesis and to establish an accurate context of the research sites, substantial text describing the study sites and the instrumentation associated with each is re-presented from the original descriptions. This dissertation acknowledges fully the substantial contribution made by the data democratization policies of researchers and research agencies in South Africa.

Abstract

Recent advances in satellite sensor technology and micrometeorological instrumentation for water flux measurement, coupled with the expansion of automatic weather station networks that provide routine measurements of near-surface climate variables, present new opportunities for combining satellite and ground-based instrumentation to obtain distributed estimates of vegetation water use over wide areas in South Africa. In this study, a novel approach is tested, which uses satellite leaf area index (LAI) data retrieved by the Moderate Resolution Imaging Spectroradiometer (MODIS) to inform the FAO-56 Penman-Monteith equation for calculating reference evaporation (ET_0) of vegetation phenological activity. The model (ET_{MODIS}) was validated at four sites in three different ecosystems across the country, including semi-arid savanna near Skukuza, mixed community grassland at Bellevue, near Pietermaritzburg, and Groenkop, a mixed evergreen indigenous forest near George, to determine potential for application over wider areas of the South African land surface towards meeting water resource management objectives.

At Skukuza, evaluated against 170 days of flux data measured at a permanent eddy covariance (EC) flux tower in 2007, the model (ET_{MODIS}) predicted 194.8 mm evapotranspiration relative to 148.9 mm measured fluxes, an overestimate of 31.7 %, (r^2 = 0.67). At an adjacent site, evaluated against flux data measured on two discrete periods of seven and eight days in February and May of 2005 using a large aperture scintillometer (SLS), ET_{MODIS} predicted 27.4 mm and 6.7 mm evapotranspiration respectively, relative to measured fluxes of 32.5 and 8.2 mm, underestimates of 15.7 % and 18.3 % in each case (r^2 = 0.67 and 0.34, respectively). At Bellevue, evaluated against 235 days of evapotranspiration data measured using a surface layer scintillometer (SLS) in 2003, ET_{MODIS} predicted 266.9 mm evapotranspiration relative to 460.2 mm measured fluxes, an underestimate of 42 % (r^2 = 0.67). At Groenkop, evaluated against data measured using a SLS over three discrete periods of four, seven and seven days in February, June and September/October respectively, ET_{MODIS} predicted 9.7 mm, 10.3 mm and 17.0 mm evapotranspiration, relative to measured fluxes of 10.9 mm, 14.6 mm and 23. 9 mm, underestimates of 22.4 %, 11.2 % and 24.1 % in each case (r^2 = 0.98, 0.43 and 0.80, respectively). Total measured evapotranspiration exceeded total modelled evapotranspiration in all cases, with the exception of the flux tower site at Skukuza, where evapotranspiration was overestimated by ET_{MODIS} by 31.7 % relative to measured (EC) values for the 170 days in 2007 where corresponding modelled and

measured data were available. The most significant differences in measured versus predicted data were recorded at the Skukuza flux tower site in 2007 (31.7 % overestimate), and the Bellevue SLS flux site in 2003 (42 % underestimate); coefficients of determination, a measure of the extent to which modelled data are able to explain observed data at validation periods, with just two exceptions, were within a range of 0.67 – 0.98.

Several sources of error and uncertainty were identified, relating predominantly to uncertainties in measured flux data used to evaluate ET_{MODIS}, uncertainties in MODIS LAI submitted to ET_{MODIS}, and uncertainties in ET_{MODIS} itself, including model assumptions, and specific uncertainties relating to various inputs; further application of the model is required to test these uncertainties however, and establish confidence limits in performance. Nevertheless, the results of this study suggest that the technique is generally able to produce estimates of vegetation water use to within reasonably close approximations of measurements acquired using micrometeorological instruments, with r^2 values within the range of other peer-reviewed satellite remote sensing-based approaches.

Contents

List of Figures

List of Tables

List of Abbreviations and Symbols

Roman Symbols

C_n^2	Structure parameter of refractive index
c_p	Specific heat capacity of dry air
d	Zero plane displacement height
D_a	Vapour pressure deficit of the air
e	Mean vapour pressure
e'	Instantaneous deviation of vapour pressure from e
e	Water vapour pressure
e_l	Lower moisture content
e_u	Upper moisture content
E	Evaporation
E_a	Water vapour transport flux
ET	Total evaporation
ET_a	Actual evaporation
ET_{LAS}	LAS-based evapotranspiration
ET_{MODIS}	MODIS-based evapotranspiration
ET_p	Potential evapotranspiration
ET_0	Reference evapotranspiration
G	Flux of soil heat storage
g_s	Stomatal conductance
H	Sensible heat flux
h	Vegetation height
k	von Karman's constant
K_c	Crop factor
K_h	Eddy diffusivity coefficient for H
K_v	Eddy diffusivity coefficient for λE
LAI	Leaf Area Index

LAI_{max}	10-year maximum MODIS LAI
L_{Ob}	Obukhov length
P	Atmospheric pressure
q	Mean specific heat humidity
q'	Instantaneous deviation of specific humidity from q
r_a	Aerodynamic resistance for water vapour
R_n	Net irradiance
r_l	Bulk stomatal resistance of an illuminated leaf
r_s	Bulk stomatal (canopy) resistance
r^2	Coefficient of determination
T	Absolute temperature
T_a	Aerodynamic temperature
T_0 (or T_s)	Surface temperature
u_z	Windspeed at height z
W	Vertical wind velocity
W_f	Wind function (linear function of windspeed at reference height above the ground)
z	Height above surface
z_T	Height of temperature measurement above surface
z_0	Roughness length
z_{oh}	Roughness length governing heat and vapour transfer
z_{om}	Roughness length governing momentum transfer

Greek Symbols

β	Bowen ratio
ε	Ratio of the molecular mass of water to the molecular mass of dry air
Δ	Slope of saturated vapour pressure vs. air temperature relationship
γ	Psychrometric constant
λ	Wavelength
λE	Evaporative latent energy flux
ρ_a	Density of air
ρ_w	Density of water
ψ_m	Businger-Dyer correction for stability

Abbreviations

m.a.s.l.	Metres above sea level
ARC-ISCW	Agricultural Research Council Institute for Soil Climate and Water
ASTER	Advanced Spaceborne Thermal Emission and Reflection Radiometer
AVHRR	Advanced Very High Resolution Radiometer
BR	Bowen ratio
BREB	Bowen ratio energy balance
BRF	Bidirectional Reflectance Factor
C-T	Cohesion-Tension theory
CSIRO	Commonwealth Scientific and Industrial Research Organisation
DAAC	Data Active Archive Centre
E	Evaporation
EC	Eddy Covariance
EOS	Earth Observation System
ET	Evapotranspiration
FAO	Food and Agriculture Organisation
fPAR	Fraction of photosynthetically active radiation
ICM	Integrated Catchment Management
IGBP	International Geosphere Biosphere Programme
ILWRM	Integrated Land and Water Resource Management
GOES	Geostationary Operational Environmental Satellite
HDF	Hierarchical Data Format
HEG	HDF-EOS to GeoTIFF Conversion Tool
IGBP	International Geosphere Biosphere Programme
IRGA	Infra-red gas analyzer
IWRM	Integrated Water Resource Management
LAI	Leaf area index

LAS	Large aperture scintillometer
LDOPE	Land Data Operational Product Evaluation
LP DAAC	Land Processes Data Active Archive Centre
LST	Land surface temperature
MISR	Multi-angle Imaging SpectroRadiometer
MODIS	Moderate Resolution Imaging Spectroradiometer
MODLAND	MODIS Land Discipline Team
MOST	Monin Obukhov Similarity Theory
NASA	National Aeronautics and Space Administration
NDVI	Normalised difference vegetation index
NTDI	Normalised temperature difference index
NTSG	Numerical Terradynamic Simulation Group
NWA	National Water Act
PES	Payments for Ecosystem Services
RSEB	Resistance Surface Energy Balance
RT	Radiative Transfer
SAFARI 2000	Southern Africa Regional Science Initiative
SANParks	South African National Parks
SEBAL	Surface Energy Balance for Land Algorithm
SEBS	Surface Energy Balance System
SLS	Surface layer scintillometer
T	Transpiration
TIR	Thermal infra-red
VI	Vegetation index
WRC	Water Research Commission

1. Introduction

1.1 Land use and water resources in South Africa

The combined physical and plant physiological process of evapotranspiration (ET) is generally the second largest component of the terrestrial water balance after rainfall, and in arid and semi-arid ecosystems returns approximately 90 % of all precipitation to the atmosphere (Wilcox, *et al*., 2003). Transpiration dominates vapour fluxes in this context, routinely accounting for some 70-90 % of total ET (Williams, *et al*., 2004), influencing rainfall quantities partitioned to infiltration, streamflow and groundwater components (Jobaggy, *et al*., 2011). Tightly coupled with production, transpiration is itself regulated primarily by water availability in dry regions (Huxman, *et al*., 2004), with strong feedbacks occurring between climate, hydrology and plant biota (Wilcox, *et al*., 2011). In these systems, changes in the nature, in terms of structure and physiology, and amount of vegetation cover typically have significant implications for catchment water yields, where even changes that elicit relatively minor variations in ET often translate into disproportionately large changes in surface flow and groundwater volumes (Jobaggy, *et al*., 2011). In South Africa therefore, a predominantly semi-arid country subject to chronic water deficits, the impacts of anthropogenic and climate-driven shifts in biotic assemblages are of particular concern in the context of water resource management (Everson, *et al*., 2011; Schulze, *et al*., 2011; Warburton, *et al*., 2012). With steadily increasing pressures on land and water in recent decades (Everson, *et al*., 2011), and little unexploited, economically viable surface water remaining (Turpie, *et al*., 2008), there is consensus that holistic approaches to water resource management, which explicitly recognise the continuity of the hydrological cycle and the role of vegetation in water balance partitioning, are critical in sustaining South Africa's future water requirements (Jewitt, 2006).

Land use impacts on water resources, and particularly commercial afforestation, were identified as an issue of potential concern in South Africa as early as 1915 (Dye & Versveld, 2007). Despite the accumulation of a considerable body of research demonstrating the significance of vegetation controls on hydrology since this time however, land use issues in the broader context appear to have received relatively little consideration in the water resource management and planning arena. For most of the 20th century, echoing trends globally, water policy and strategy thinking had instead been dominated by a focus on surface water, where conventional responses to rising demand comprised the expansion of supply-

side engineering infrastructure to ever higher degrees (Turpie, *et al*., 2008). Surface water resources by the end of the last century had been developed to nearly unprecedented levels, with the combined storage capacity of large impoundments exceeding 73 % of the country's total annual runoff (Ashton, *et al*., 2008). By this time, prompted by growing global consciousness of the vulnerability of water resources, particularly since the United Nations Mar del Plata Conference on Water in 1977, which first established water issues as a priority on the international agenda, fundamental shifts in attitudes towards its use and management had begun to occur (Rahaman & Varis, 2005). A defining trend in international policy during these decades was a gradual departure from the expansion of new supply-side systems and infrastructure, toward improved management, efficiency of use and conservation of existing water resources (Badenhorst, *et al*., 2002).

1.2 Integrated Water Resource Management

Integrated Water Resource Management (IWRM), the contemporary framework for which emerged from the 1992 International Conference on Water and the Environment in Dublin, and subsequent UN Conference on Environment and Development in Rio, set the foundations for far reaching reforms in the international water policy arena at this time (Rahaman & Varis, 2005). IWRM sought to promote coordinated development of land, water and related resources at the catchment scale, emphasizing economic, social and ecological sustainability, and principles of good governance and public participation (Global Water Partnership, 2000). It was seen as a solution to some of the failures of the earlier single sector approaches to water resource management, which proved inadequate to deal with the challenges of complex, rapidly changing social-ecological systems (Pollard & du Toit, 2008); after a series of international conferences in subsequent years, IWRM soon became positioned as the dominant water resource management paradigm in both developed and developing world contexts (Rahaman & Varis, 2005). In South Africa in the 1990s, IWRM was seen as a particularly attractive option given the prevailing socio-political climate at the time (Calder, 2005). Major overhauls of Apartheid-era legislation, including those regulating the water sector, had begun immediately subsequent to the first democratic elections in 1994, and the country was uniquely poised to integrate IWRM into national policy. The new 1998 National Water Act (NWA, or "the Act") and associated policy documents ushered in fundamental reforms to water administration as it was under the former 1956 Water Act, strongly embracing the IWRM principles of integration, equity in allocation, sustainability, and stakeholder participation (Pollard & du Toit, 2008), and considered by some to represent

among the most advanced examples of the operationalizing of IWRM in the world (Jonker, 2007).

While water sector reforms introduced under the banner of IWRM are wide ranging, the key element from the perspective of this study is its implications for policy relating to the integration of land use and water resource management issues, and this is reflected in a number of statutes and policy documents. The White Paper on a National Water Policy for South Africa, which established a set of guidelines for the drafting of South Africa's new water law, states that "since many land uses have a significant impact upon the water cycle, the regulation of land use shall, where appropriate, be used as an instrument to manage water resources within the broader integrated framework of land use management" (DWAF, 1997). This directive was enacted into law primarily through the declaration of certain land-based activities in terms of Section 36 of the NWA as stream flow reduction activities (SFRAs), which, as such, become subject to regulation as a water use; Section 36 (2) of the NWA defines an SFRA as "…any activity (including the cultivation of any particular crop or other vegetation)…[that]…is likely to reduce the availability of water in a watercourse to the Reserve, to meet international obligations, or to other water users significantly". The Act also empowers the Minister to determine methods for volumetric assessments of streamflow reductions resulting from such land-based activities. At present, only commercial forestry has been declared an SFRA (its regulation in terms of Section 36 of the NWA replaces the earlier Forest Act), although other land uses have or are being considered for classification in terms of this section of the Act (Calder, 2005). The National Water Resource Strategy (NWRS, 2004), drafted to give effect to the NWA, also acknowledges the integrated nature of catchment hydrological systems, referring to the need for IWRM as a framework to understand and manage the complex linkages between the different components of the hydrological cycle (Pollard & du Toit, 2008).

IWRM in South Africa therefore, through the National Water Act and National Water Resource Strategy, provides a clear mandate for the management of catchments as interlinked ecological and hydrological systems, including recognition of the connectivity of the water cycle and interactions with the land resource (Pollard & du Toit, 2008). Moreover, Catchment Management Strategies, described in Section 8 of the NWA as plans for the "protection, use, development, conservation, management and control of water resources", required of all Catchment Management Agencies established in terms of the Act, provide a strategic

framework for implementing these statutes and policies. There is, however, some consensus that a higher degree of integration of land and water resource management beyond what is provided for by IWRM in its present form in South Africa is ultimately required; Integrated Catchment Management (ICM), and Integrated Land and Water Resource Management (ILWRM) have been held as examples of such approaches (Jewitt, 2006). These frameworks, closer to true integration of land and water resource management, are designed to consider land use interactions with the catchment hydrological cycle more holistically than what policy based on IWRM currently allows; although ICM and ILWRM are not yet feasible within the present statutory and institutional environment, it has been suggested that IWRM could eventually be "upgraded" and recast to fit these criteria if and when the necessary structures have been put in place (Ashton, 2000).

1.3 Technical challenges to operationalizing IWRM in South Africa:

1.3.1 Difficulties of measuring the water use of land-based activities & predicting hydrological responses to catchment land-use change

Integrating land use into water resource management, whether to the extent required in terms of the present IWRM framework and Section 36 of the NWA, or within more explicit frameworks, such as those implied by the ICM and ILWRM models, is faced with a number of key technical challenges however, arguably the greatest of which are the difficulties of measuring the water use of land-based activities, and predicting catchment hydrological responses to changes in land use management (Jewitt, 2006). With the exception of gauged experimental catchments, where streamflow responses to management can be empirically measured relative to climatically and physiographically similar controls, quantitative estimation of water resource impacts for the majority of the South African land surface presents significant difficulties for hydrologists (Warburton, *et al*., 2012). Streamflow in catchments results from the integration of complex surface and subsurface hydrological processes operating at multiple time and spatial scales, (Scott, 1999) including both lateral and vertical water fluxes (Warburton, *et al*., 2012); soil water storage, and it's partitioning to the water balance components of evaporation, transpiration, infiltration and deep recharge, and ultimately to various parts of downstream catchment streamflow regimes, remains little understood (Jewitt, 2006). Given the complexities of predicting catchment hydrological responses without recourse to detailed field measurements, there have been a wide variety of physical and conceptual models designed to simulate these processes (Royappen, *et al*., 2002). Probably most notable of these in the South African context is ACRU, developed

within the School of Bioresources Engineering and Environmental Hydrology, University of KwaZulu-Natal (Gush, *et al*., 2002); ACRU is currently being used by the Department of Water Affairs to assess commercial forestry applications in terms of streamflow reductions, for the purposes of water use authorization and allocation under Section 36 of the NWA.

Hydrological models such as ACRU are indispensable as a means for assessing the impacts of changes in catchment physical conditions on water balance partitioning and streamflow characteristics in uninstrumented catchments, and predicting the likely impacts of proposed land use changes; common to all modelling approaches however, they are associated with several sources of uncertainty, relating to gaps in understanding regarding some of the processes being represented, and the need to simplify others (Warburton, *et al*., 2012). The means to more directly measure or estimate fluxes of the critical water balance components is crucial for verifying the performance of hydrological models, and also for improving scientific understanding of catchment hydrological processes for the range of environmental and climatic variability. Evapotranspiration, a key component of the water balance in South African systems with fundamental implications for catchment hydrology and water resources, is of particular significance in this respect (Jovanovic & Isreal, 2012). Despite its importance however, it is arguably one of the most difficult processes to measure reliably, especially over wide areas, given marked variation of fluxes in space and time in response to microclimatic and surface heterogeneity. This is typically compounded in arid and semi-arid systems, where precipitation often occurs as sporadic "pulses", driving complex, dynamic vegetation physiological responses to prolonged periods of water stress (Huxman, *et al*., 2004). A further level of complexity may arise given that there is often a need to distinguish between and separately measure the physical process of evaporation from soil and canopy surfaces, and the plant physiological one of transpiration, described by some as "green water" flows, requiring complicated measurement methodologies (Jewitt, 2006).

1.3.2 Evapotranspiration measurement techniques

Since the late 1990s in South Africa, and internationally, scientific investigation into vegetation water use has largely centred on two main approaches: ground-based micrometeorological methods, notably eddy covariance (EC) (Swinbank, 1951), and scintillometry as a relatively new operational method (Savage, *et al*., 2004; Savage, *et al*., 2010), and more recently, various satellite-based remote sensing techniques, with some of the main operational approaches being the Surface Energy Balance for Land Algorithm (SEBAL)

and the Surface Energy Balance System (SEBS) (Bastiaanssen, *et al*., 1998a; Bastiaanssen, *et al*., 1998b; Su, 2002, Jarmain, *et al.*, 2009; Gibson, *et al*., 2009, Gibson, *et al.*, 2011; Műnch, *et al*., In Press). Assuming certain criteria are fulfilled, micrometeorological techniques are capable of providing reliable, areally-averaged estimates of evapotranspiration for flux "footprints" ranging in dimension between tens of metres (Eugster & Zeeman, 2006) to several square kilometres (Meijninger, *et al*., 2002), either directly, or as a residual of the surface energy balance equation. Remote sensing approaches such as SEBS and SEBAL, by contrast, provide spatially distributed estimates of evapotranspiration; the latter belong to a class of remote sensing models that use satellite-derived land surface temperature to calculate sensible heat flux, estimating evapotranspiration as a residual of the surface energy balance equation.

1.3.3 Satellite-based techniques for measuring evapotranspiration

Satellite-based remote sensing techniques have attracted particular interest for their ability to provide continuous, spatially resolved flux estimates over wide areas, and are at present the only means by which this can be achieved (Glenn, *et al*., 2007). These attributes of remote observation are a key requirement in water resource management applications, given the high time and space variability of catchment hydrological processes, which cannot adequately be resolved on the basis of either point measurements or "lumped" catchment observations (Jensen & Illangasekare, 2011). Satellite data has been explored extensively as a means for estimating moisture flux densities at the earth's surface since the late 1970's, and four broad classes of techniques have emerged: those based on the surface energy balance (including SEBS and SEBAL, as mentioned above), the catchment water balance, the Penman-Monteith equation, and empirical/statistical relation of vegetation indices or satellite-derived land surface temperature to ground-measured fluxes (Verstraeten, *et al*., 2008). Given that they are unable to measure flux stores and exchanges directly, high quality flux data from ground-based instrumentation for validation and calibration procedures is key to the success of remote sensing approaches (Cleugh, et al., 2007; Verstraeten, *et al*., 2008). Until relatively recently however, the availability of quality flux data has been restricted, largely due to technical constraints and expenses of available ground-based measurement methodologies, for instance, micrometeorological techniques and lysimeters.

1.3.4 Opportunities for combining satellite & ground-based instrumentation

There have been several important advances in both satellite sensor and micrometeorological technologies and theory in recent years, particularly since the late 1990s, which present new opportunities for combining remote sensing with ground-based instrumentation to obtain evidence-based, verifiable estimates of evapotranspiration over large parts of South Africa's land surface (Glenn, *et al*., 2007). A number of sophisticated satellite sensor systems, including, perhaps most notably, the Multi-angle Imaging SpectroRadiometer (MISR), Advanced Spaceborne Thermal Emission and Reflection Radiometer (ASTER), and the Moderate Resolution Imaging Spectroradiometer (MODIS), mounted aboard NASA's Terra and Aqua satellites, have been returning high quality global information on earth surface spectral and thermal properties to the research community free of charge for approximately the last decade. With improved spectral resolution, on-board calibration systems and well characterised radiometric, spectral, spatial and polarization sensitivities, MODIS in particular represents important technical improvements in earth observation capabilities over its predecessors (Justice, *et al*., 2002). Perhaps most significantly, MODIS has pioneered the development and operationalizing of a range of multidisciplinary, remotely sensed global biophysical datasets, stratified according to land, atmosphere and ocean products (Privette, *et al*., 2002). Of particular interest with respect to ecohydrological research objectives are the leaf area index (LAI) products; LAI provides critical information on vegetation phenological dynamics, and is a state parameter in all models describing mass exchanges within the geobiosphere (Knyazikhin, *et al*., 1999).

Micrometeorological methods for the measurement of evapotranspiration, such as EC, scintillometry and Bowen ratio energy balance (BREB, or simply BR) have been available for several decades, although have only relatively recently become popular with advances in instrumentation, theory and analytical techniques, largely within the last two decades (Shuttleworth, 2007). Driven by the growing interest in the global carbon budget, permanent EC flux towers managed by the FLUXNET consortium have been deployed in a wide range of ecosystems and production landscapes worldwide (Glenn, *et al*., 2007); these instruments deliver continuous flux measurements with a reported accuracy range of 10-30 %, and are considered by some to represent the standard in CO_2 and water flux measurement technology (Consoli, 2011). In South Africa, portable EC, scintillation and BR instruments have been tested extensively in different systems since around the turn of this century, and have now become well established as a research technique (Savage, *et al*., 1997; Savage, *et al*., 2004;

Dye, *et al*., 2008); data originating from many of these studies are available in the public domain or upon request from researchers, and represent an invaluable resource in terms of the opportunities for validation of experimental satellite-based models. Complementing flux data from these systems, a network of some 530 automatic weather stations, managed by the Agricultural Research Council's Institute for Soil and Water Research (ARC-ISCW), provide continuous measurements of weather variables required to calculate reference evaporation using meteorological equations (discussed in Section 2.5 of Chapter 2).

1.3.5 Satellite remote sensing and the Penman-Monteith equation

Several recent studies have explored the use of remote sensing data to parameterize the Penman-Monteith equation (Monteith, 1965) to derive continuous, distributed estimates of evapotranspiration over large areas, specifically with a view to developing a global evapotranspiration algorithm (MOD16 ET) within the suite of MODIS land products (Cleugh, *et al*., 2007; Mu, *et al*., 2007; Leuning, *et al*., 2008; Mu, *et al*., 2011). The Penman-Monteith equation is a biophysically robust, well established method for approximating evapotranspiration; it combines an energy balance and aerodynamic formula to estimate latent heat flux, or the energy transferred in the change of state from liquid water to vapour in the process of evaporation, and includes a bulk surface resistance term that describes the resistance to vapour transfer presented by plant stomatal controls, vegetation canopies and/or soil conditions (Cleugh, *et al*., 2007). The equation relies on widely available point-measured meteorological data, including air temperature, solar radiation, humidity and wind speed, but its routine implementation as a means to estimate spatially distributed evapotranspiration has been restricted by the requirement for information on aerodynamic and surface resistances to vapour transfer (or conversely, conductance) (Moran, *et al*., 1996). Both aerodynamic resistance, a function of wind speed, aerodynamic roughness of vegetation and atmospheric stability, and surface resistance, primarily a function of bulk stomatal conductances, are typically highly variable in space and time. Remote observation by polar orbiting daily return satellites such as Terra and Aqua, which retrieve spatially distributed information of surface spectral properties at near-real time, offers potential solutions to the challenges related to heterogeneity in surface flux estimation, and there have been ongoing efforts to exploit spectral data for this purpose in the last decade. Researchers from the Numerical Terradynamic Simulation Group (NTSG) at the University of Montana, and Commonwealth Scientific and Industrial Research Organisation (CSIRO), report a range of techniques for deriving information on aerodynamic and surface resistance, the latter primarily from the

standard MOD15A2 LAI product, for estimating evapotranspiration within a Penman-Monteith formulation (Cleugh, *et al*., 2007; Mu, *et al*., 2007; Mu, *et al*. 2011). The results of these studies indicate that satellite approaches based on the Penman-Monteith logic, supported by validated information on vegetation physiological activity provided by MODIS (primarily LAI), offer significant potential as a means for estimating the water use of land-based activities over wide areas.

1.4 The future of water resources in South Africa: Responding to the challenges

There is consensus among scientists that present trends in human pressures on land and water (Everson, *et al*., 2011), and climate-related shifts in terrestrial ecosystem structure and functioning (Schulze, *et al*., 2011) are likely to accelerate in the 21st century, the combined effects of which on hydrology and water resources are as yet imperfectly understood (Wilcox, *et al*., 2011). In its National Water Resource Management Strategy, the Department of Water Affairs predicts that the country will likely face a national water deficit by 2025 (NWRS, 2004), with few unexploited, economically viable resources remaining (Turton, 2008). Allocation of already scarce water in South Africa will likely become increasingly contentious, as policy moves towards a more representative, participatory approach to management in which all interests are recognised (Royappen, *et al*., 2002). Knowledge of how existing land-use systems impact water resources, and how they may be impacted by intentional and climate-induced changes at various scales is therefore a research imperative (Everson, *et al*., 2011; Schulze, *et al*., 2011; Warburton, *et al*., 2012). This knowledge will be critical in informing decisions regarding optimal resource distribution amongst competing users, and enhancing water use efficiency within in existing land-use systems (Műnch, *et al*., In Press). In this context, integrated approaches to water resource management, which explicitly consider the complex relationship between the land resource and hydrology, are key to sustaining the nation's water needs into the 21st century. Additionally, as the concept of water as an ecosystem service gains popularity, accompanied by new institutions and mechanisms to incorporate the value of these services into the formal market, knowledge of the water use of land-based activities will be required to establish payment contracts for service delivery by catchment managers.

The technical difficulties of measuring the water use of land-based activities at time and spatial scales relevant to catchment management applications continues to present significant challenges to integration of land and water resource management, both to the extent required

in terms of IWRM in its present incarnation, but particularly as demanded by ICM or ILWRM, recognised as future ideals in South Africa (Jewitt, 2006). Advances in micrometeorological and remote sensing technologies in recent years now provide new possibilities for evaluating land surface evapotranspiration at improved spatial and temporal resolution (Glenn, *et al*., 2007), and there is a need to explore the potential for meeting water resource management objectives in the South African context (Münch, *et al*., In press). Several existing pre-packaged open source and proprietary remote sensing-based models, such as SEBS, SEBAL, the Mapping EvapoTranspiration with high Resolution and Internalised Calibration (METRIC^{tm}) and the Vegetation Index/Temperature Trapezoid (VITT) models have been evaluated in South African conditions in earlier studies (Jarmain, *et al*., 2009; Gibson, *et al*., 2009; Gibson, *et al*., 2011; Műnch, *et al*., In Press). Jarmain *et al*. (2009) assessed a number of these approaches in different systems across the country, reporting large variability in performance, both between models as well as in the ability to simulate different energy balance components by the same model. Gibson *et al*. (2011), in their application of the SEBS model in the heterogeneous G10K quaternary catchment in the Western Cape Province, reported consistent over-prediction of evapotranspiration by this approach. In a follow up to the study by Gibson, *et al.,* (2011) in the sparsely vegetated P10A catchment in the Eastern Cape, consistent over-prediction of evapotranspiration, in combination with the complex parameterization procedures and resulting uncertainty, lead Műnch *et al*. (In Press) to call for continued exploration of parsimonious satellite based techniques for evapotranspiration assessment.

1.5 Aims & objectives

Several recent studies have demonstrated the potential of remote sensing approaches that use MODIS LAI in combination with the Penman-Monteith equation to derive continuous, spatially resolved estimates of vegetation water use over large areas (Cleugh, *et al*., 2007; Mu, *et al*., 2007; Leuning *et al*., 2008; Mu, *et al*., 2011). Typically, the challenge to routine implementation of the Penman-Monteith method relates largely to the difficulties of obtaining information on surface resistance to vapour transfer, measured as s^{m-1} (Cleugh, *et al*., 2007), which is a function of bulk stomatal conductances in vegetated systems, and which is typically highly variable in space and time in natural conditions (Kelliher, *et al*., 1995). These studies report a range of techniques of varying degrees of complexity for deriving spatially and temporally resolved surface resistance values within a Penman-Monteith formulation, typically applying empirically-derived, biome-specific stomatal conductance

values scaled up to canopy level using MODIS LAI data, and which are discussed in Section 2.6.4; the reader is referred to Mu, *et al*. (2011) for more detail.

In this study, an alternative, parsimonious technique based on a similar logic is tested, in which the standard 8-day MOD15A2 LAI product is used to derive information on vegetation dynamics, and effectively adjust the FAO-56 equation (Allan *et al*., 1998) according to vegetation physiological status, an approach first described by Palmer and Weideman (2011). The FAO-56 equation is a modified formulation of the Penman-Monteith method, which is widely used primarily in agricultural applications both in South Africa and internationally to calculate reference evaporation (ET_0); it incorporates standard parameter values for crop height, surface resistance and albedo representative of an assumed reference surface comprising a flat extensive crop in full physiological activity, and which is never water limited, providing a universal measure of vegetation water use based only on meteorological forcings (discussed in Section 2.5.2 of Chapter 2). The utility of the concept of ET_0 is that it yields a standard, universal measure of the evaporative potential of the atmosphere based on a well-defined surface and routine meteorological data, and which can theoretically be related to any surface of interest by applying site-specific indicators of vegetation physiological status. The technique described by Palmer and Weideman (2011) (hereinafter ET_{MODIS}) uses remotely sensed LAI to derive these indicators, applying the relationship of LAI at time T1 to long term maximum LAI for the pixel of interest, and thus proposes a simple solution to the difficulties of obtaining site-specific information on vegetation physiological status for use within a Penman-Monteith formulation for estimating latent heat flux.

This study aims to establish the viability of ET_{MODIS} in a range of conditions across South Africa, by validating model results over a variety of temporal scales against flux data measured using several micrometeorological instruments in earlier studies. The approach is tested at four sites in three distinct ecotypes: semi-arid savanna near Skukuza in the Limpopo Province, mixed community grassland near Ashburton in the KwaZulu-Natal Province, and mixed evergreen indigenous forest near George in the southern Cape, to establish its potential for routine implementation over wider areas of the country. The study responds to the need to develop parsimonious, evidence-based techniques for water flux estimation that are continuous, spatially and temporally resolved, and applicable at scales relevant to addressing land use issues as they relate to water resource management in South Africa.

1.6 Structure of this thesis

This thesis comprises six chapters, which, including the introduction, is structured according to a literature review, methods and results sections, discussion, and conclusion. The literature review (Chapter 2) is organised as follows: a summary of the background and current state of the art of methods for the assessment of evapotranspiration is provided, with specific reference to the South African experience, including recent advances in micrometeorological and satellite remote sensing techniques (Section 2.1). In Section 2.2, a discussion of the biophysical properties of the evaporative process is presented, including a description of atmospheric structure insofar as it influences turbulence and water fluxes at the earth's surface (Section 2.2.1). Cohesion-tension theory (Dixon & Joly, 1894), describing the plant physiological process of soil moisture transfer to the atmosphere (transpiration) (Section 2.2.2), and functional convergence theory (Field, 1991), describing the scaling of plant photosynthetic ability according to the availability of resources, the theoretical basis upon which ET_{MODIS} is predicated, are also included in this discussion (Section 2.2.3). The surface energy balance equation, which describes the way in which energy is balanced at the earth's surface by inputs or outputs of energy from non-radiative origins, providing the physical basis for models describing vertical energy, momentum and mass exchanges in the planetary boundary layer (or atmospheric boundary layer) (Allen, 2005a), is described in Section 2.3.

This is followed in Section 2.4 by a review of methodologies for the assessment of evapotranspiration that have direct bearing on this study, and comprises a section on micrometeorological methods, including EC, BR and two types of scintillometer (LAS and SLS); a review of meteorological equations for estimating evapotranspiration, with a focus on the Penman-Monteith and FAO-56 equation for reference evaporation, is provided in Section 2.5, followed by a summary of satellite-based approaches in Section 2.6. Finally, MODIS and the MOD15A2 LAI product are described in Section 2.7. Chapter 3 comprises a description of the methods employed in this study, including a discussion of model theoretical basis (3.1), and approach used in validation (3.2). A description of each of the three study areas in terms of climate, physical and vegetation characteristics, as well as dates and duration of ET_{MODIS} input (MOD15A2 and FAO-56/Class A-pan) and validation (micrometeorological) data, is provided in Section 3.3.

Results of the study are presented in Chapter 4, and are reported in terms of:

- long-term (~10 year) trends and patterns observed in remotely sensed LAI at each validation site;
- trends in remotely sensed LAI, and retrieval quality for the particular year in which validation is performed at respective sites;
- modelled (ET_{MODIS}) relative to measured water fluxes, and ET_0 at respective validation sites; and
- regression analyses of modelled versus measured data at respective sites.

A discussion of the results is presented in Chapter 5, and includes a general summary and comparison of the key indicators listed above across the four validation sites (Section 5.2), followed by a more detailed analysis addressing each site independently (Section 5.3). Finally, an analysis of uncertainties in the approach and validation of model performance is provided in Section 5.4, followed by an appraisal of the opportunities and constraints of the approach as a means to derive distributed estimates of vegetation water use over wider areas of the South African land surface (5.5); conclusions and recommendations for further research are provided in Chapter 6.

2. Literature Review

2.1 Vegetation and water resources: A South African perspective

2.1.1 South African paired catchment studies

Land use impacts on water resources, given the country's particular climatic conditions and development needs, were recognised as an issue of potential concern in South Africa as early as 1915, and have been subject to intensive scientific investigation since the 1930s (Van der Zel, 1995). Much of the understanding of ecohydrological processes at this time was based on experimental catchment research, directed primarily at evaluating the long-term (annual) impacts of commercial afforestation on catchment streamflow (Görgens & van Wilgen, 2004). From 1936 onwards, in response to the concerns regarding the impacts of the rapidly expanding commercial forestry sector on catchment water yields, a series of paired catchment experiments was established in high rainfall upper catchment areas across the country, originally dominated by low biomass, seasonally dormant grasslands or *Machia*-type shrublands. Experiments monitored hydrological responses to treatment relative to adjacent physiographically similar control catchments over a period of more than half a century (Scott, *et al*., 2000). Paired catchment studies provided well-documented empirical evidence that changes in the nature and extent of vegetation cover may alter the volume and timing of streamflow components significantly (Bosch, 1979; Bosch & Hewlett, 1982; Scott & Lesch, 1997). Studies reported measurable declines in base flows and long-term water yields following afforestation, understood to be attributable primarily to increased water use by trees, and driven by mechanisms which modify both storm and low-flow generating mechanisms, including increases in the amount of standing plant biomass, canopy cover, leaf area, surface roughness, rooting depth, and changes in the timing of senescence (Blight, *et al*., 2005).

Long-term streamflow data generated in these experiments running from 1935 to around 1980 represented an invaluable resource in the development and validation of a number of empirical methods for predicting hydrological responses to changes in catchment management; the Nänni curves (Nänni, 1970), Van der Zel curves (Van der Zel, 1997) and later the Scott, or CSIR curves (Scott & Smith, 1997) were all used to assess permit applications for forestry required in terms of the Afforestation Permit System under the Forest Act (Act 72 of 1968). These approaches allowed for initial estimates of changes in

streamflow characteristics likely to accompany afforestation, however they were based entirely on data from commercial plantation species (pine and eucalypt) growing in a few high rainfall catchment areas (in excess of 1100 MAP), and were therefore unrepresentative of vast areas of the South African landscape and for native vegetation types (Gush, *et al*., 2002). South African paired catchment experiments, and the empirical models based upon these data, while useful in an applied sense (restricted to commercial afforestation applications in high rainfall areas), offered little insight into the multiple complex ecohydrological processes driving streamflow responses in natural conditions and for the range of (typically drier) climate variability.

2.1.2 Direct measurement techniques

Individual ecohydrological processes driving streamflow were to remain inadequately explained on the basis of catchment experiments, and in the 1970s and 80s, coinciding approximately with their discontinuation in South Africa, greater emphasis was placed on direct measurement techniques, and the development of conceptual understanding to address gaps in knowledge (Schulze, *et al*., 2000; Hughes, 2004; Everson, *et al*., 2011). Process studies in the 1960s and 70s contributed substantially to improving existing understanding of rainfall-runoff and streamflow generation mechanisms, extending beyond that previously limited largely to forestry (Royappen, Dye, *et al*., 2002; Hughes, 2004). Knowledge gained from this research supported the development of a growing number of process-based and conceptual hydrological models of varying levels of complexity, which were designed to simulate hydrological processes by applying various mathematical algorithms (Hughes, 2004).

To address this lack of representivity, the Water Research Commission, in conjunction with the then Department of Water Affairs and Forestry commissioned a study based on the ACRU model to produce a series of look up tables indicating reductions in streamflow for each quaternary catchment, based on local conditions including rainfall, evaporation, soil depth and type, *etc*. (Gush, *et al*., 2002).

2.1.3 Empirical & physically-based equations

Up until the late 1980s, direct measurement of evapotranspiration by micrometeorological techniques remained limited by the theoretical and technical challenges of measuring near-surface climate variables and surface energy and momentum exchanges (Farahani, *et al*.,

2007). Similarly, water balance approaches, including lysimeters and microlysimeters were expensive and largely limited to research applications. For these reasons, empirical and physically-based equations for estimating evapotranspiration were (and continue to be) widely used, particularly in agrohydrological and irrigation engineering applications where estimates of crop water use are needed with few data requirements and less emphasis on accuracy (Shuttleworth, 2007).

Early perceptions were that evapotranspiration was predominantly a simple physical surface-atmosphere energy transfer process, with little physiological control exerted by vegetation; this perception prompted a focus particularly in the early 20th century on the exploration of simple empirical equations for explaining relationships between surface and atmospheric variables and potential evaporation (used to describe the upper limit of water which would be evaporated by the atmosphere if it were available) (Farahani, *et al*., 2007). These comprised equations based on temperature, including the Thornthwaite (1948), Blaney-Criddle (1950) and Hamon (1963) equations, equations based on radiation, including Turc (1961), Makkink (1957) and Priestley-Taylor (1972) equations, and equations based on both radiation and temperature, including Jensen-Haise (1963) and Hargreaves-Samani (1985), many of which remain in use, although incorporating various modifications (Farahani, *et al*., 2007; Jovanovic & Israel, 2012).

In 1948, Penman developed a physically-based equation to describe the process of energy transfer in the lower atmosphere, representing a significant landmark in the ability to model surface moisture fluxes; the Penman (1948) equation combined an energy balance and aerodynamic formula to estimate latent heat flux, the energy transferred in the evaporation of water. This was later improved by Monteith, to give the Penman-Monteith equation (Monteith, 1965) requiring only routine climate variables widely available (described in Section 2.5.1); the need for vegetation specific parameters limited its use as a means to calculate actual evapotranspiration, however (Moran, *et al*., 1997). To address inconsistencies in the way that the concept of potential evaporation was being interpreted and applied, the Food and Agriculture Organisation (FAO), in consultation with the International Commission for Irrigation and Drainage and the World Meteorological Organisation, established a universally consistent definition of a “reference surface” by which to define potential evapotranspiration (Allen, *et al*., 1998). The resulting FAO-56 equation, based on the Penman-Monteith approach (Monteith, 1965) has become the international standard for the

calculation of reference evapotranspiration (ET_0) and is widely used to calculate crop water requirements in agricultural applications in South Africa, based on data measured by networks

2.1.4 Automated measurement of near-surface climate variables

Significant advances in the fields of agro and ecohydrology have come with the advent and expansion of automatic weather station networks in recent decades, which allow for continuous, automated measurements of surface meteorological variables required to calculate ET_0 at high time steps and over wide areas (Farahani, *et al*., 2007). Previously, meteorological variables required to perform these calculations, including air temperature, humidity, solar radiation, wind (speed and direction), and precipitation, had to be recorded manually using simple instrumentation and recorded on paper, an especially labour intensive task significantly restricting the extent to which these data could feasibly be collected and managed.

In South Africa, the ARC-ISCW has deployed some 530 of these automated stations since the 1940s, managing and distributing data online to researchers upon request. The network is being expanded on an ongoing basis, and extensive data at hourly time-steps are now available for experimental and applied purposes for large parts of the country going back several decades in many cases. ET_0 is calculated by the FAO-56 method on an hourly basis using meteorological data measured at each weather station.

Since the late 1990s, research into ET measurement technologies in South Africa has centred largely on two main approaches: ground-based micrometeorological methods, particularly scintillometry as a relatively new operational method (Savage, *et al.*, 2004, Savage, *et al.*, 2010), and more recently, various satellite-based remote sensing techniques, with some of the main operational approaches being the Surface Energy Balance for Land Algorithm (SEBAL) (Jarmain, *et al*., 2009) and the Surface Energy Balance System (SEBS) (Jarmain, *et al*., 2009; Gibson, *et al*., 2009; Gibson, *et al*., 2011; Mùnch, *et al*., In press; Műnch, *et al*., In press.). Micrometeorological methods, including BR and EC were first assessed for their applicability in South Africa by Savage *et al*. (1997), and scintillometry somewhat later (Savage, *et al*., 2004).

2.1.5 Advances in micrometeorological techniques

With advances in understanding of the physics of turbulence and heat and radiation transfer in the lower atmospheric boundary layer since the 1970s, and rapid improvement in electronics and sensor technology in the early 1980s, there has been important progress in the development of micrometeorological methods for evaporation measurement in recent years (Shuttleworth, 2007). Scintillometry (Savage, *et al*., 2004), eddy covariance (EC) (Swinbank, 1951) and Bowen ratio energy balance (BR) (Bowen, 1926; Sverdrup, 1943) in particular have become relatively widely used by researchers within the last decade, both in South Africa and internationally. These instruments are capable of high quality spatially-averaged estimates of flux densities for discrete "footprints" of vegetation (Savage *et al*., 2010), typically varying in dimension between tens of m^2 (Eugster & Zeeman 2006) to several km^2 in the case of the large aperture scintillometer (LAS) (Meijninger, *et al.*, 2002). The EC method, in contrast to both BR and scintillometry, provides a direct measure of CO_2 and water vapour flux based on the statistical correlation of vertical vapour or sensible heat fluxes (H) transported in turbulent wind eddies above the canopy (Allen, *et al*., 2011). Scintillometry and BR, on the other hand, provide indirect estimates of latent heat flux (λE) based on the surface energy balance (described in Section 2.3), invoking various theoretical assumptions to account for turbulent transfer in the lower atmospheric boundary layer (Shuttleworth, 2007). Measurements are variously averaged over time periods ranging between two to 60 minutes, allowing high temporal resolution of diurnal variation in flux densities (Savage, *et al*., 2004).

Largely within the last two decades, driven by advances in theory and instrumentation (Shuttleworth, 2007), and the growing interest in global climate change and carbon cycling (Glenn, *et al*., 2007), there has been a proliferation of high quality micrometeorological flux data from a range of ecosystems and climate regions globally (Baldocchi, 2001). A series of permanent EC flux towers has been established in nearly every type of natural ecosystem and production landscape worldwide, managed by the FLUXNET consortium and presently numbering around 500 instruments (Glenn, *et al*., 2011).

Satellite-based approaches offer several distinct advantages over ground-based instrumentation, in that they are capable of continuous, spatially and temporally resolved flux estimates at regional and catchment scales (Glenn, *et al*., 2007). These attributes of remote observation are critical from the perspective of refining understanding of ecohydrological

processes, because catchment hydrological responses to diverse land-use systems and changes in ecosystem structure typically demonstrate a high degree of spatio-temporal variation, and may not be adequately interrogated on the basis of either point measurements or catchment-scale water balance approaches (Jensen & Illangasekare, 2011).

2.1.6 Advances in satellite remote sensing capabilities

Satellite remote sensing has been explored extensively as a means of inferring information on mass, energy and momentum fluxes from surface thermal and spectral properties since the late 1970's, and there has long been interest in the potential of these approaches for water resource management applications specifically (Jackson, *et al*., 1977; Carlson & Buffum, 1989; Kustas & Norman, 1997; Bastiaanssen, *et al*., 1998a; Bastiaanssen, *et al*., 1998b; Su, 2002). Given that satellite sensors are unable to measure flux exchanges directly, these approaches are generally based on quantifying relationships between observed radiances and various parameters required to calculate flux densities, such as LAI, vegetation indices, or land surface temperature, using physically-based or statistical/semi-empirical algorithms (Cleugh, *et al*., 2007). Several potential sources of error are introduced in the approximation of biophysical processes however (Zeweldi, *et al*., 2009), and quality flux information from ground-based instruments at appropriate spatial scales is key for model calibration and validation, and in improving satellite algorithm performance (Savage, *et al*., 2010). New opportunities for calibration and validation in global terrestrial ecosystems, which have accompanied the advent and expansion of both permanent and portable micrometeorological systems described above, as well as the expansion of ground-based automatic weather station networks, have dramatically improved the potential for remote sensing approaches for flux estimation since the turn of this century (Glenn, *et al*., 2007).

Recent technological advances have culminated in the emergence of sophisticated satellite sensor systems, embodied in the National Aeronautics and Space Administration´s (NASA) Earth Observation System (EOS), the implementation arm of the Earth Systems Enterprise (Privette & Roy, 2005). EOS, conceived in the 1980s and realised largely during the 1990s, comprises a series of coordinated polar-orbiting satellites, and was established to enhance understanding of the planet's climate system by generating long-term observations of atmospheric and surface (marine and terrestrial) spectral and thermal properties. EOS consists of three flagship satellites, including Terra, launched in 1999 and aimed at systematic land, atmospheric and ocean measurements, Aqua, launched in 2002 and designed to make water

cycle observations, and Aura, launched in 2004, aimed at atmospheric chemistry measurements. These systems are equipped with a collection of 13 different sensors, perhaps most notable of which are the MISR, ASTER and MODIS (abbreviations previously defined), the latter of which is mounted on both the Terra and Aqua platforms, allowing surface observation from different view and illumination angles at morning (Terra) and afternoon (Aqua) overpass times. With improved spectral resolution, on-board calibration systems and well characterised radiometric, spectral, spatial and polarization sensitivities, MODIS in particular introduces several important technical advances in earth observation capabilities (Justice, *et al*., 2002).

Technological advances aside, EOS, and MODIS, are perhaps most significant for the fact that they herald the start of the era of multidisciplinary earth observation initiatives (Privette, *et al*., 2002); spectral information returned by MODIS is being used by science teams contracted to NASA and differentiated according to land, ocean and atmospheric disciplines, to develop a series of validated, high quality global geophysical datasets, variously operational and freely available to the public over the last decade. Among these, the combined leaf area index/fraction of photosynthetically active radiation (LAI/FPAR) products provide continuous, near-real time information on global vegetation phenological canopy dynamics, and have been widely anticipated by the international research community. They include the 8-day MOD15A2 product from the Terra satellite, the 8-day MYD15A2 product from the Aqua satellite, the Terra/Aqua combined 8-day MCD15A2 product, and the combined Terra/Aqua 4-day MCD15A3 product. LAI is a well established plant structural characteristic that provides important information on surface vegetation processes (Darvishzadeh, *et al.*, 2008). It is defined as the one-sided green leaf area per unit ground area in broadleaf canopies, and the projected needle leaf area in coniferous canopies; it is a key variable in most ecosystem productivity models, global climate, hydrology, biogeochemistry and ecology models, and is applied in numerous NASA EOS interdisciplinary projects (Shabanov, *et al*., 2005). Most recently, these LAI datasets have been used as inputs in developing a global evapotranspiration algorithm within the suite of MODIS land products (Mu, *et al*., 2011), described in Section 2.6.4.

2.2 The biophysics of evapotranspiration

Evaporation is defined as the process whereby a liquid or a solid substance is transformed to a gaseous state, in which energy is absorbed or transferred and removed from the evaporating

surface (Allen, *et al.,* 1998b). Energy required to break the hydrogen bonds of liquid water molecules in this process is derived from solar radiation, advection, and heat stored in water and land masses, of which the former is dominant. Total evaporation in terrestrial ecosystems comprises evaporation from saturated and moist soils, evaporation of intercepted rain water from plant canopies, sublimated water vapour from ice and snow, and transpiration, the exchange of plant water for atmospheric CO_2 required for photosynthesis from stomata on plant leaves and stems (Mu, *et al.,* 2011). By convention, in applying the term evapotranspiration, the plant cellular process of transpiration (T) is distinguished from the physical one of evaporation (E), although these processes are in fact strictly congruous (Monteith, 1985), and use of the term in the international literature is declining (Savage, *et al*., 2004). It has been suggested, however, that the term transpiration be retained in favour of plant evaporation, as the latter incorrectly implies that plants themselves exert no control of water loss to the atmosphere; the terms evapotranspiration to describe the combined physical and plant cellular processes, and transpiration for the plant cellular process specifically, are therefore applied throughout this thesis.

2.2.1 Atmospheric structure: the atmospheric/planetary boundary layer

The atmospheric or planetary boundary layer is a relatively shallow layer of influence above the earth's surface (between 100-2000 m in thickness, varying in response to air temperature) in which friction results in significant energy, mass and momentum exchanges between the surface and the atmosphere (Savage, *et al*., 2004). It is characterised by rapid variations in the properties of flow variables including wind velocity, air temperature and mass concentration such as CO_2 and water vapour pressure, largely carried by turbulent motion. It extends vertically to a sharp boundary with the upper free atmosphere, above which flow is generally laminar. The lowest 10-15% is referred to as the surface boundary layer, which is itself comprised of an outer and inner (or internal) boundary layer.

2.2.2 Transpiration and cohesion-tension theory

Evaporation from a vegetated surface is controlled by radiant energy availability, atmospheric humidity deficit, turbulence in the near-surface boundary layer, soil moisture availability, and plant stomatal control of the ability of the surface to transmit water vapour to the atmosphere (termed stomatal conductance, or conversely, resistance) (Kelliher, *et al.,* 1995). Transpiration dominates total evaporation in most terrestrial ecosystems, (Williams, *et al*., 2004), and is therefore a key term in the water balance.

It is generally accepted that soil moisture transport from the soil profile to the atmosphere via plant roots, xylem, and eventually stomata in the process of transpiration can be explained in terms of Cohesion-Tension (C-T) Theory (Dixon & Joly, 1894). C-T Theory proposes that water rises in a metastable state under tension driven by surface tension at the evaporating surfaces of the leaf. Water is evaporated primarily from cell walls of substomatal chambers as a result of the lower water potential of water vapour in the air, causing a curvature in the water menisci of apoplastic water within the cellulosic microfibril pores of cell walls (Tyree, 1997). Surface tension at the leaf results in a decrease in xylem pressure in plant water directly behind the meniscus, resulting in a decrease in water potential in adjoining cell walls and protoplasts. The water column is maintained in a metastable state by the cohesion of water molecules to each other, and adhesion to walls of the xylem conduits by hydrogen bonds. Tension at the evaporating surface of the leaf is transmitted to the roots via a continuous water column, causing water potential in root apices to fall below that of the surrounding soil moisture, and therefore an uptake of soil moisture to replace evaporated water at the surface. Plant water is evaporated at the air/water interface at the meniscus by the breaking of hydrogen bonds, derived from the sources described earlier.

2.2.3 Functional Convergence Theory

Functional convergence theory (Field, 1991) hypothesizes that plants scale leaf area and light harvesting ability according to the availability of resources in order to optimize carbon fixation. Plant functional convergence is manifested in a number of traits which perform in very similar ways, irrespective of species, despite enormous variation in leaf life span, rate of photosynthesis and respiration, leaf growth rate, leaf nitrogen content and leaf specific area. Reich, *et al*., (1997) found intraspecific relationships among these traits, across a diversity of plant species and biomes, demonstrating convergent evolution and global generality in plant functioning. Reich, *et al*., (2003) further argue that patterns of functional trait variation within and amongst habitats can be explained by trade-offs reflecting adaptations to resource and environmental gradients. While functional convergence in leaf traits is comparatively well understood, there are relatively few studies addressing convergence in plant water relations and productivity. McClenahan, *et al*., (2004) demonstrate convergence in several traits that define plant hydraulic architecture in Australian woodlands, heathlands and mangroves, suggesting that this convergence allows us to generalize plant function over relatively large homogenous areas. Following from this, remote sensing of canopy light absorption also enables an important component of canopy carbon assimilation rates to be estimated over

extensive areas. Modelling of carbon exchange and net storage is facilitated, owing to natural selection for a narrow range of light-use efficiencies among a wide range of plant functional types. This "functional convergence" arises from resource allocation strategies that appear to maximise the benefits of carbon (energy) and nutrients (e.g. mainly nitrogen) relative to the costs of acquisition (Goetz & Prince, 1999). Convergence is most evident on a leaf mass per unit ground area basis, a measure that more closely reflects the costs of resource acquisition than does leaf area.

2.3 The surface energy balance

The surface energy balance describes the way in which energy in the form of solar and atmospheric radiation is balanced at the earth's surface by inputs or outputs of energy from non-radiative origins (Allen, *et al.*, 2005a), and provides the physical basis for models describing vertical energy, momentum and mass exchanges in the planetary boundary layer, also called the atmospheric boundary layer (described in Section 2.2.1). In the energetic sense, rather than as a residual water loss in the catchment water balance, evapotranspiration is conceived of as the partitioning of energy at the surface into that required for either the evaporation of water (latent heat) or heating of the overlying atmosphere (sensible heat) (Shuttleworth, 2007). In its shortened form, the expression neglects various less significant terms, such as canopy heat storage and advection (although the latter may in fact be significant in certain conditions), and for a flat, extensive surface can be written as (Savage, *et al.*, 2010):

$$R_n = G + H + \lambda E$$

Equation 1

where:

R_n is the net radiance;

G is the soil heat flux density based on soil heat flux and soil temperature;

H is the sensible heat flux density; and

λE is the latent heat flux density.

(all units are in W m^{-2}, where 1mm ET day^{-1} = 28.36 W m^{-2}).

Given accurate measurements of R_n and G, and estimates of H, which requires an ability to account for turbulent transfer in the near-surface atmospheric boundary layer, λE can be calculated as a residual of the energy balance (Equation 1) from Equation 2:

$$\lambda E = R_n - G - H$$

Equation 2

The surface energy balance reflects net radiation inputs (R_n), latent heat exchanges (λE), and the sum of sensible heat fluxes to or from the air (H) and to or from the soil (G) (Savage, *et al.* 2004). H is defined as the absorption or transference of heat energy flux due to a change in temperature between the surface and the overlying air, without the influence of a phase change (*i.e.* the vaporisation of water), while λE, by contrast, accounts for the energy absorbed in the phase change of water, without significant change in temperature (Clulow, 2007). ET can be calculated directly from latent heat flux (W m^{-2}), where 1 mm ET = 28.36 W m^{-2}. The former is driven by the vertical temperature differences between the evaporating surface (vegetation canopy or soil surface) and adjacent overlying air mass, while the latter is driven by vertical water vapour pressure differences between the air immediately above the evaporating surface and the adjacent overlying air mass (Savage, *et al.*, 2004).

In solving for the above, the determination of H presents particular difficulties, and requires accurate measurements of temperature gradients above the surface (Allen, *et al.*, 1998a). The aerodynamic expression for calculating H can be written as follows (Allen, 2005):

$$H = \rho c_p \frac{T_s - T_a}{r_a}$$

Equation 3

where:

T_s is surface temperature;

T_a is aerodynamic temperature;

r_a is aerodynamic resistance to heat transfer between a mean height within the surface to some height z above the surface;

ρ is air density; and

c_p is the specific heat capacity of air.

r_a (s m^{-1}) is aerodynamic resistance, which determines the transfer of heat and water vapour from the canopy to the atmosphere above the canopy (Allen, 2005).

Aerodynamic resistance (Equation 4) is calculated in terms of roughness length (z_o), and zero plane displacement (*d.)* z_o describes the aerodynamic roughness of the surface, and is a factor of the height (*h*) and distribution of the roughness elements, while *d* refers to the mean level at which momentum is absorbed by the individual elements of the plant, and is the height at which these elements, when condensed, assume the properties of a displaced surface where wind speed is zero (Clulow, 2007). Calculation of *d* is complicated by the effect of wind, which alters the effective displacement height.

The traditional aerodynamic resistance formula is expressed as:

$$r_a = \frac{\left(In\left(\frac{z_u - d}{z_{om}}\right) - \psi_m\right)\left(In\left(\frac{z_T - d}{z_{oH}}\right) - \psi h\right)}{\kappa^2 u_z}$$

Equation 4

where:

z_u is the height above the surface at which wind speed is measured;

d is the zero plane displacement of the logarithmic wind profile;

z_{om} is an assumed roughness length governing the transfer of momentum from the surface;

ψ_m is the Businger-Dyer correction factor for momentum transfer to account for buoyant stability or instability of the boundary layer;

z_T is the height above the surface at which air temperature is measured;

z_{oh} is an assumed roughness length governing the transfer of H from the surface;

ψ_h is a correction factor for the transfer of H to account for buoyant stability or instability of the boundary layer;

κ is the von - Karman constant (0.41); and

u_z is the wind speed measured at the z_u height.

The aerodynamic resistance formula as expressed in terms of Equation 4 has also been criticized for its use of z_{oh}, which is commonly expressed as a constant fraction of z_{om}, although this relationship can in reality vary significantly in arid conditions and sparse canopies (Allen, 2005).

2.4 Micrometeorological methods for the assessment of evapotranspiration

With advances in instrumentation and analysis since the late 1990's, the use of micrometeorological methods for flux measurement, such as EC (Swinbank, 1951), BR (Bowen, 1926), (Sverdrup, 1943), and more recently, scintillometry (Savage, *et al*., 2004), has become increasingly common in South Africa and internationally (Dye, *et al*., 2008, Jarmain, *et al*., 2009, Savage, 2009, Savage, *et al*., 2010). Micrometeorological techniques rely on high frequency measurements of scalars above the canopy to derive estimates of H and λE (Rana & Katerji, 2008), either directly, or indirectly as a residual in the surface energy balance (Equation 1) (Savage, *et al*., 2004). They possess certain advantages over other ground-based approaches for flux estimation, in that they deliver non-destructive measurements for extended periods at hourly time steps or less, with little requirement for supervision (Shuttleworth, 2007). Instruments provide either point (EC and BR) or path-averaged (scintillometers) measurements of flux scalars for discrete fetches of vegetation, or flux 'footprints' (Savage, *et al*, 2010) typically varying in size between tens of m^2 (Eugster & Zeeman, 2006) to several km^2 in the case of the large aperture scintillometer (LAS) (Meijninger, *et al.,* 2002). Although other techniques also based on micrometeorological principles are available, such as the Infra red (Savage, *et al*., 2004) and Surface Renewal (SR) (Paw & Brunet, 1991), the EC, BR and scintillation methods have direct bearing on this study, and are therefore discussed in more detail here.

2.4.1 Eddy covariance (EC)

Driven largely by the interest in global climate change and the carbon cycle, the EC technique (sometimes called eddy correlation) has become a particularly popular method for research, and is considered by many to be the universal standard for energy and CO_2 flux measurement (Consoli, 2011). Coordinated through the international FLUXNET consortium, some 500 permanent EC flux towers have now been established on five continents spanning a wide range of natural and agricultural systems (Glenn, *et al.*, 2011). Instruments deliver areally-averaged estimates of water vapour and CO_2 fluxes at high temporal resolution (typically integrated over two minute intervals) over footprints varying between several tens to thousands of square metres (Eugster & Zeeman, 2006).

The EC method differs from the BR and scintillation techniques in that it provides a 'direct' measure of ET (Savage, *et al*., 2010). The method is based on the statistical correlation between the vertical fluxes of vapour or *H* transported in vertical motions of turbulent eddies (Allen, *et al*., 2011). The instrument typically comprises a sonic anemometer and infra-red gas analyzer (IRGA), which measure vertical wind velocity (*W*) and water vapour mixing ratios (*h*) at a given point above the canopy, at sampling rates capable of accounting for all eddies contributing to vapour transport (frequencies varying between 5-20 Hz, but commonly 10 Hz) (Allen, *et al*., 2011). Flux calculations are based on the statistical relationship described by Swinbank (1951):

$$E = \rho a\overline{W'q'} = \frac{0.622}{P}\rho a\overline{W'e'}$$

Equation 5

where:

ρ_a is the density of moist air;

P is the atmospheric pressure;

q' is the instantaneous deviation of specific humidity from mean specific humidity (*q*);

e' is the instantaneous deviation of vapour pressure from mean vapour pressure (*e*); and

W' is the instantaneous deviation of vertical wind velocity from mean vertical wind velocity (*W*).

E is evaporation rate (units mass per unit surface area per unit time).

The overbar in Equation 5 indicates averaging of the products, typically over 15 - 30 minute intervals (Allen, *et al*., 2011). Vapour transport across the horizontal plane is calculated based on the covariance of *w* and *h* (Baker, 2008), requiring various retrospective flux correction procedures (Shuttleworth, 2007).

2.4.2 Bowen Ratio Energy Balance method (BR)

The BR technique works by computing the ratio of *H* to λE, known as the Bowen ratio (β) (Bowen, 1926) (Equation 7), based on vertical temperature and humidity gradients above the canopy (Dye, *et al*., 2008). Temperature and humidity are measured simultaneously every two seconds, averaged over 20 minute periods, at two points of known height (z_1 and z_2) using fine wire thermocouples and hygrometers. Given measurements of R_n and *G* obtained using net radiometers and soil heat flux plates, β is used to calculate λE by Equation 2.

H and λE flux densities are calculated using the functions:

$$H = \lambda \rho_a K_h \left(\frac{(T_1 - T_2)}{(z_1 - z_2)} \right)$$

Equation 6

$$\lambda E = \left(\frac{\lambda \rho_a \varepsilon K_v}{P} \right) \left(\frac{(\bar{e}_1 - \bar{e}_2)}{(z_1 - z_2)} \right)$$

Equation 7

where:

K_h is an eddy diffusivity coefficient for *H;*

K_v is an eddy diffusivity coefficient for λE*;*

ε is the ratio of the molecular mass of water (M_w) to the molecular mass of dry air (M_a);

ρ_α is the density of air;

P is atmospheric pressure;

$(\bar{e}_1 - \bar{e}_2)/(z_1 - z_2)$, the vapour pressure gradient; and

$(T_1 - T_2)/(z_1 - z_2)$, the temperature gradient.

Assuming diffusivity coefficients K_v *and* K_h are equal, a rational assumption because they are transported by the same eddies, their ratio can be calculated using β*:*

$$\beta = \gamma \frac{[T_l - T_u]}{[e_l - e_u]}$$

Equation 8

where:

β is the Bowen ratio

γ is the psychrometric constant,

T_l is the lower temperature,

T_u is the upper temperature,

e_l is the lower moisture content, and

e_u is the upper moisture content.

Using Equation 2 and the computed Bowen ratio (Equation 6), Bowen, (1926) showed H and λE flux densities (Equations 3 and 4) to be:

$$H = \beta \frac{(R_n - G)}{(\beta + 1)}$$

Equation 9

and

$$\lambda E = \frac{(R_n - G)}{(\beta + 1)}$$

Equation 10

To permit calculation of the energy balance, R_n is measured using a net radiometer, and G is calculated from average soil temperature, where soil water content and heat flux is measured at 80 mm below the soil surface (Dye, *et al*., 2008). Air temperature profile difference is calculated from air temperatures measured using high resolution fine-wire thermocouples, while water vapour pressure difference is computed from the water vapour pressure measured with a hygrometer.

2.4.3 Scintillometry

Scintillometry first emerged in the 1960s, making significant progress in the 1970s with advances in the theories describing atmospheric turbulence (Shuttleworth, 2007), although the technique only became popular in the 21st century (de Bruin, 2002). Also an indirect method, it is based on the propagation of electromagnetic radiation through the turbulent atmosphere above the canopy (Dye, *et al*., 2008), and relies on Monin Obukhov Similarity Theory (MOST) to account for turbulent transfer (Savage, *et al*., 2004). To date, two types of scintillometer have been used in South Africa: the large aperture scintillometer (LAS), designed for path distances of between 250-3000 m, and the surface layer scintillometer (SLS), designed for operation over path lengths of 50-250 m (Savage, *et al*., 2004).

Large aperture scintillometer (LAS)

The LAS consists of a transmitter that emits an electromagnetic beam of known wavelength towards a precisely located receiver, which registers attenuation in signal caused by distortions in the beam. The dominant cause of distortions, and signal attenuation, are fluctuations in structure parameter of the refractive index of air (C_n^2), caused by turbulent wind eddies that result in small variations in temperature and humidity across the plane,

known as 'scintillations'. C_n^2 can be conceived of as the 'turbulent strength' of the atmosphere (Meijninger, 2002), which describes its ability to transport H and λE (Clulow, 2007). C_n^2 is linked to the structure function parameter for air temperature (C_T^2), which in turn is used to derive path-averaged estimates of H using MOST to account for turbulent heat transfer in the surface layer.

Surface layer scintillometer

> *"The SLS consists of a transmitter and a receiver unit separated by between 50 and 250 m with a laser beam between the transmitter and receiver. The receiver unit measures the radiation intensity fluctuations at 1 kHz,caused by atmospheric refractive scattering of turbulent eddies in the path of the SLS beam. The so-called inner scale of refractive index fluctuations {/$_o$) is calculated from the beam path length and the variances of the logarithm of the amplitude of the two beams and the structure parameter refractive index fluctuations C_n^2 is calculated from the covariance of the logarithm of the amplitude fluctuations between the two beams. Using an iterative method, and applying MOST, sensible heat flux density may be calculated from inputs of air temperature, atmospheric pressure, beam path length and the SLS beam height above the level corresponding to a wind speed of 0 m s^{-1}. The latent energy flux density is then estimated as a residual using the energy balance equation and measurements of net irradiance and soil heat flux density"* (Savage, *et al*., 2004).

2.5 Meteorological equations for estimating evapotranspiration

Measuring ET by directly by the methods described above is expensive and technically demanding, and it has often been necessary to rely on various semi-empirical and/or physically-based equations to obtain estimates. This is particularly true in an applied context such as agriculture and irrigation engineering, where there may be a need to estimate crop water use relatively easily with limited data requirements, and with less stringent demands in respect of data accuracy (Shuttleworth, 2007). Numerous equations based on meteorological data are available that provide an ability to estimate evaporation with relatively few data needs; historically, because the process was thought to be largely physical with little influence exerted by vegetation, these equations were primarily based on simple statistical relationships between temperature and/or radiation, for example, and potential evaporation (Farahani, *et al*., 2007; Jovanovich & Israel, 2012).

Potential evaporation (ET_p), a concept which seems to have first been proposed by Thornthwaite (1948), is typically used to refer to the upper limit of evaporation possible for a given combination of surface and atmospheric conditions, and is useful in that it provides a measure of the evaporative potential of the atmosphere independent of vegetation (or surface) factors (Lhomme, 1997). Examples of some of these approaches include equations based on temperature, such as the Thornthwaite (1948), Blaney-Criddle (1950) and Hamon (1963) equations; equations based on radiation, including Turc (1961), Makkink (1957) and Priestley-Taylor (1972) equations; and equations based on both radiation and temperature, including Jensen-Haise (1963) and Hargreaves-Samani (1985). Several of these remain in use, although incorporating various modifications (Israel & Jovanovich, 2012). More recently, as recognition of the complexity of the evaporative process evolved, physically-based approaches, particularly the Penman (1948) and modified Penman-Monteith (1965) equations, which combine aerodynamic and energy balance formulae to estimate the latent heat of evaporation, have gained prominence (Farahani, *et al*., 2007; Jovanovich & Israel, 2012). Since its introduction in 1965, the Penman-Monteith equation in particular has become well established as a physically robust method for describing the process of evaporation; the Penman-Monteith has direct relevance to this study, and is discussed in Section 2.5.1.

2.5.1 The Penman-Monteith equation

The Penman-Monteith equation (Monteith, 1965) is a well established method for calculating ET for uniform vegetated or bare soil surfaces, based on standard point-measured micrometeorological data and surface parameters (Moran, *et al.*, 1996). It builds on the earlier Penman combination equation (Penman, 1948), in which Penman combined an energy balance and aerodynamic formula, expressed as:

$$\lambda E = \frac{\Delta\,(R_n - G) + \gamma \lambda E_a}{\Delta + \gamma}$$

Equation 11

where:

R_n is the net radiation flux at the surface;

G is the soil heat flux;

Δ is the slope of saturation vapour pressure versus temperature curve;

γ is the psychrometric constant; and

E_a is the water vapour transport flux.

E_a can be conceived of as the drying power of air (Clulow, 2007), and is defined empirically as:

$$E_a = W_f\ (e_s - e_z)$$

Equation 12

where:

W_f is the wind function, expressed as a linear function of wind speed at a reference height above the ground (typically 2 m);

e_s is the saturated water vapour pressure at mean air temperature; and

e_z is the mean ambient water vapour pressure at the reference height.

By expressing the slope of saturation water vapour pressure versus air temperature relationship (Δ) in terms of Equation 12, Penman eliminated surface temperature from the final result (Ayra, 2001).

$$\Delta \simeq \frac{e_s(T_0) - e_s\ (T_z)}{T_0 - T_z}$$

Equation 13

where:

T_0 is the surface temperature; and

T_z is the air temperature at height z above the surface.

In so doing, it becomes possible to solve the equation using routine point-measured weather data (Clulow, 2007).

Monteith (1965) improved on Penman's (1948) equation by adding a more rigorous aerodynamic transfer formula and a bulk surface resistance term, expressed as:

$$\lambda EorET = \frac{\Delta\,(R_n - G) + \rho_a c_p (e_s - D_a)/r_a}{\left(\Delta + \gamma\left(1 + \frac{r_s}{r_a}\right)\right)\lambda\rho_w}$$

Equation 14

where:

Δ is the slope of saturation vapour pressure versus temperature curve;

R_n is the net radiation flux at the surface;

G is the sensible heat exchange from the surface to the soil (positive if the soil is warming);

ρ_a is the density of air;

c_p is the specific heat of dry air;

$D_a = e_s\,(T_a) - e_a$ is the vapour pressure deficit of the air (humidity deficit), and $e_s\,(T_a)$ is the saturation vapour pressure at air temperature (Cleugh, *et al*., 2007);

γ is the psychrometric constant;

r_a is the aerodynamic resistance to turbulent heat and/or vapour transfer from the surface to some height z above the surface, and is generally considered analogous to r_a in Equation 5 (Allen, 2005);

r_s is a bulk surface resistance term representing the resistance presented by plant stomatal controls, vegetation canopies and/or soil conditions to vapour conductances;

λ is the latent heat of vaporisation, defined as the energy required to convert water to vapour (joules per kilogram); and

ρ_w is the density of liquid water.

In computing ET, the Penman-Monteith method algebraically eliminates surface temperature and humidity at the evaporating surface in favour of a bulk surface resistance term r_s (Kelliher, *et al,*. 1995), which is a factor of soil moisture content and soil resistance to water transport where evaporation is concerned, and plant LAI and stomatal resistance where transpiration is concerned (Glenn, *et al*., 2007). The model assumes that whole canopy exchange can be adequately represented by simulating radiation capture and partitioning of energy into H and λE as if it occurred at a single level, implying that there are no intermediate aerodynamic or convective resistances between vegetation and soil layers, known as the 'big leaf' approach (Allen, *et al.*, 2005b). At this source-sink level, the control of exchanges between the hypothetical big leaf and the adjacent air mass (r_s), is approximated by the parallel average sum of stomatal and boundary layer resistances (Shuttleworth, 2007).

The terms A (or R_n-G), T_a and D_a can be obtained from radiation and soil heat flux measurements, air temperature and humidity measurements respectively (Cleugh, *et al.*, 2007). Accounting for r_a and r_s in natural ecosystems is more difficult however, and has restricted the routine implementation of the Penman-Monteith as a means of estimating ET_a in heterogeneous systems. For this reason, it is most often used in one of its modified forms to estimate reference ET (ET_0) (discussed below) for uniform vegetated or bare soil conditions (Moran, *et al*., 1996). More recently, satellite data has been explored as means to derive information on surface parameters required to calculate evaporation using the Penman-Monteith in heterogeneous systems, discussed in Section 2.6.4.

2.5.2 The FAO-56 Penman-Monteith equation

Since the concept was first introduced in 1948, definitions of ET_p have been varied and inconsistently applied (see Lhomme, 1997 for a review), leading to uncertainty regarding the comparability of the different approaches used in its calculation (Clulow, 2012). To help address these problems, the Food and Agriculture Organisation (FAO), in consultation with the International Commission for Irrigation and Drainage and the World Meteorological Organisation, established a universally consistent definition of a "reference surface" by which to define potential evapotranspiration, which it described as follows:

> *"A hypothetical reference crop with an assumed crop height of 0.12 m, a fixed surface resistance of 70 s m^{-1} and an albedo of 0.23"* (Allen, *et al*., 1998).

This is consistent with an extensive surface of green grass (or alfalfa) of uniform height in full physiological activity, completely shading the ground and not water limited; evaporation calculated for the reference surface thus defined is officially referred to as reference evaporation (ET_0) to distinguish it, and thereby eliminate confusion, from the term ET_p. The FAO methodology has a clear agrohydrological focus, having been developed primarily to address issues of crop water requirements; the principles are equally applicable in natural ecosystems although higher levels of surface heterogeneity need to be accounted for. The FAO panel identified the Penman-Monteith equation as the most reliable method by which to calculate ET_0, recognising it as an improvement over the earlier FAO-24 guidelines (Doorenbos & Pruitt, 1977) based on Penman's (1948) equation, and devised standardized procedures for its calculation, relating specifically to calculation of aerodynamic and surface resistance (or conductance) parameters (described below).

Calculating aerodynamic resistance

In the FAO-56 method, aerodynamic resistance to heat/vapour transfer (r_a) is computed using empirically derived parameters for zero plane displacement height (d), roughness length governing momentum transfer (z_{om}), and roughness length governing transfer of heat and vapour (z_{oh}) (Allen, 2005):

$d = 0.67\ h$

$z_{om} = 0.123\ h$

$z_{oh} = 0.1\ z_{om}$

where h is vegetation height (all units in metres).

Following Equation 5, assuming a vegetation height of 0.12 m and a standard measurement height of 2 m, the function for r_a in the FAO-56 becomes:

$$r_a = \frac{\ln\left[\frac{2-0.67(0.12)}{0.123\ (0.12)}\right] \ln\left[\frac{2-0.67(o.12)}{(0.1)\ 0.123\ (0.12)}\right]}{(0.41)^2\ u_z} = \frac{208}{u_z}$$

Equation 15

where:

u_z is wind speed measured at z_u height (2 m); and

0.41 is the von-Karman constant.

Calculating surface resistance

The bulk surface resistance term r_s in the Penman-Monteith equation describes the combined effects of the soil, canopy surface and stomatal controls, as well as the effects of surface roughness on turbulent transfer (Dye, *et al*., 2008). In the FAO-56 method, for a fully vegetated surface, it is approximated using active (sunlit) LAI, where LAI_{active} = 0.5 LAI, assuming that approximately only half of the leaf area is contributing to heat and vapour transfer (Allen, *et al*., 1998). Strictly, where the criterion of full canopy cover is not met, the effects of soil evaporation would need to be accounted for in the resistance factor.

Allen, *et al.,* (1998) define r_s as:

$$r_s = \frac{r_l}{LAI_{active}}$$

Equation 16

where:

r_l is bulk stomatal resistance of a well illuminated leaf (s m^{-1})

LAI_{active} is active (sunlit) leaf area index [m^2 (leaf area) m^{-2} (soil surface)].

The general equation

LAI = 24 h

is used to approximate LAI for a clipped grass surface.

Using the above assumptions, in the FAO-56 r_s becomes:

$$r_s = \frac{100}{0.5\ (24)(0.12)} = 70\text{s m}^{-1}$$

Equation 17

Where r_l of a single leaf under well watered conditions is 100 s m^{-1}.

For standard reference height crops of grass (hc = 0.12 m) and alfalfa (hc = 0.5 m), resulting rs values are 70 s m-1 and 45 s m-1, respectively (Howell & Evett, 2004).

The FAO-56 equation, incorporating the functions for r_a and r_s described above, therefore takes the form:

$$ET_0 = \frac{0.408\Delta(R_n - G) + \gamma \frac{900}{T+273} U_2\ (e° - e_a)}{\Delta + \gamma(1 + 0.34U_2)}$$

Equation 18

where:

R_n is net radiation at the crop surface [MJ m^{-2} day^{-1}],

G is soil heat flux density [MJ m^{-2} day^{-1}],

T is mean daily air temperature at 2 m height [°C],

u_2 is wind speed at 2 m height [m s^{-1}],

$e°$ is saturation vapour pressure [kPa],

e_a is actual vapour pressure [kPa],

$e° - e_a$ is saturation vapour pressure deficit [kPa],

Δ is slope vapour pressure curve [kPa $°C^{-1}$],

γ is psychrometric constant [kPa $°C^{-1}$].

Crop factors and reference evaporation for non-standard conditions

The utility of the concept of ET_0 lies in the ability to produce a standardised measure of evapotranspiration for a known reference surface; however, to obtain estimates of actual water use (ET_a), it is necessary to relate the reference surface to the surface under assessment, including in non-standard conditions (*e.g.* conditions of water stress) (Allen, et al., 1998). The FAO-56 guidelines provide for this through the application of crop (K_c) and water stress coefficients (K_s).

In agricultural conditions, crop (K_c) and water stress coefficients (K_s) are applied to obtain estimates of ET_a, and crop water use in non-standard conditions, from ET_0 (Allen et al. 1998). K_c values are typically empirically derived, usually obtained by growing plants in precision weighing lysimeters and comparing actual water use with ET_0 (Allan, 2005); the resulting coefficient is then applied as a multiplier to derive ET_a, as follows:

$$ET_c = K_c ET_0$$

Equation 19

2.6 Satellite-based approaches for the assessment of evapotranspiration

The naturally high spatial variability of ET, particularly in heterogeneous land-use and natural ecosystems, imposes particular limitations on conventional ground-based methods for its assessment, and satellite remote sensing is at present the only means by which continuous, spatially resolved estimates of ET can be obtained over large landscape units (Glenn, *et al*., 2007). These attributes of remote observation are critical from the perspective of advancing understanding of ecohydrological processes, because diverse land-use systems and changes in vegetation cover drive complex, non-linear catchment hydrological responses, which may not be adequately interrogated on the basis of either point measurements or catchment-scale observations (Jensen & Illangasekare, 2011).

Satellite data has been explored extensively for this purpose since the late 1970's (Jackson, *et al*., 1977; Carlson & Buffum, 1989; Kustas & Norman, 1997, Bastiaanssen, *et al*., 1998a; Bastiaanssen, *et al*., 1998b; Su, 2002), and Verstraeten, *et al*. (2008) identify four main operational approaches in the literature:

- empirical models which describe the statistical relationship between ground measured ET fluxes and remotely sensed vegetation indices (VIs) or land surface temperatures (LSTs) (Nagler, *et al*,. 2005);

- physically based approaches, which typically use satellite thermal infrared (TIR) land surface temperature data (Kalma & Jupp 1990, Bastiaanssen, *et al.,* 1998a, Bastiaanssen, *et al.,* 1998b, Su, 2002) to solve for *H* in computing the surface energy balance;

- models based on determining the components of the water balance (Price, 1990, D'Urso, 2001); and

- models based on the Penman-Monteith logic (Cleugh, *et al.,* 2007, Mu, *et al.,* 2007, Leuning, *et al.,* 2009, Mu, *et al.,* 2011).

Efforts to develop regional and global scale models of surface/atmosphere exchanges using satellite data are complicated by the fact that satellite sensors cannot measure fluxes directly, and quantities of interest must instead be indirectly estimated in terms of their relationship to satellite-measured radiances, often using various physically-based or empirical/semi-empirical algorithms (Cleugh, *et al*., 2007). These algorithms must both adequately represent biophysical complexity, yet also be simple enough to parameterize and execute at multiple time and spatial scales on a continual basis. Most approaches work by physical or empirical relation of electromagnetic radiances to leaf area index (LAI), gross and net primary productivity, vegetation indices, or land surface temperature (Cleugh, *et al*., 2007; Zeweldi, *et al*., 2009). This approximation of biophysical processes introduces potential sources of error however (Zeweldi, *et al*., 2009), and quality data from ground-based instruments at scales which at least partially overlap with satellite pixel footprints are required to evaluate model performance (Savage, *et al*., 2010), in the absence of which errors of uncertainty cannot be readily quantified (Zeweldi, *et al*., 2009). Since the late 1990s, high quality flux data have become routinely available from EC flux tower networks in a wide range of ecosystems and climate regions (Baldocchi, 2001), allowing for iterative improvements in RS algorithms, and reduced errors of uncertainty in satellite modelled data (Verstraeten, *et al*., 2008).

A review of the four basic approaches listed above is provided below.

2.6.1 Remote sensing ET models based on empirical relation to vegetation indices and land surface temperature

Typically, these approaches use evapotranspiration data measured at flux towers to develop best-fit equations with remotely-sensed vegetation indices, particularly NDVI, and other derived data from satellites (Glenn, *et al*., 2007). There have been significant advances in these approaches in the last decade, accompanying the expansion of permanent flux tower networks, coordinated by the international FLUXNET network, into global ecosystems. Glenn, *et al*., (2010) provide a comprehensive review of empirical approaches based on vegetation indices, and synthesize the results of several published models, reporting coefficients of determination, a measure of the extent to which models are able to describe the variation in measured data, ranging between 0.45 – 0.96; the reader is referred to this paper for further information.

2.6.2 Parameterization of the surface energy balance using remotely sensed land surface temperature

In these approaches, estimates of land surface temperature are derived from the thermal infrared (TIR) band on satellites such as the Landsat series, the Geostationary Operational Environmental Satellite (GOES), the AVHRR series, ASTER, and MODIS, to solve for H by means of Equation 1 (Glenn, *et al*., 2010). By these approaches, if heat transfer coefficients are known or can be estimated, and aerodynamic resistance (r_a) adequately accounted for (Equation 3), H can be computed as the difference between air temperature at a reference height and TIR-based land surface temperature. λE can then be calculated as a residual of the shortened energy balance (Equation 2).

Common operational examples based on the use of remotely sensed land surface temperature in a energy balance formulation include SEBAL (Bastiaanssen, *et al*., 1998a; Bastiaanssen, *et al*., 1998b), SEBS (Su, 2002; Gibson ,*et al*., 2009; Gibson, *et al*., 2011), NTDI (McVicar & Jupp, 1999), RSEB (Kalma & Jupp, 1990; Cleugh, *et al*., 2007), the Triangle method (Gillies & Carlson, 1995; Nemani & Running, 1989; Nishida, *et al*., 2003), and the Dual Source model (Norman, *et al*., 1995; Kustas & Norman, 1999).

2.6.3 Remote sensing models based on the water balance

Remote sensing techniques based on water balance approaches appear less frequently in the literature. Verstraeten, *et al*., (2008) cite two references for this technique: Price (1990) and D'urso, *et al*., (2001), and the reader is referred to these publications for further information.

2.6.4 Remote sensing models based on the Penman-Monteith equation

The Penman-Monteith equation has received particular attention as a theoretical basis in remote sensing approaches in recent years (Cleugh, *et al.,* 2007; Mu, *et al.,* 2007; Leuning, *et al.,* 2009; Mu, *et al.,* 2011). The logic is appealing because it combines the variables driving land/atmosphere energy fluxes in a theoretically robust manner, overcoming some of the challenges encountered in a number of operational satellite-based models that use remotely sensed radiative surface temperature to calculate *H* in a surface energy balance formulation (Cleugh, *et al*., 2007). These issues have been discussed in earlier publications (Cleugh, *et al.,* 2007; Glenn, *et al.,* 2007; Gibson, *et al*., 2011).

The Penman-Monteith equation has been utilized in several ways within satellite-based approaches for moisture flux estimation (*e.g*. Moran, *et al*., 1996; Mauser & Schadlich, 1998; Granger, 2000). Most recently however, researchers from the Numerical Terradynamic Simulation Group (NTSG) at the University of Montana, and Commonwealth Scientific and Industrial Research Organisation (CSIRO), have published several papers reporting techniques for deriving information on aerodynamic and surface resistance, the latter primarily from the standard MOD15A2 LAI product, for estimating evapotranspiration within a Penman-Monteith formulation (Cleugh, *et al*., 2007; Leuning, et al., 2008; Mu, *et al*., 2007; Mu, *et al*. 2011). Cleugh and colleagues (2007) used a simple function to account for the surface resistance term in the Penman-Monteith equation, by using MOD15A2 LAI to scale biome-specific stomatal conductance values to canopy scales. They reported an improvement in evaporation estimates achieved by other established approaches based on the surface energy balance (specifically, the Resistance Surface Energy Balance model), suggested to be due to the fact that the Penman-Monteith includes an energy constraint on the rate of evaporation. Mu, *et al*., (2007) improved on the approach of Cleugh and colleagues by adding vapor pressure deficit and minimum air temperature constraints on stomatal conductance, using the Enhanced Vegetation Index (in place of NDVI) to estimate fraction of vegetation cover, and adding a function to describe soil evaporation.

This approach was further improved (Mu, *et al*., 2011) by introducing a simplified calculation of vegetation cover fraction; combining ET as the sum of both night time and daytime fluxes; incorporating a soil heat flux calculation; improving estimates of stomatal conductance, aerodynamic resistance and boundary layer resistance; separating dry canopy surface from the wet; and dividing soil surface into saturated wet surface and moist surface. This approach ultimately provided the basis for an operational global evapotranspiration algorithm utilizing MODIS inputs, and termed the MOD16 ET product.

2.7 MODIS

MODIS is a wide field-of-view satellite sensor with a swathe of 2,330 km and 36 spectral bands, with 250 m, 500 m and 1 km pixel resolution (Privette, *et al*., 2002). The instrument is a key component of NASA's Earth Observing System (EOS), the implementation arm of the Mission to Planet Earth Programme initiated in the 1980s and later renamed the Earth Sciences Enterprise (ESE) (Privette & Roy, 2005). EOS comprises three flagship satellites: Terra, launched in 1999 and directed at obtaining measurements of systematic land, atmospheric and oceanic processes, Aqua, launched in 2002, focusing on water cycle measurements, and Aura, launched in 2004 primarily to generate information on atmospheric chemistry. The three platforms are equipped with a total of 13 different sensors; both Terra and Aqua are equipped with the MODIS instrument (Justice, *et al*., 2002).

MODIS introduces a number of significant advances over its predecessors (primarily the AVHRR), including improved spectral resolution, on-board calibration systems and well characterised radiometric, spectral, spatial and polarization sensitivities (Justice, *et al.*, 2002, Privette, *et al*,. 2002). MODIS spectral resolution, with 36 bands and 12 bit radiometric resolution, exceeds any other global coverage moderate resolution imager presently in operation; key features of the Terra/MODIS system are described in Table 1. Technical improvements notwithstanding, EOS and Terra/Aqua MODIS are notable for operationalizing multidisciplinary remotely-sensed geophysical datasets (Privette, *et al.*, 2002). Science teams under contract with NASA, dedicated to land, ocean and atmospheric disciplines, have been tasked with the development of a range of global datasets based on spectral information returned by the MODIS instrument; level 2 and 3[1] products developed

[1] MODIS products are distinguished on the basis of the degree of processing involved, where level 0 products denote raw digital number images; level 1 products denote both uncalibrated and calibrated radiance values; and level 2 and 3 products denote higher levels of processing, typically derived from lower level products.

by the MODIS Land team (MODLAND) include the leaf area index/fraction of photosynthetically active radiation (LAI/fPAR), net primary production (NPP), global primary production (GPP), and ET datasets, among others (Shabanov, *et al.*, 2005). Upon generation, MODIS products are accessible online and free of charge to the public through the EOS Distributed Active Archive Centres (DAACs): the Land Process (LP) DAAC for land products, and the GSFC Earth Sciences (GES) DAAC for atmospheric products (Privette & Roy, 2005).

Table 1: General characteristics of Terra/MODIS for terrestrial remote sensing (from Justice, *et al.*, (2002).

Orbit	705 km, sun - synchronous, near - polar nominal descending equatorial crossing at 10:30 local time (specific overpass times can be obtained from http://www.earthobservatory.nasa.gov/MissionControl/overpass.html)
Swathe	2,330 km ± 55 ° cross-track
Spectral bands	36 bands, between 0.405 and 14.385 μm with onboard calibration subsystems
Spectral calibration	band 1 - 4, 2% for reflectance, band 5 - 7, under investigation (some scene-dependent electronic crosstalk)
Data rate	11 Mbps (peak daytime)
Radiometric resolution	12 bits
Spatial resolutions at nadir	250 m (bands 1-2), 500 m (bands 3-7), 1000 m (bands 8-36)
Duty cycle	100%
Repeat coverage	daily, north of ~ 30° latitude, every two days for < ~ 30° latitude
Gridded land products geolocation accuracy	within 150 m (1 sigma) at nadir
Band to band registration for bands 1-7	within 50 m in the along scan direction, within 100 m in the along track direction

2.7.1 Leaf area index and the MOD15A2 LAI/FPAR product

LAI is a well-established plant structural characteristic that provides important information on surface vegetation processes (Darvishzadeh, *et al.*, 2008), and is a state parameter in all models describing fluxes of mass, energy and momentum within the geobiosphere (Knyazikhin, *et al.*, 1998). It is defined as the mean one-sided green leaf area per unit ground area of canopy cover in broadleaf canopies, and the projected needle leaf area in coniferous canopies (Zhang, *et al.*, 2004). Derivation of LAI from remotely-sensed data is based on the analysis of multi-spectral, multi-directional surface reflectance signatures of photosynthesizing vegetation elements at the earth's surface, and two approaches have generally been used: the first involves establishing empirical or semi-empirical relationships between LAI and vegetation indices, which are various combinations of spectral reflectances at different wavelengths of the electromagnetic spectrum sensitive to vegetation characteristics, while the second is based on the inversion of the radiative transfer model

(Garrigues, *et al*., 2008). These approaches work by employing various assumptions and approximations regarding canopy structure and associated radiometric properties, which allow the canopy radiative transfer regime to be mathematically described; inversion of these models against satellite observations of surface spectral qualities then yields information on canopy structure, including LAI (Kauwe, *et al*., 2011). Garrigues, *et al*., (2008) review several studies which developed different physical algorithms, yielding LAI datasets varying in quality as well as spatial coverage and temporal availability. These authors describe five LAI datasets produced using AVHRR data since 1996, and three datasets produced from SPOT/VEGETATION data since 1998, including CYCLOPES, GLOBCARBON, and a regional dataset produced by the Canada Centre for Remote Sensing for the Canadian land surface area. Other datasets, in addition to the Terra/Aqua MODIS datasets, include one produced from each of ADEOS/POLDERENVISAT/MERIS systems, which cover a restricted time period only; LAI datasets from Terra/MISR and MSG/SEVIRI were also produced, although seemingly for limited spatial coverage only. MODIS employs both physical and empirical approaches in the derivation of LAI, dependent on the state of atmospheric and surface conditions (discussed below).

The MODIS instrument measures earth atmospheric and surface reflected solar radiation, using state-of-the-art on-board calibration and processing systems for geolocation, cloud filtering and correction of atmospheric contamination of surface reflectances (Myneni, *et al*., 2007). Corrected spectral data is then ingested by a suite of algorithms to generate geophysical datasets on an operational basis at near-real time at a global scale. The MOD15A2 product delivers global LAI information based on one of two approaches: the main approach invokes radiative transfer theory to solve for the inverse problem of LAI based on measured reflectances and biome-specific canopy architecture information, while a backup algorithm based on biome-specific NDVI-LAI relationships is activated in the event that the main approach fails. At present, only two bands are utilised by the radiative transfer (RT) algorithm, including the visible red and near infrared wavelengths (648 and 848 nm, respectively) (Privette, *et al*., 2002). The standard MOD15A2 LAI/FPAR product from the Terra platform is generated as an 8-day composite at 1 km pixel resolution, in which the LAI with the highest corresponding FPAR value over the eight day compositing period is returned; compositing is performed to eliminate to the extent possible the effects of cloud and atmospheric contamination, which typically result in algorithm failure. Other global LAI datasets produced by the MODLAND Science team include the 8-day MYD15A2 product

from the Aqua satellite, the Terra/Aqua combined 8-day MCD15A2 product, and the Terra/Aqua combined 4-day MCD15A3 product.

In the main approach, advanced 3-dimensional radiative transfer theory is used to solve for LAI given sun and view directions, atmospherically corrected bidirectional reflectance factors (BRF) for each MODIS band, band uncertainties, and an eight biome land cover class based on the International Geosphere Biosphere Programme (IGBP) classification (Knyazikhin, *et al*., 1998). Presently (Collection 5), land cover classes include: grasses and cereal crops, shrubs, broadleaf crops, savannas, broadleaf forests (with evergreen and deciduous subclasses), and coniferous forests (with evergreen and deciduous subclasses). The global land cover dataset (the MOD12Q1 product), updated on a quarterly basis, is used to define unique model configurations and fixed parameter values appropriate to each biome (Privette, *et al*., 2002). Look-up tables are generated for each biome by running the model for various combinations of LAI and fractional vegetation cover. In algorithm execution, modelled and observed reflectances are compared for a suite of canopy structures and soil patterns consistent with the range for expected natural conditions, and all values that differ by less than the uncertainty of the observed reflectances are considered acceptable solutions. The mean LAI values returned by this solution set are reported.

When no acceptable solutions are found, the backup algorithm is activated, which generates estimates based on an empirical LAI/NDVI relationship regardless of BRF effect and surface reflectance uncertainties (Shabanov, *et al*., 2005). Since the main approach typically fails (*i.e.* no acceptable solutions are found) in the event of cloud cover or aerosol contaminated reflectances, LAI estimates generated by the backup algorithm are generally considered unreliable (Myneni, *et al*., 2007). The quality of LAI produced by the main RT algorithm are determined by two key factors: the first are uncertainties regarding inputs to the algorithm, specifically land cover and surface reflectances, while the second refers to model uncertainties, or the consistency between RT simulations stored in the look-up tables for each biome, and corresponding MODIS surface reflectances (Shabanov, *et al*., 2005). Information regarding the quality of LAI retrievals is provided in quality control datasets accompanying the MOD15A2 product (described below), and interrogation of these data is required to determine the confidence limits within which the product may be used; the full list of datasets comprising the MOD15A2 LAI/FPAR collection 5 (V005) products is provided in Table 2 .

MODIS products are delivered in Hierarchical Data Format (HDF-EOS), projected to Sinusoidal 10° grids (Collection 4 and 5) (Tan, *et al*., 2005). They are produced as an unsigned 8-bit integer variable, with values that may range from 0-255. In the case of the LAI and FPAR datasets, values range between 0-100, and are stored with a scaling factor (0.1 for LAI and 0.01 for FPAR) which must be applied to each cell, or pixel, to derive biophysical values for analysis. The HDF file format is typically not fully compatible with most GIS platforms, and a tool for conversion to Geotiff format, the HDF–EOS to GeoTIFF Conversion Tool (HEG Tool), has been developed to meet user requirements. HEG also allows users to convert EOS data from its original map projection to user specified projections, and to request subsets of EOS data products by spatial coordinates or band specification. The tool is available online through the EOS Data Pools, and is also available as a stand-alone product which can be downloaded to a user workstation.

Table 2: Science Data Sets for MODIS/Terra Leaf Area Index/FPAR 8-Day L3 Global 1km SIN Grid V005 (MOD15A2).

Science Data Sets (HDF Layers) (6)	**Units**	**Bit Type**	**Fill**	**Valid Range**	**Multiplicative Scaling Factor**
Fpar_1km	%	8-bit unsigned integer	249–255	0–100	0.01
Lai_1km	m^2plant/m^2ground	8-bit unsigned integer	249–255	0–100	0.1
FparLai_QC	Class flag	8-bit unsigned integer	255	0–254	N/A
FparExtra_QC	Class flag	8-bit unsigned integer	255	0–254	N/A
FparStdDev_1km	%	8-bit unsigned integer	248–255	0–100	0.01
LaiStdDev_1km	m^2plant/m^2ground	8-bit unsigned integer	248–255	0–100	0.1

36 tiles span the global east-west (horizontal) axis, and 18 span the north-south (vertical) axis, with each tile approximately 1,200 x 1,200 km in dimension. The South African land surface extent is represented by four grid tiles, comprising tiles H19V11, approximately coextensive with the Northern Cape region, H19V12, approximately coextensive with the Western Cape area, H20V12, approximately coextensive with the Eastern Cape area, and H20V11, approximately coextensive with the KwaZulu-Natal and Mpumalanga area. In the case of the MOD15A2 product, 46 8-day composited datasets are typically produced in a year.

MOD15A2 quality assessment information

The collection 5 products have been extensively validated against ground measured LAI in most global vegetation types, (Heinsch, *et al.*, 2006, Hill, *et al.*, 2006, Fuentes, *et al.*, 2008) and algorithm performance iteratively improved over the course of each collection. Data are delivered with comprehensive uncertainty information provided in two quality assessment datasets (denoted FparLai_QC and FparExtra_QC, Table 2) of which of primary relevance is the FparLai_QC dataset. Information contained in each bit field of the FparLai_QC dataset can be accessed by 'unpacking' the datasets using a tool developed by the Land Data Operational Product Evaluation (LDOPE) facility, tasked with supporting the MODLAND science team's quality assessment activities; the tool can be downloaded and installed from the LP DAAC website. Once unpacked, the five bit layers (bit numbers 0, 1, 2, 3-4, and 5-7) may be interrogated for information regarding the retrieval method and sensor used, cloud conditions and retrieval quality (Table 3).

Table 3: MOD15A2. Collection 5 FparLai_QC.

Bit No.	Parameter Name	Bit Combination	FparLai_QC
0	MODLAND_QC bits	0	Good quality (main algorithm with or without saturation)
		1	Other Quality (back-up algorithm or fill values)
1	Sensor	0	Terra
		1	Aqua
2	DeadDetector	0	Detectors apparently fine for up to 50% of channels 1,2
		1	Dead detectors caused >50% adjacent detector retrieval
3-4	CloudState (inherited from Aggregate_QC bits {0,1} cloud state)	0	0 Significant clouds not present (clear)
		1	1 Significant clouds were present
		10	2 Mixed cloud present on pixel
		11	3 Cloud state not defined, assumed clear
5-7	SCF_QC (confidence score)	0	0, Main (RT) method used, best result possible (no saturation)
		1	1, Main (RT) method used with saturation. Good, very usable
		10	2, Main (RT) method failed due to bad geometry, empirical algorithm used
		11	3, Main (RT) method failed due to problems other than geometry, empirical algorithm used
		100	4, Pixel not produced at all, value couldn't be retrieved (possible reasons: bad L1B data, unusable MODAGAGG data)

3. Materials & Methods

3.1 Model theoretical basis

An alternative, parsimonious approach to deriving ET_a from that published by Leuning, *et al.* and Mu, *et al*. (2011) has been proposed (Palmer & Yunusa, 2011; Palmer & Weideman, 2011), who invoked functional convergence theory to scale ET_a from ET_0 (as calculated by the FAO-56). Functional convergence theory (Field, 1991) (discussed in Section 2.2.3) hypothesizes that plants have evolved to calibrate leaf area and light harvesting ability according to the availability of resources in order to optimize carbon fixation, such that leaf area is an objective indicator of vegetation physiological activity and plant water use. ET_a, incorporating the effect of vegetation controls on vapour fluxes in terms of bulk surface resistance, approaches ET_p under conditions of plentiful soil moisture availability, when plant root systems are able to supply water to the atmosphere via stomata at a rate almost commensurate with demand; when soil moisture becomes limiting, however, this relationship declines to some fraction < 1 (Jovanovich & Israel, 2012). Following this logic, the relationship of LAI at time T1 to maximum LAI (LAI_{max}), signalling the physiological status of an ecosystem relative to its optimum, can theoretically be applied to relate ET_a to ET_0, assuming that ET_0 represents the upper limit of water use possible within the system when $LAI/LAI_{max} = 1$. Implicit in this approach is the assumption that the system has achieved growth optimum within the ~10 year time span of MODIS data availability, and that efficiency levels are possible to the extent that all available energy defined by the FAO-56 is used.

Equation 20 describes the proposed relationship between LAI, ET_0 and ET_a:

$$ET_{MODIS} = P - M(FAO - 56) \times \frac{LAI}{LAI_{max}}$$

Equation 20

where

P-M is ET_0 calculated using the FAO-56 method from local point-measured weather data;

LAI is the LAI value returned by MODIS at time T1; and

LAI_{max} is the maximum LAI value returned for that pixel over the entire MODIS data span.

In some cases, owing to an absence of operational climate stations within reasonable proximity to flux validation sites at which FAO-56 could be calculated, FAO-56 ET_0 input to ET_{MODIS} is substituted by class A-pan evaporation data; A-pan data provide a measure of the evaporative potential of the atmosphere, describing the effect of temperature, humidity, rain fall, solar radiation and wind only, neglecting the influence of aerodynamic and vegetation factors, and thus is more correctly considered a measure of potential evaporation (ET_p). The term ET_0 on the other hand is strictly reserved for application to evaporation estimated on the basis of the FAO-56 method. Instances in which class A-pan data are utilised in parameterizing ET_{MODIS} are clearly indicated in the text.

3.2 Model validation

Model performance may be evaluated using various statistical tests, however nearly all studies report the coefficient of determination (r^2), a statistical description of the extent to which the variation in measured ET is explained by the model, with values ranging between 0 (no agreement) to 1 (perfect agreement) (Glenn, *et al*., 2010). In this study, ET_{MODIS} is evaluated by fitting a linear regression to modelled data and data measured using micrometeorological systems. It is assumed that micrometeorological data are an accurate reflection of moisture fluxes in each case; it should be remembered however that these systems are themselves subject to errors of uncertainty, reportedly in the order of 20 – 30 % in the case of the EC system (Glenn, et al., 2007).

In the approach taken in this study, model execution and validation is performed at the scale of an individual 1 x 1 km MODIS pixel at each site. It would similarly be possible to aggregate unlimited numbers of pixels in defining a study area, typically an entire catchment, treating each pixel either individually, a more time and resource-demanding approach, or averaging values over the entire user-defined area; by treating each pixel individually however, it is possible to more precisely define uncertainty in model inputs, and therefore results.

3.3 Study areas

Site selection was based on the availability of existing high quality ET_a data as measured using micrometeorological systems, generated independently by various researchers in earlier studies, allowing for objective evaluation of model performance in each case. Criteria considered in site selection in this study included continuity and duration of flux data

availability, and the requirement for flux footprint dimensions which at least partially correspond with MODIS pixel resolution (1 km^2). Obviously, validation data are also required to overlap temporally with the period of satellite data availability.

Ideally, for validation purposes, flux data should be continuous and representative of seasonal variation in flux densities at a particular site, and the site should, to the greatest extent possible, comprise homogeneous land cover/land-use and terrain within the collocated MODIS pixel footprint. In the first case, continuous data over long durations provide the opportunity to evaluate the performance of the model against a large number of data points, increasing confidence in statistical tests of accuracy. Seasonal representivity allows evaluation of model performance under variable environmental conditions in a given system, which may represent a divergence from certain assumptions implicit in the model (*i.e.* the FAO-56 vegetation parameter values for a reference surface), and present particular challenges in terms of pixel retrieval quality (*e.g.* high levels of atmospheric contamination/cloud cover at certain times of the year, or low levels of vegetation cover and LAI in dry periods which may exceed sensitivity thresholds of the MODIS instrument). In the second case, surface homogeneity within collocated test pixels eliminates the effect of "mixed pixels", where LAI retrievals may rather be based on a single spectrally dominant land cover within the pixel footprint, and which may not be representative of the flux footprint of the micrometeorological instrument used for validation. In addition to these selection criteria, automatic weather stations required to calculate ET_0 using the FAO-56 method, or in the absence of which, manual weather stations providing class A-pan data, required as a model input, should be available within reasonable proximity to the site.

Given the inherent difficulty of measuring fluxes over extended time periods using ground-based instrumentation (with the exception of permanent EC flux towers), and often high land-use/land cover heterogeneity in many areas, these criteria have been met in relatively few earlier studies in South Africa, and three sites were finally selected which fulfilled these requirements to the greatest extent possible. Validation data used in this study were derived from the following sources:

- the Southern African Regional Science Initiative (SAFARI 2000) (Scholes, *et al*., 2001; Privette, & Roy, 2005), a collaborative research initiative involving the ongoing observation of surface/atmosphere exchanges above a number of ecosystems in southern

Africa, and in particular a semi-arid savanna ecosystem near Skukuza, Kruger National Park; a permanent EC flux tower has been erected at this site, and has provided near-continuous water and CO_2 flux measurements for the *Combretum/Acacia* dominated system since April 2000. In addition, as part of a Water Research Commission (WRC) funded study into water use efficiency (WUE) of various natural ecosystems in South Africa, Dye, *et al.*, (2008) measured water fluxes using a LAS over three periods in 2005 at an adjacent location;

- an investigation into the suitability of a dual beam SLS for measuring grassland ET (Savage, *et al.*, 2004; Savage, *et al.*, 2010). These authors used an SLS, in combination with a portable Eddy Covariance and Bowen Ratio system, to estimate water fluxes at this mixed community grassland site near Ashburton, Pietermaritzburg (Bellevue) on a more or less continuous basis between January 2003-June 2005;

- as a continuation of the WRC study described above, Dye, *et al.*,(2008) used a LAS to estimate ET_a for a transect above a mixed evergreen indigenous forest (Groenkop) near George in the southern Cape over three periods in 2004.

Site locations and relevant specifications are provide in Figure 1 and Table 6, and described in further detail in the following section.

Figure 1: Study areas selected for model validation.

Table 4: Summary of data specifications and availability at validation sites.

Site	Site Coordinates	Vegetation Type	Validation ET_a Data Specifications (Micrometeorological Instruments)			
			Instrument	Instrument Altitude (m.a.s.l.)	Path Length (m) / Fetch (m^2)	Periods of Flux Measurement
Skukuza (Kruger National Park) Mpumalanga	25.01973 S 31.49688 E	Semi - arid savanna	Eddy covariance flux tower	365	600	Continuous
	25.07509 S 31.52915 E		Large aperture scintillometer	Transmitter: 369 Receiver: 393	4250	23rd Aug - 3rd Sep 2004; 31st Jan - 11th Feb 2005; 9th - 20th May 2005
Bellevue (Pietermaritzburg) KwaZulu-Natal	29.63480 S 30.43290 E	Mixed community grassland	Surface layer scintillometer (patched with EC and BR)	671	SLS path length: 101m; SLS Fetch (NW wind) transmitter:90m receiver: 138m EC fetch:135m	14th January 2003 - June 2005
Groenkop forest (George) Western Cape	33.94167 S 22.55000 E	Indigenous mixed evergreen forest	Large aperture scintillometer	Transmitter: 289 Receiver: 134	Path length: 3200	20 - 23rd Feb; 4 - 10 Jun; 28th Sep - 4th Oct 2004

		MODIS LAI Data Specifications			ET_0 Data Specifications		
Duration/No. Days Usable Data	**Reference**	**MODIS Tile**	**MODIS Pixel (Column/Row)**	**Successful Retrievals Available**	**Site Location**	**Altitude (m.a.s.l.)**	**Duration/No. Days Usable Data**
175 days total	SAFARI 2000	H20V11	1224/602	365 days in 2007 (46 retrievals, 46 using best possible solution)	Malekutu (FAO-56) 25.27893 S, 31.17804 E	538	353 days in 2007
22 Days total in 2005	Dye at al. (2008)		1229/609	365 days in 2005 (46 retrievals, 45 using best possible solution)			365 days in 2005
316 total in 2003	Savage *et al.* (2010)	H20V11	1098/1157	365 days in 2003 (46 retrievals, 45 using best possible solution)	Faulklands (A - pan) - 29.54999 S 30.53333 E; Bellevue (FAO-56) 29.63480 S 30.43290 E	740	A - pan: 365 in 2003; FAO-56: 231 in 2003
18 Days total in 2004	Dye *et al* (2008)	H19V12	1320/473	365 days in 2004 (46 retrievals, 15 using best possible solution)	Outeniqua (A - pan) - -33.91667 S, 22.41667 E; FAO-56 for dates & location corresponding with LAS data	361	A - pan: 365 days in 2004 FAO-56: 18 days in 2004

3.3.1 Semi-arid savanna (Skukuza)

Site description

Detailed surface/atmosphere flux measurements have been made at this site 13 km WSW of Skukuza (Figure 2) since April 2000 as part of the Southern Africa Regional Science Initiative (SAFARI 2000) (Scholes, *et al*., 2001). SAFARI 2000 is a collaboration between international and southern African researchers designed to identify and develop an understanding of coupled land/atmosphere processes in the region, particularly the effects of biogenic, pyrogenic, and anthropogenic emissions on the functioning of biogeohysical and biogeochemical systems (Swap, *et al*., 2002). As such, the site and programme activities have been comprehensively described in numerous earlier publications (Scholes, *et al*., 2001; Swap, *et al*., 2002; Privette & Roy, 2005).

Rainfall in the area is strongly seasonal (November and April), with long-term mean annual rainfall of 560 mm (Schulze,& Lynch, 2007). Centred on an EC flux tower (25.01973 S 31.49688 E) the site is located on a gentle slope at the ecotone between broad-leaved *Combretum apiculatum*-dominated savanna on the coarse sand ridge-top, and fine-leaved *Acacia nigrescens* savanna on sandy clay loam on the mid-slope (Scholes, *et al*., 2001). The ecotone comprises a 10 m wide band of sedges. The landscape is gently undulating, and soils are approximately 0.6 m deep. The woody basal area at the site is 6.8 m^2/ha, with a tree density of 128 ± 16 plants/ha and crown cover of 24 ± 4 %. Shrubs (woody plants taller than 0.5 m but less than 2.5 m) increase crown cover to 7.6 %. Basal area weighted mean height of trees is 9 m, with a maximum height of 13 m. Scholes, *et al.*, (2001) recorded 19 woody plant species, dominated by *Combretum apiculatum, Sclerocarya birrea* and *Acacia nigrescens.* The grass layer is dominated by *Panicum maximum*, *Digitaria eriantha, Eragrostis rigidor* and *Pogonarthria squarrosa* (Archibald, *et al*., 2009).

Instrumentation & data specifications

Validation data

Fluxes at the site are measured on a continuous basis by an EC flux tower (ET_{EC}) located at coordinates 25.01973 S 31.49688 E (Figure 2), oriented true north and at an altitude of 365 m.a.s.l. (Scholes, *et al*., 2001). The tower is instrumented with a sonic anemometer (WindMaster, Gill Instruments Ltd., Lymington, UK) measuring wind velocity in three dimensions and a closed-path infrared gas analyzer (LI-6262, LI-COR Inc., Lincoln, NE, USA) measuring water vapour and [CO_2] (Archibald, *et al*., 2009). Sensors are positioned at

a height of 17 m, and the footprint extends approximately 600 m upwind (Scholes, *et al*., 2001). ET_{EC} data used in this study were from 2007, for which 178 days clean data spanning both the wet and dry seasons were available. Three daily ET_{EC} values (days 88, 154 and 185) in the 2007 flux tower data were considered unrealistically high, and were subsequently rejected from the dataset, resulting in a total of 175 days data considered acceptable for model validation.

In a WRC funded study into the comparative water use efficiency of indigenous ecosystems versus commercial plantations, Dye *et al*., (2008) deployed a LAS a few kilometres from the flux tower site (Figure 2) over three periods spanning winter, summer and autumn in 2004 and 2005, and data (ET_{LAS}) were used as an additional, independent validation dataset in this study. The transmitter was located at latitude 25.0602 E, longitude 31.5157 S, and the receiver at latitude 25.0915 E, longitude 31.5431 S, with the beam aligned in a NNW/SSE direction, and a path length of 4.25 km. ET_{LAS} data were available for seven days in August 2004 (days of year 239 - 245), seven days in February 2005 (days of year 33 - 39), and eight days in May 2005 (days of year 131-138).

Micrometeorological data

Daily micrometeorological data required to calculate ET_0 (FAO-56 method) were obtained for years 2005 and 2007 from an automatic weather station (ARC-ISWC) located approximately 42 kilometres SW of the validation sites (Malekutu 25.27893 E, 31.17804 S: altitude 538 m.a.s.l) (Fig. 2). 353 days of ET_0 data were available from this station in 2007, and for all dates corresponding with the ET_{LAS} data in 2005; no ET_0 data were available in 2004, however.

MODIS LAI data

The standard eight day Terra MOD15A2 LAI/FPAR product (Collection 5) was acquired from the LP DAAC National Centre, EROS, Sioux Falls, South Dakota, USA, for the Mpumalanga area (MODIS tile H20V11) for the period 26 February 2000-31 December 2009. Images were converted from HDF-EOS to GeoTIFF format for use in Idrisi image processing software, and reprojected from Sinusoidal to Geographic WGS'84 using the HEG tool. LAI values were extracted from MODIS pixels corresponding with the both the EC flux tower position (column 1224 / row 602) and the beam path of the LAS (column 1229 / row 609) (Figure 2). This provided a database of nearly 10 years of continuous LAI data, assumed

representative of the phenological variability in leaf area which could be expected at each site. 365 days of MOD15A2 LAI data (46 8-day composited datasets) were available in both 2005 and 2007. The FparLai_QC layer delivered with the LAI product was interrogated using the LDOPE tool to determine retrieval quality at these pixels for the years corresponding with the validation period in each case.

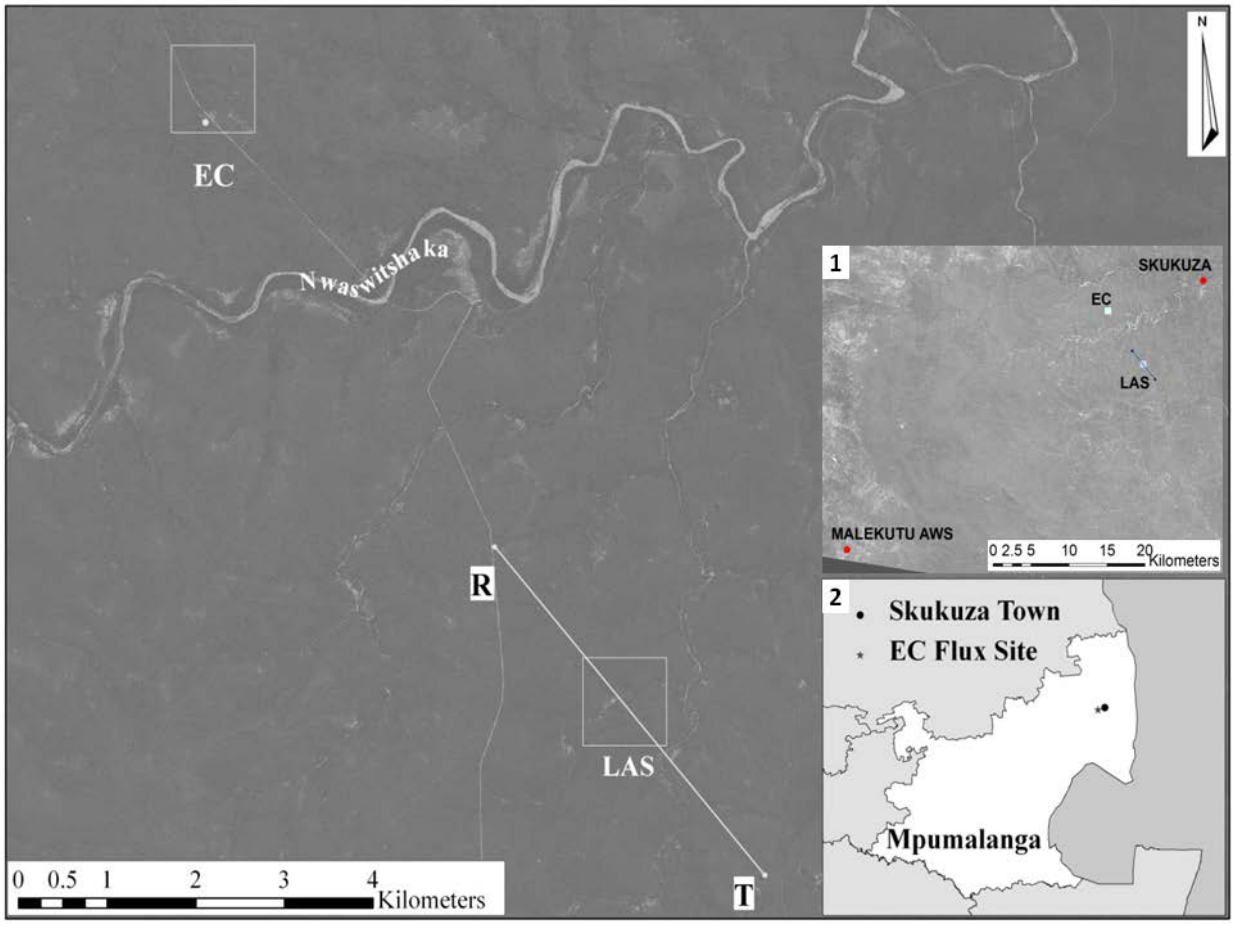

Figure 2: Location of EC flux tower and LAS at the Skukuza site, showing beam path of the LAS instrument (R = receiver and T = transmitter); respective MODIS validation pixel locations are illustrated in white outline. The location of the Malekutu automatic weather station (AWS) with respect to the validation sites is indicated in inset 1; location of the sites in relation to the Mpumalanga Province and the town of Skukuza is indicated in inset 2.

3.3.2 Mixed community grassland, Bellevue (Pietermaritzburg)

Site description

This site, located near Ashburton, Pietermaritzburg, at coordinates 29.6348 S, 30.4329 E (Figure 3) was used by Savage, *et al.*, (2004; 2010) to establish the suitability of an SLS

instrument to determine *H* between the periods January 2003 - June 2005, and is described in some detail by these authors. It comprises an open and mixed grassland community, dominated by *Diheteropogon amplectens*, *Themeda triandra*, *Tristachya leucothrix* and *Cymbopogonexcavatus*, at an altitude of 671 m above sea level (Savage, *et al*., 2010). The area experiences summer rainfall, with a long-term (58 years) mean annual rainfall of 724 mm (Schulze & Lynch, 2007). The site has an average gradient of 1° 15', sloping to the SE. Soils are derived from Dwyka Tillite, with a soil profile consisting of a loam A horizon (0 - 0.3 m) overlying clay B1 and B2 horizons extending to 1 m. Fetch distances in the prevailing SE wind direction were 90 and 138 m for the SLS transmitter and receiver respectively. Fetches in the next most dominant NW wind direction were 146 and 114 m respectively. Beyond these distances and to the south, the site is exposed and there is a substantial increase in slope, while the area to the north and west consists of residential housing and tall trees. With the exception of the latter, the site is surrounded by natural grassland and occasional trees.

Data specifications

Validation data

A commercially available dual beam SLS (model SLS40-A, Scintec Atmospärenmessetechnik, Tübingen, Germany) was used, with a beam path length of initially 50, then 101m (Savage, *et al*., 2010). The beam heights were set at 1 and 1.6 m, and fetch distances in prevailing wind directions as indicated above. The beam path was oriented in a NW/SE direction, aligned with prevailing winds (Figure 3). Further technical specifications are provided by Savage, *et al*., (2004; 2010). A portable EC and BR system were deployed simultaneously to allow comparison of results between the three instruments, and used to patch missing or unreliable SLS data where necessary (hereinafter notated ET_{ave}); meteorological data were recorded by an automatic weather station deployed at the site, permitting calculation of ET_0. A total of 316 days ET_{ave} data were acquired in the year 2003.

Micrometeorological data

Weather data required to calculate daily ET_0 by the FAO-56 method were recorded by an automatic weather station deployed at the site by Savage, *et al*., (2004), however, several substantial gaps occurred in these data in 2003, and only 231 days of usable data were acquired. Class A evaporation pan data from a manual weather station (ARC-ISCW) located approximately 13.3 kms to the NE of the site (Faulklands, 29.54999 S, 30.53333 E; altitude

740 m.a.s.l.) were therefore acquired to allow patching of the FAO-56 data where necessary (Fig. 3).

MODIS LAI data

The same process as described earlier was followed in acquiring and converting the MOD15A2 Collection 5 data, and in the interrogation of uncertainty information, for the Bellevue site. LAI values were extracted for the MODIS pixel approximately corresponding with the position of the SLS beam path (MODIS tile H20V11, column1098 / row 1157) (Figure 3) for the period 26 February 2000-31 December 2009 to determine annual phenological variability in LAI at the site. 365 days of LAI data (or 46 8-day composited datasets) were successfully retrieved in 2003.

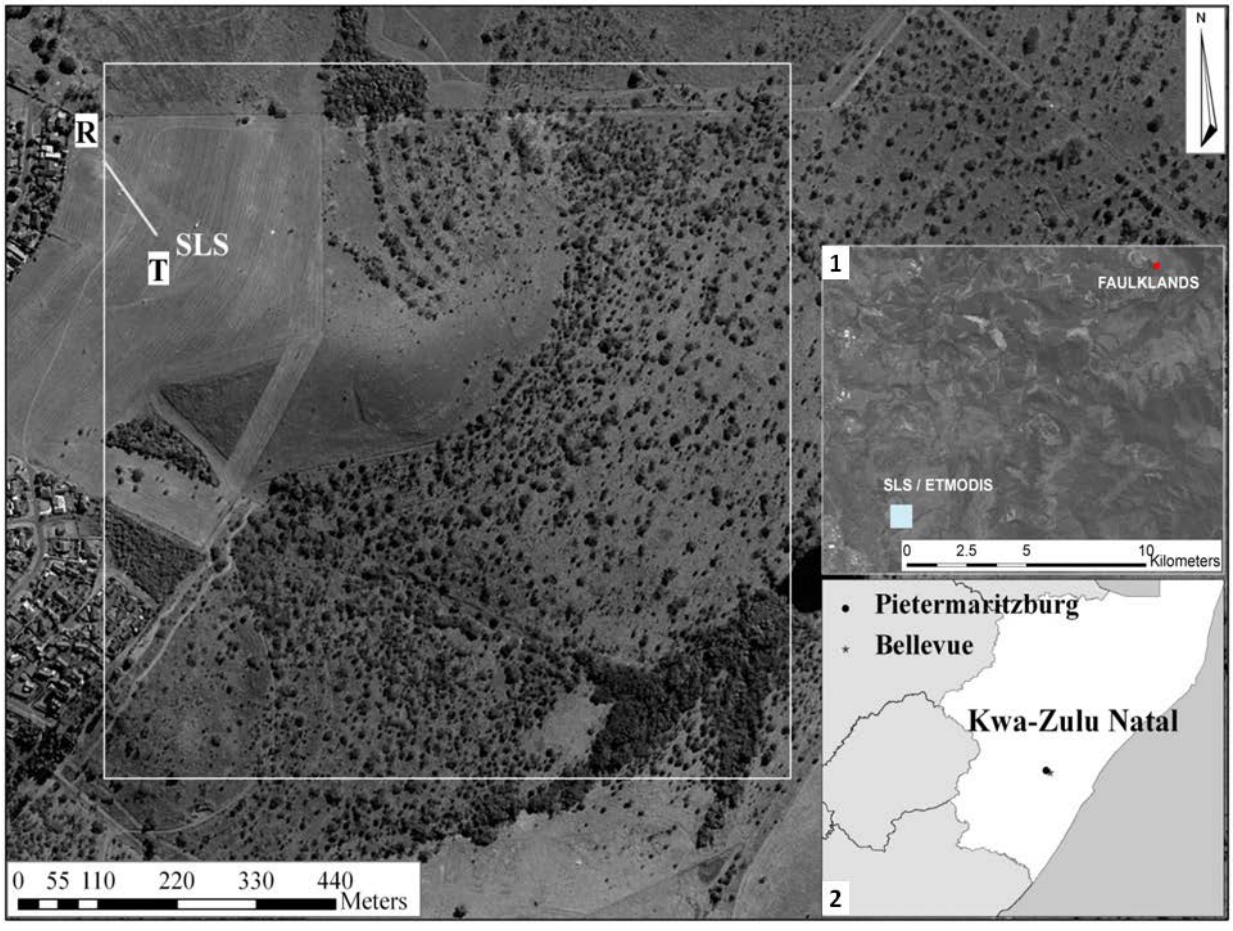

Figure 3: Location of SLS at Bellevue near Pietermaritzburg (R = receiver and T = transmitter) (beam path position is approximate), and corresponding MODIS pixel in white outline. Location of the site with respect to the Faulklands manual weather station is

indicated in inset 1; site position in relation to Pietermaritzburg and KwaZulu-Natal Province is indicated in inset 2.

3.3.3 Groenkop mixed indigenous forest (George)

Site description

This site in the Groenkop Forest, located near the town of George (Figure 4), is a research station, and has been comprehensively described in a number of publications (Geldenhuys, 1982; Geldenhuys, 1998; Van der Merwe, 1999; Dye, *et al*., 2008). It comprises an approximately 40 ha block (coordinates 33.94167 S, 22.55000 E) bordering the northeast corner of the Saasveld campus of the Nelson Mandela Metropolitan University, and lies at altitudes between 190 - 300 m.a.s.l. (Geldenhuys, 1998). The area experiences rainfall throughout the year, although most occurs during autumn (March) and early summer (October/November), with a mean annual rainfall of 860 mm. It is underlain predominantly by Table Mountain Sandstones, commonly including bands of conglomerate and shale (Dye, *et al*., 2008). Mean minimum temperature varies between 19.7 °C in February to 8.9 °C in August.

The forest lies at the western limit of the Coastal Platform Forests (Geldenhuys, 1993), a belt of mixed evergreen forests on the southern Cape coastal platform within the Southern Cape Afro-temperate Forest (von Maltitz, *et al*., 2003). It is extensive and relatively flat, with a canopy height estimated at 24 m (Dye, *et al*., 2008). The forest appears to be in equilibrium, with high standing biomass and low mean annual volume increment. The canopy is not completely closed, and numerous gaps occur which permit the infiltration of sunlight to the understory. Dye, *et al*., (2008) estimate a LAI of two for the canopy, and two for the understory. Stem size distribution indicates a pronounced inverse J-shaped skew, having many smaller trees suppressed by a fewer larger individuals accessing the majority of resources. Geldenhuys,(1993) classify the forest as typically *Podocarpus latifolius - Curtisia dentata - Burchellia bubalina* platform forest.

The northern areas immediately below the foothill zone are dominated by multi-stemmed *Platylophus trifoliatus*, scattered *Ocotea bullata* and *Ilex mitis*, associated with the main species of the platform forest (Dye, *et al*., 2008). There is no shrub layer present but a dense layer of *Rumohra adiantiformis* occurs. Topsoil is fine textured and 250 mm in depth, overlying a leached horizon of 200 mm over a deep ferri-humic horizon. In the southern reaches, the forest grades to typical coastal platform forest dominated by *Olea capensis*

subsp. *macrocarpa*, *Podocarpus latifolius* and *Pterocelastrus tricuspidatus* as canopy dominants amongst a range of other species. A shrub layer is present here, comprised of *Trichocladus crinitus* of varying heights. Topsoil, 350-450 mm deep, overlies poorly drained clayey subsoil, and fluctuations in the water table are in evidence on level terrain and well drained subsoil on the slopes (Dye, *et al*., 2008).

Instrumentation & data specifications

Validation data

Dye, *et al.*,(2008) used a LAS to measure *H* along a 3.2 km beam path at the site over three periods in summer, winter and spring in 2004, for which a total of 18 days data was obtained. The description of instrument set-up provided here is taken from their report, which provides more technical details if required.

The transmitter was erected near the upper edge of the forest at coordinates, 33.93781 S, 22.55600 E, and the receiver at the lower edge, at coordinates 33.95497 S, 22.52941 E, with the beam aligned in a SW/NE orientation. The mean height of the beam of the canopy was calculated to be 36.34 m. Except for ± 100 m on either side of the beam path, the vegetation was entirely closed canopy indigenous evergreen forest, and the section near the centre of the beam, at which it is most sensitive to fluctuations, comprised the gently sloping research site. The beam crossed the Kaaiman's River gorge at its SW extreme, although Dye, *et al.*, (2008) considered the effects on flux estimates negligible, because the instrument is known to not be particularly sensitive to fluctuations in these regions of the beam. ET_{LAS} data were available for four days in February 2004 (days of year 51-54), seven days in June 2004 (days of year 156-162), and seven days in September/October 2004 (days of year 272-278).

Micrometeorological data

No automatic weather stations operational at time periods corresponding with LAS data availability were found to exist within reasonable proximity to the Groenkop site, and it was necessary to use class A-pan data as a substitute for the FAO-56 in modelling annual ET for 2004; data for this purpose were obtained from a manual weather station (ARC-ISCW) located approximately 12.5 kms WNW of the site (Outeniqua 33.9167 S, 22.4167 E; altitude 361 m.a.s.l.) (Fig. 4). The FAO-56 was, however, calculated by Dye *et al.* (2008) for the 18 days corresponding with LAS measurements at the site, and these were used as model inputs when evaluating model performance against the LAS.

MODIS LAI data

MOD15A2 data was acquired from the LP DAAC for the period 26 February 2000-31 December 2009 for the Western Cape region (MODIS tile H19V12). Data were converted from HDF-EOS to GeoTiff format and reprojected using the HEG tool, by the same procedure applied to the Skukuza and Bellevue data. A single MODIS pixel was selected corresponding with the location of the LAS beam path, and avoiding the Kaaiman's River gorge (column 1320 / row 473) (Figure 4), from which LAI values for the ± 10-year period were extracted to derive information on phenological leaf area variability in the forest. 366 days of LAI data were available in 2004.

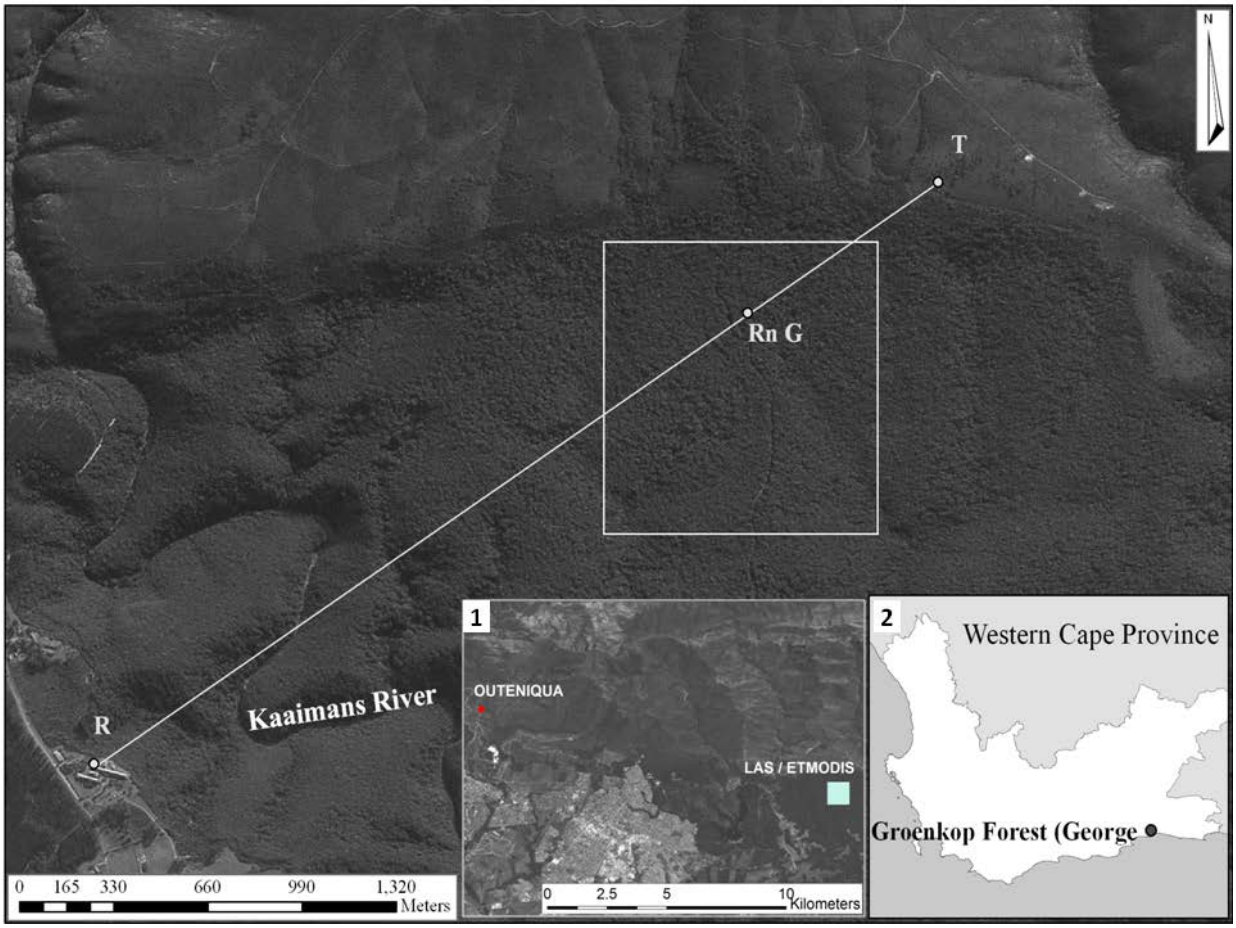

Figure 4: Location of LAS at Groenkop Forest near George (R = receiver and T = transmitter, *Rn* and *G* indicate positions of net radiation and soil heat flux measurements respectively), and corresponding MODIS pixel in white outline. Location of Outeniqua manual weather station with respect to the validation site is indicated in inset 1; site location in relation to the Western Cape Province is indicated in inset 2.

4. Results

4.1 Introduction

Results are presented separately for each of the study sites (and in the case of Skukuza, separately in respect of the EC and LAS sites), and reported in terms of the following:

- Frequency distribution of MOD15A2 LAI values retrieved since launch (approximately 10 years, from February 2000 to December 2009) for the MODIS pixel corresponding with the geolocation of the validation site;

- Seasonal variation, including means and standard deviation, in remotely sensed LAI for the equivalent time period at the validation pixel;

- 8-day MOD15A2 LAI values, and retrieval quality, at the validation pixel for the year in which ET_{MODIS} is applied at each site;

- Modelled evapotranspiration data, in relation to measured evapotranspiration (*i.e.* using micrometeorological systems) and ET_0 (FAO-56/class A-pan) values, for the year in which validation is performed;

- Model performance, evaluated by fitting a linear regression model to modelled and measured evapotranspiration data to determine coefficients of determination (r^2 values).

4.2 Semi-arid savanna (Skukuza)

4.2.1 ET_{MODIS} vs. ET_{EC}

The frequency distribution of LAI values retrieved at the EC Flux Tower site over the period from 25 February 2000 to 31 December 2009 (a total of 439 retrievals) demonstrates that values were positively skewed, with most retrievals in the range of 0.3 to 1 (Figure 5A). The maximum value observed over the ± 10-year period was 3.1, retrieved over days 337-344 in 2004, with a minimum of 0.1 retrieved over days 249-256 in 2001.

Means and standard deviation in annual LAI retrieved over the nearly 10-year period are provided in Figure 5B. These data indicate marked seasonal variation in annual LAI in this semi-arid savanna system, with an amplitude (peak to trough difference) of 113 % (LAI = 1.12) of the mean annual LAI for the 10 year period (0.99). Greatest inter-annual variation in MOD15A2 LAI values is evident in the wet season (November to April), with relatively smaller variation in the dry season.

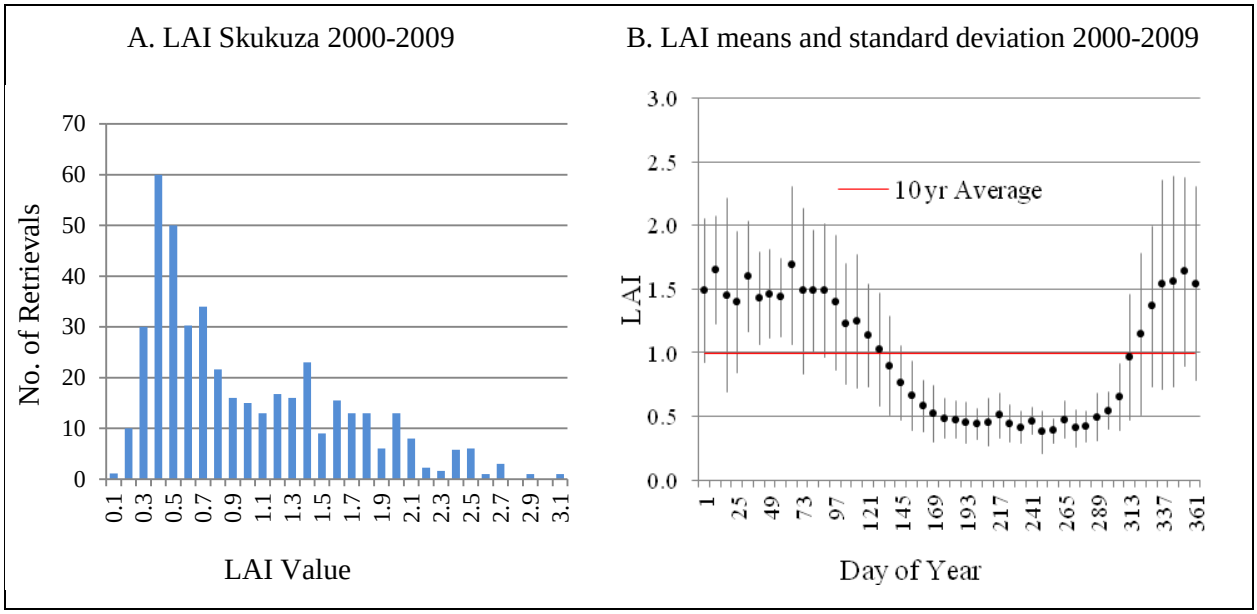

Figure 5: Frequency distribution in MODIS LAI values (A), and means and standard deviation (B) retrieved at the EC flux tower site near Skukuza over the period 25 February 2000 to 31 December 2009.

MODIS LAI retrievals for the year 2007 at the flux tower site are provided (Figure 6), including retrieval quality information extracted from bits 5-7 of the FparLai_QC SDS. Bits 5-7 provide a per pixel five level confidence score of retrieval quality, as described in Chapter 2.7.1 (Table 3). All 46 8-day composites in 2007 at the site were produced using best possible quality retrievals, performed using the radiative transfer (RT) approach without saturation (FparLai_QC bits 5-7 = 0). Maximum LAI in 2007 was 2.2, retrieved over days 361-365 using the RT approach (Figure 6).

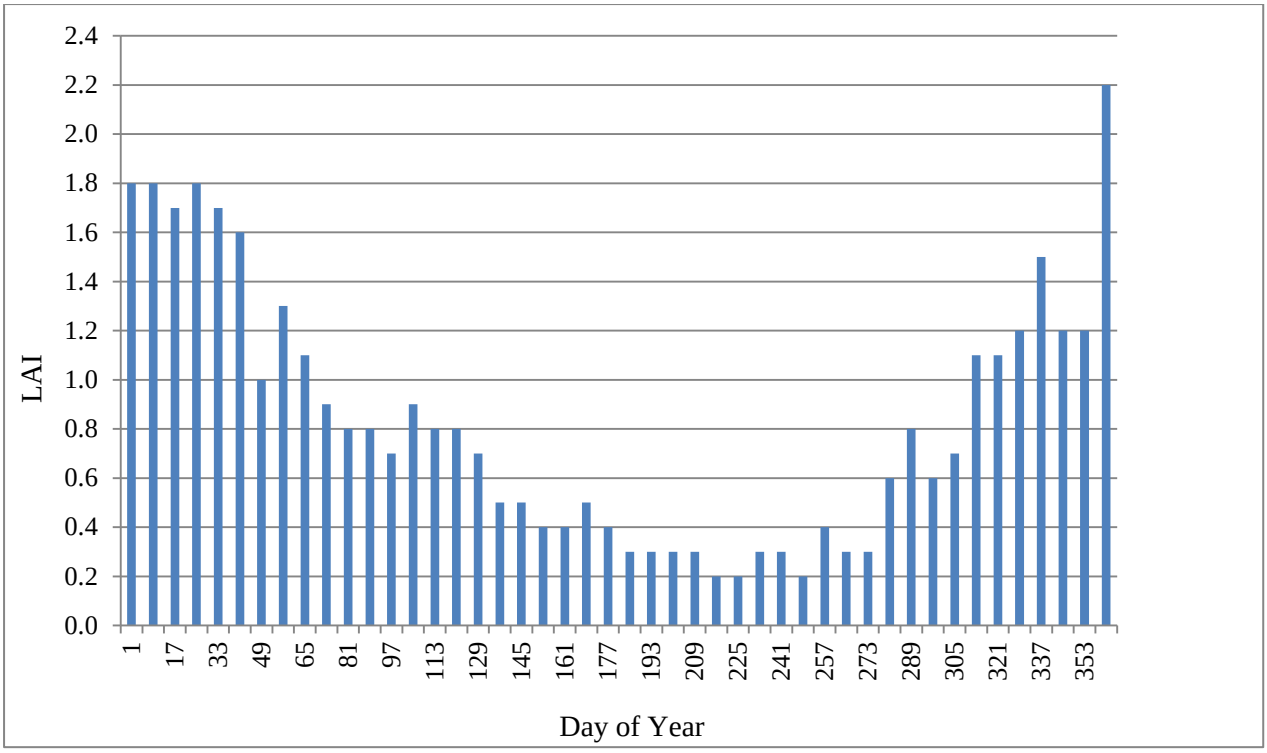

Figure 6: MODIS LAI retrieved at the Skukuza flux tower site in 2007; all retrievals were performed using the main RT algorithm.

Daily ET for the 353 days for which ET_0 data was available in 2007 was modelled by applying ET_{MODIS} (Equation 20), parameterized using long-term MOD15A2 LAI_{max} (LAI_{max} = 3.1), 8-day MOD15A2 LAI, and daily ET_0 (FAO-56; Malekutu weather station) (Figure 7). By this approach, a total of 408.4 mm ET_a was predicted over 353 days in 2007, relative to total ET_0 of 1420.5 mm for the same period, and rainfall of 530.8 mm for 350 days for which rain data was available in 2007. ET_{EC} is plotted here for comparative purposes.

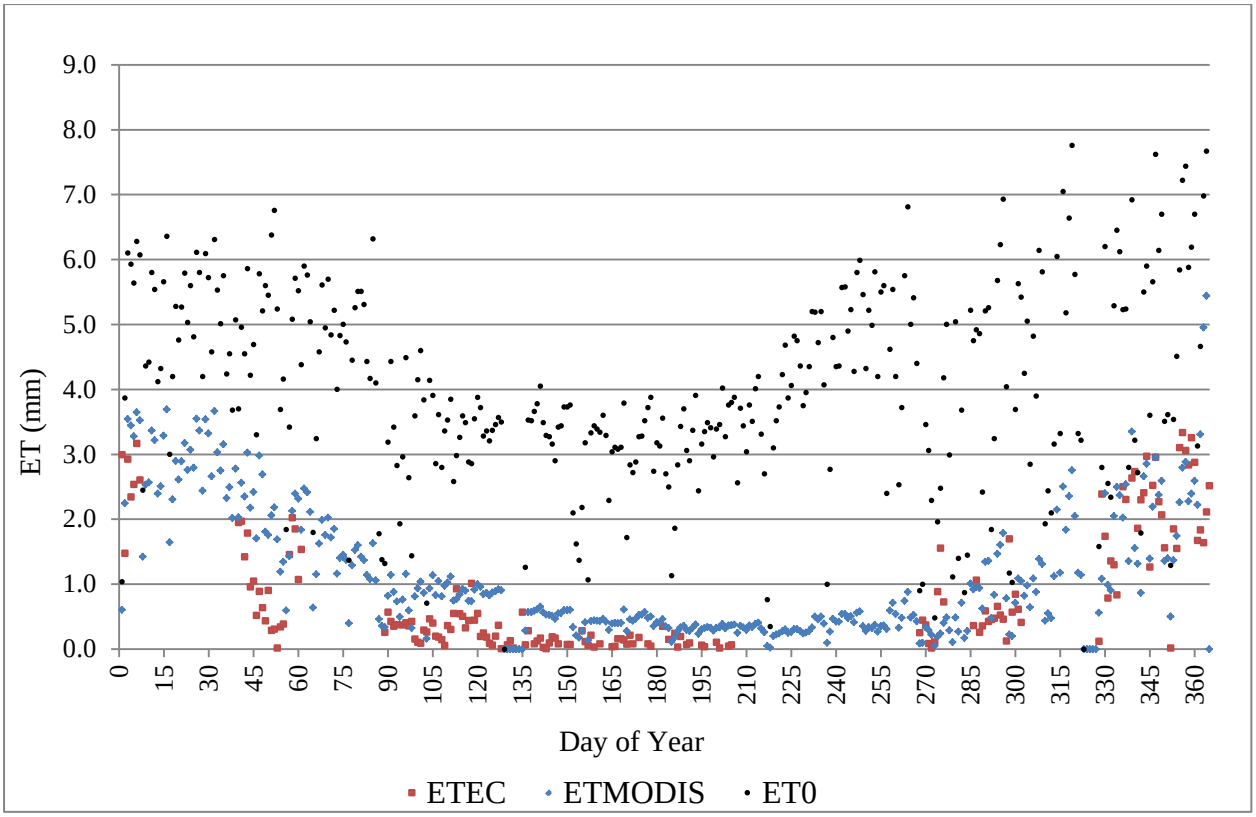

Figure 7: Modelled ET (ET_{MODIS}) vs. ET_0 (FAO-56; Malekutu), ET_{EC} over 365 days in 2007, Skukuza flux tower site.

A comparison of accumulated ET_{MODIS} and ET_{EC} was performed for periods where both modelled and measured data were available, comprising a total of 170 days spanning both summer and winter in 2007 (Figure 8). ET_{MODIS} predicted a total of 194.8 mm over this period, while ET_{EC} totalled 147.9 mm, and represents an overestimation of 31.7 % in modelled ET relative to measured ET. Visually, modelled and measured values clearly demonstrate better agreement during the summer growing season relative to the dry winter period.

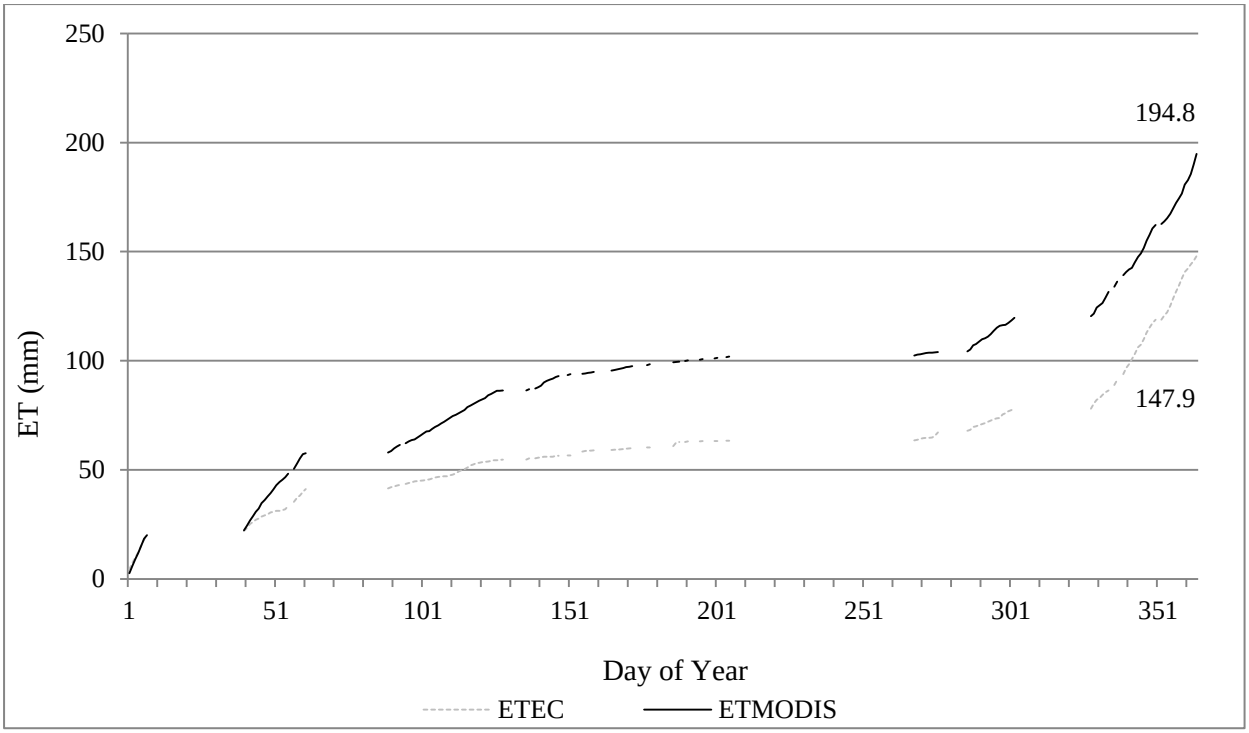

Figure 8: Accumulated ET_{MODIS} vs. ET_{EC} at the flux tower site for 170 days of corresponding data in 2007 (LAI max = 3.1).

The relationship between ET_{MODIS} and ET_{EC} was evaluated by fitting a linear regression model for the 170 days in 2007, where slope (y value) < 1, indicating that ET_{MODIS} over-predicts evapotranspiration when ET_{EC} values are low, and under-predicts evapotranspiration when ET_{EC} values are high; linear regression returned a coefficient of determination (r^2) value of 0.67 (Figure 9).

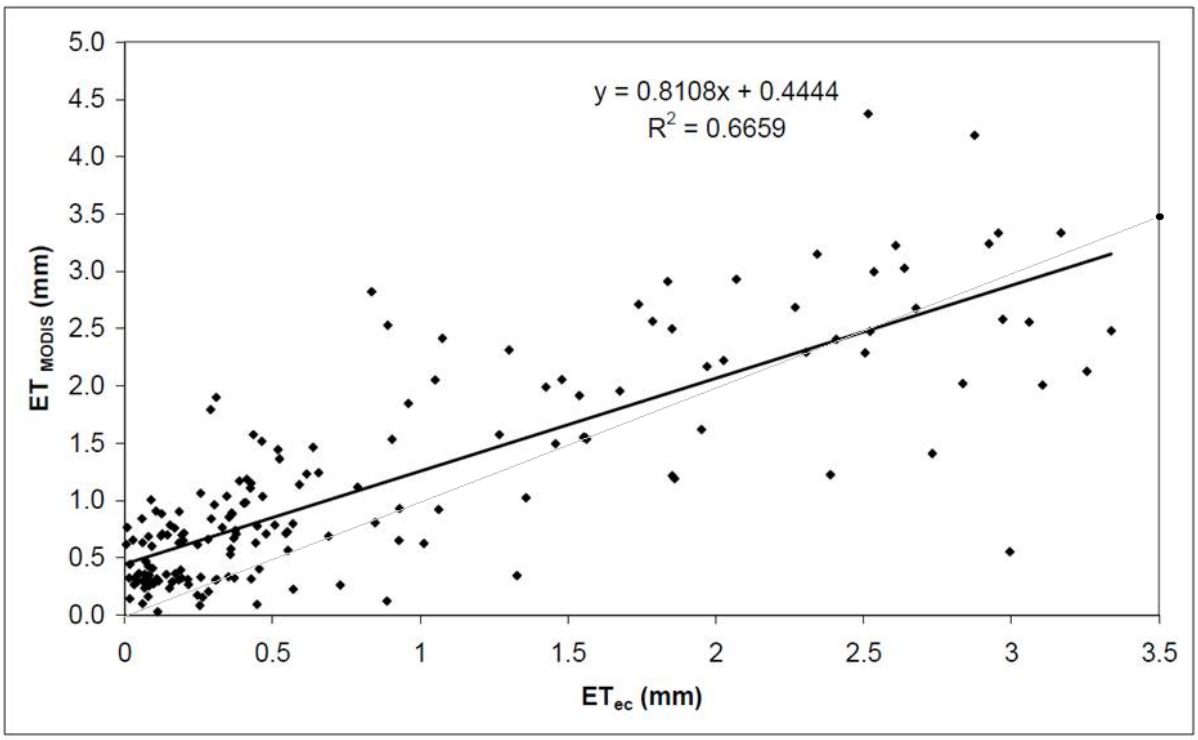

Figure 9: Linear regression model of the relationship between ET_{MODIS} and ET_{EC} over 170 days of corresponding data in 2007, Skukuza; 1:1 line shown in grey.

4.2.2 ET_{MODIS} vs. ET_{LAS}

Frequency distribution in LAI retrieved at the LAS site for the period of MODIS data availability (25 February 2000-31 December 2009), comprising a total of 439 MODIS retrievals, is provided (Figure 10A). The maximum value observed over the ± 10-year period was 2.9, retrieved over days 337-344 in 2004, with a minimum of 0.1 retrieved over days 329-336 in 2001, 353-360 in 2003, and 249-256 in 2005 (Figure 10A). A predominance of retrievals in the range of ~ 0.3-0.8 LAI were returned at this site over the period of observation.

Means and standard deviation in annual LAI retrieved over the nearly 10 year period are provided (Figure 10B). There is a marked similarity in these indices as compared with observations at the flux tower site, with most inter-annual variation occurring in the wet season (November; April), with relatively less in the dry season. Similarly, seasonal variation in annual LAI compares with that at the flux tower location, with an amplitude of 113 % (1.16 LAI) of the mean annual LAI for the 10 year period (1.02). Again, an analysis of these results must consider the margin of remote observation error (0.66 LAI).

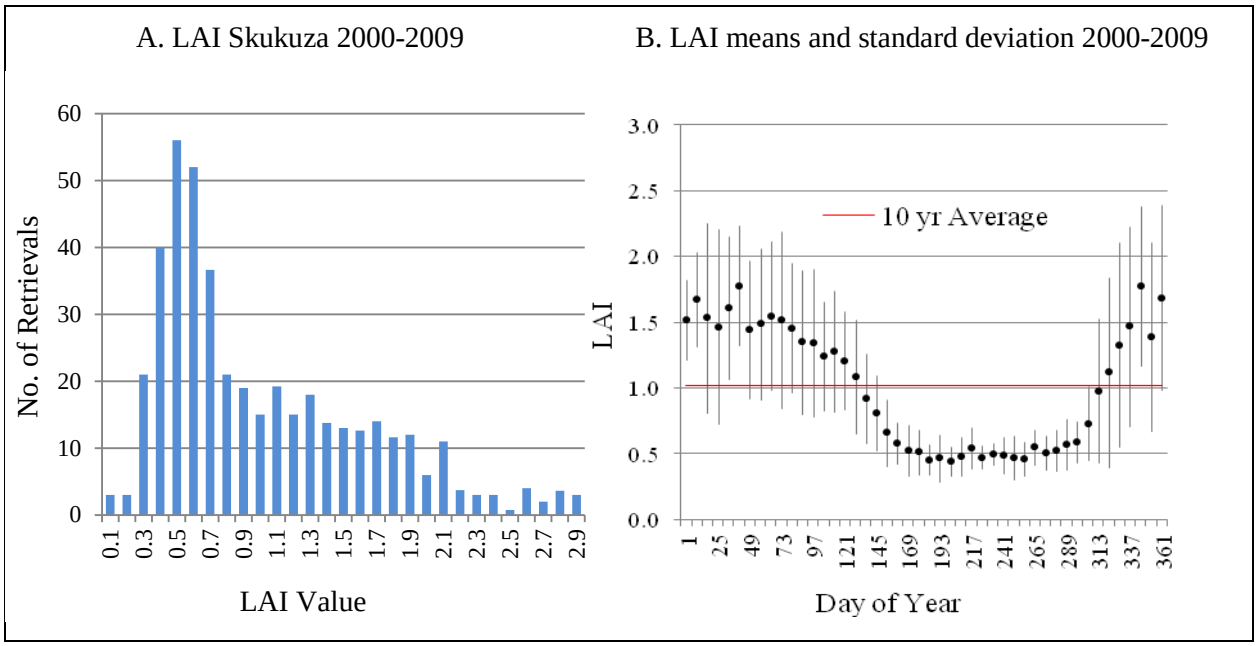

Figure 10: A) Histogram of the frequency distribution in MODIS LAI values, and B) means and standard deviation retrieved at the LAS site near Skukuza over the period 25 February 2000 to 31 December 2009.

LAI retrievals for the year 2005 at the LAS site are provided (Figure 11), including retrieval quality information extracted from bits 5-7 of the FparLai_QC SDS (see Table 3, Chapter 2.7.1 for a description of the FparLai_QC SDS and associated bit fields). With the exception of one 8-day composite spanning days 361-365), all retrievals were performed using the main RT approach without saturation (FparLai_QC bits 5-7 = 0). The empirical backup algorithm was invoked over days 361-365 as a result of RT algorithm failure due to reasons other than view/illumination geometry (FparLai_QC bits 5-7 = 3). Maximum LAI observed in 2005 was 1.9, retrieved over days 33-48 and 345-353, using the main approach without saturation.

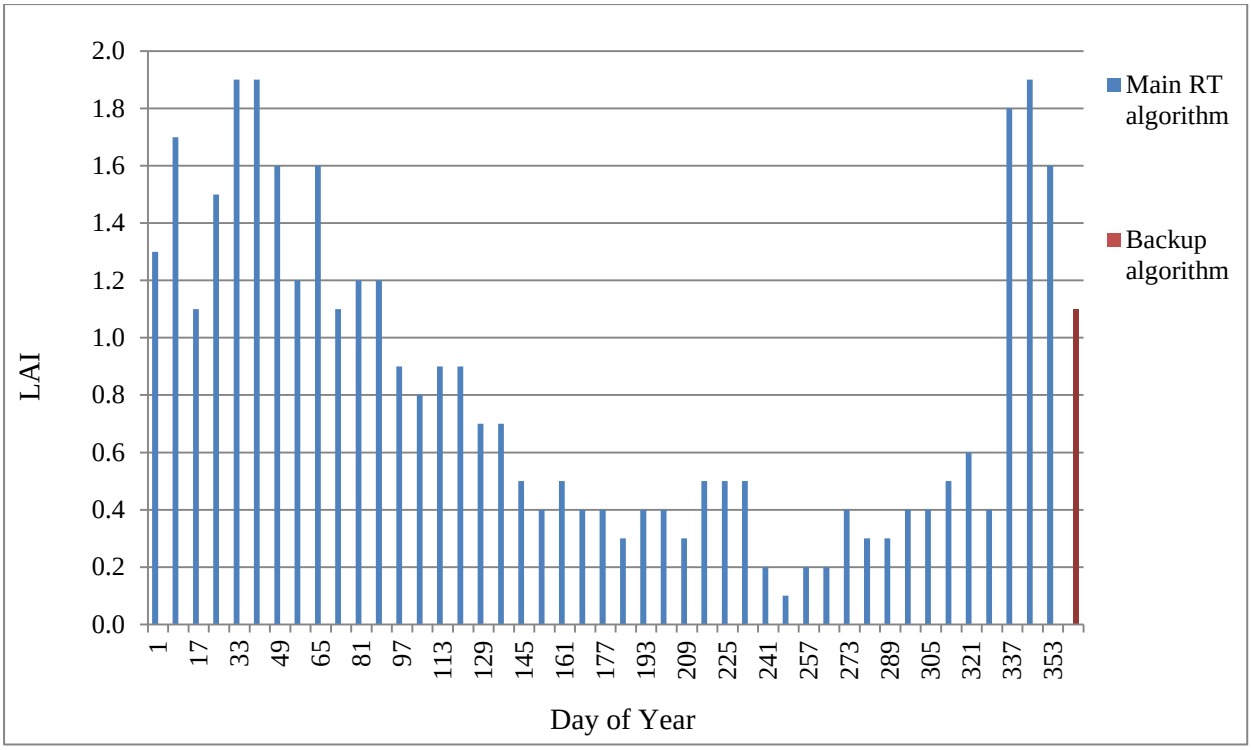

Figure 11: Composited LAI at the Skukuza LAS site in 2005, indicating LAI values retrieved by methods other than the main RT approach (without saturation).

Daily ET for 365 days in 2005 was modelled by applying ET_{MODIS} (Equation 20), parameterized using long-term MOD15A2 LAI_{max} (LAI_{max} = 2.9), 8-day MOD15A2 LAI, and daily ET_0 (FAO-56; Malekutu weather station) (Figure 12). Using this approach, a total of 435.2mm ET was predicted in 2005, relative to a total ET_0 of 1451.7 mm, and rainfall of 229.0 mm. ET_{LAS} is plotted here to provide comparison.

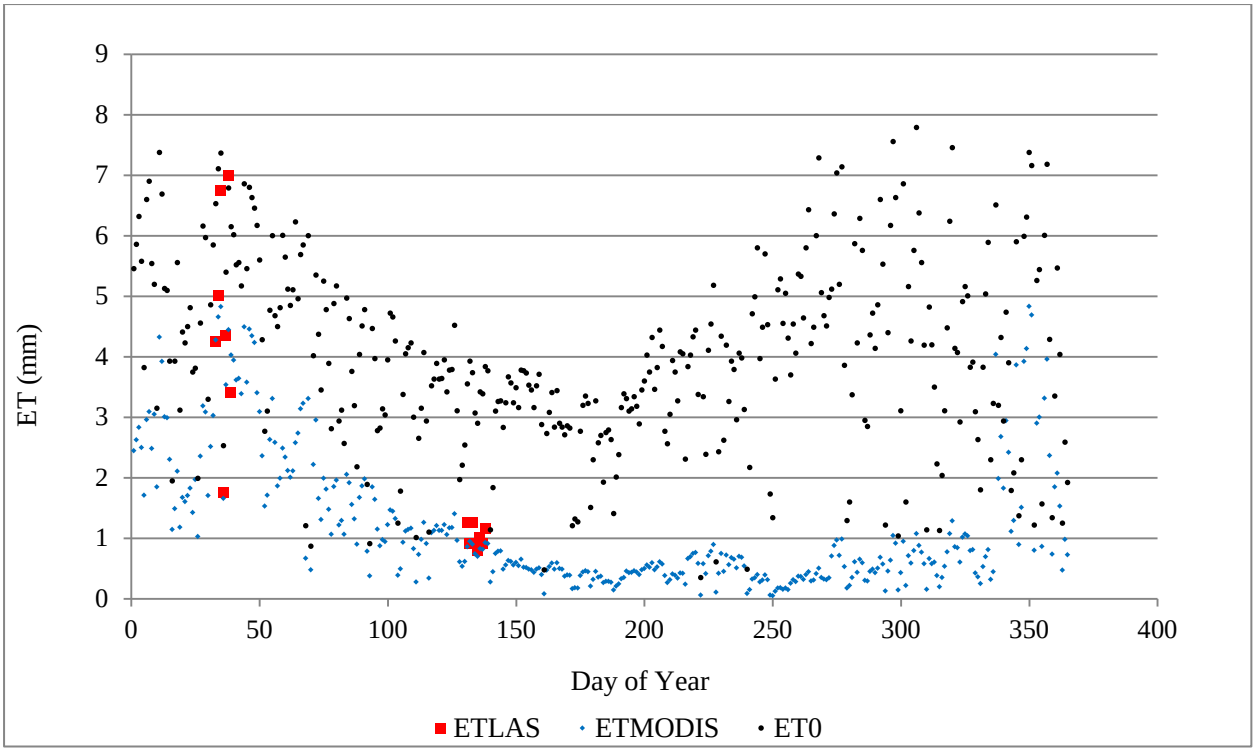

Figure 12: ET_{MODIS} vs. ET_0 (FAO-56; Malekutu), ET_{LAS} (15 days) over 365 days in 2005, Skukuza.

The absence of ET_0 data from any automatic weather station in the Skukuza area for days corresponding with the 2004 ET_{LAS} measurements meant that ET_{MODIS} could only be validated using the 2005 ET_{LAS} datasets. This comprised two periods of 7 days in summer (2^{nd}-8^{th} February), and 8 days in autumn (11^{th}-18^{th} May). Modelled ET is plotted against ET_{LAS} and ET_0 for the periods of data availability (Figures 13A &14A), and linear regression models provided (Figures 13B & 14B).

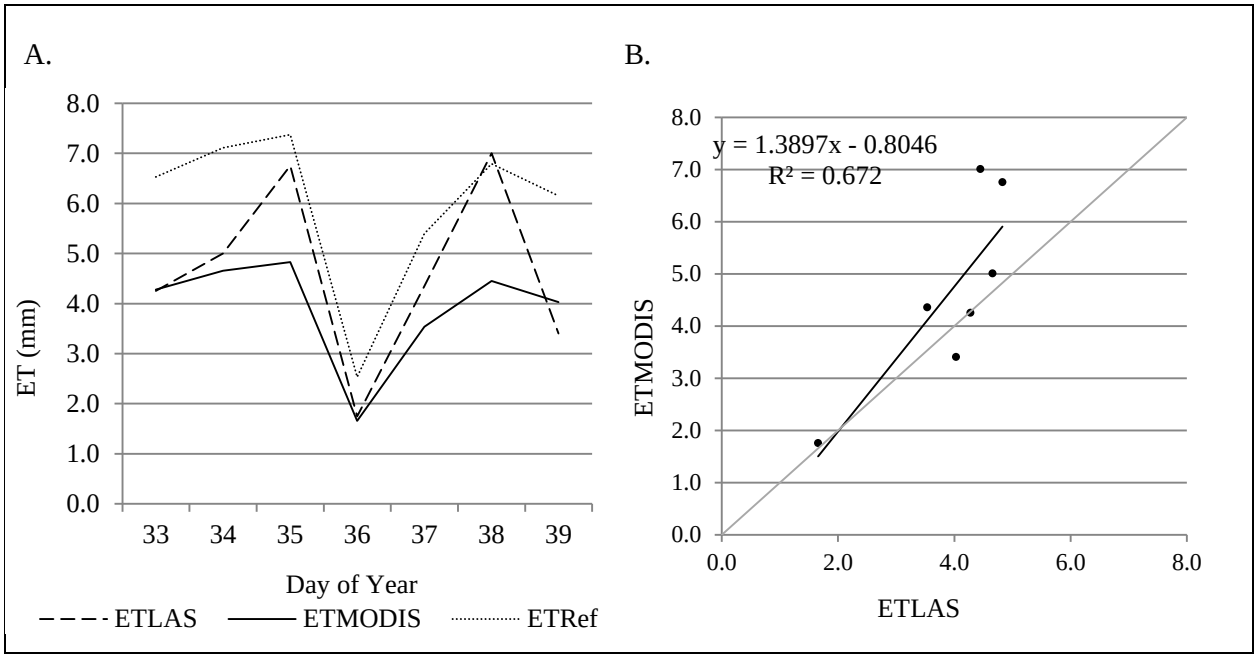

Figure 13: A) ET_{MODIS} vs. ET_{LAS} over a seven day period at Skukuza in February 2005, and B) linear regression model, showing 1:1 line.

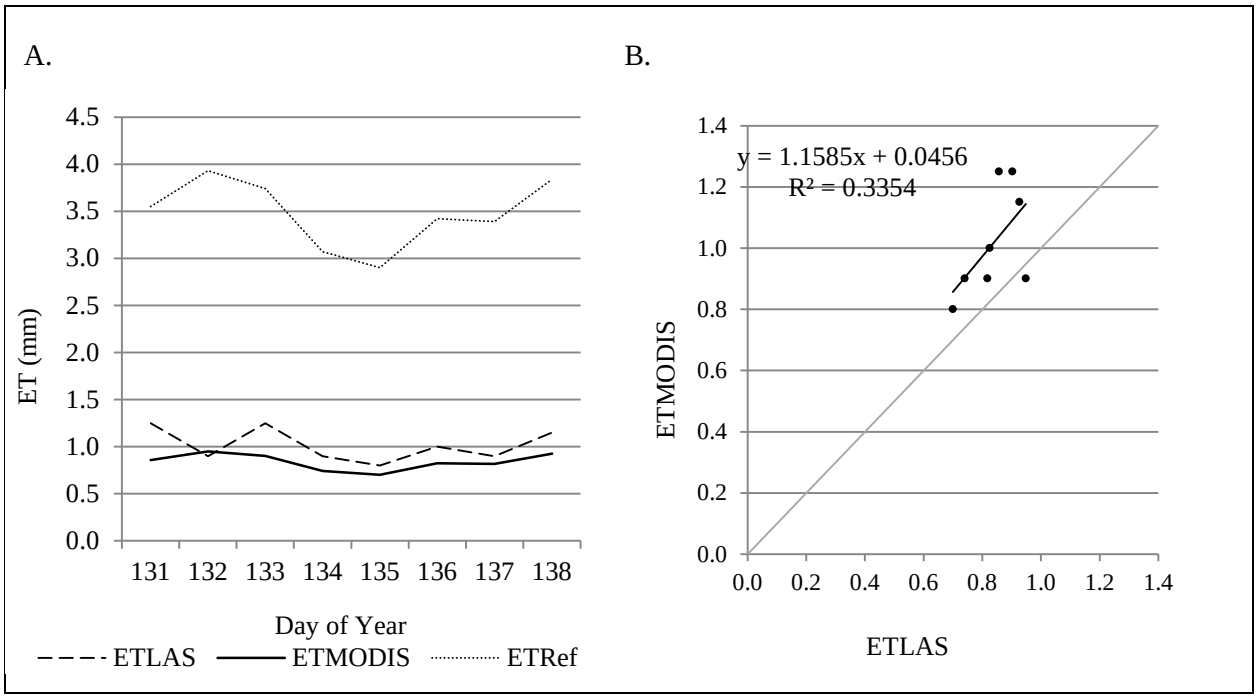

Figure 14: A) ETMODIS vs. ETLAS over a seven day period at Skukuza in May 2005, and B) linear regression model, showing 1:1 line.

ET_{MODIS} predicted a total of 27.4 mm ET for the seven days in February, relative to 32.5 mm ET_{LAS}, and 6.7 mm for the eight days in May, relative to 8.2 mm ET_{LAS}, representing an underestimation by ET_{MODIS} relative to ET_{LAS} in each instance of 15.7 % and 18.3% respectively. Given the relative sparseness of data points available for model validation, no comparison of annual accumulated ET was performed in this instance.

4.3 Mixed community grassland, Bellevue (Pietermaritzburg)

Frequency distribution in LAI retrieved at the Bellevue site for the period of data availability (25 February 2000-31 December 2009), comprising a total of 439 retrievals is provided in Figure 15A. The maximum LAI value observed over the ± 10 year period was 2.2, retrieved over days 33-40 in 2006, with a minimum of 0.1 retrieved on a number of occasions over the almost 10 year observation period. From this figure, it is evident that a large majority of retrievals were 0.3 LAI, although the reason for this abnormal distribution in values is not immediately clear.

Means and standard deviation in annual LAI retrieved over the nearly 10 year period are provided (Figure 15B). Most inter-annual variation in LAI is evident in the wet season, with relatively less occurring in the dry season. Seasonality is less pronounced than in the semi-arid savanna, with an amplitude of 92 % (0.78 LAI) of the mean annual LAI for the 10-year period (0.86).

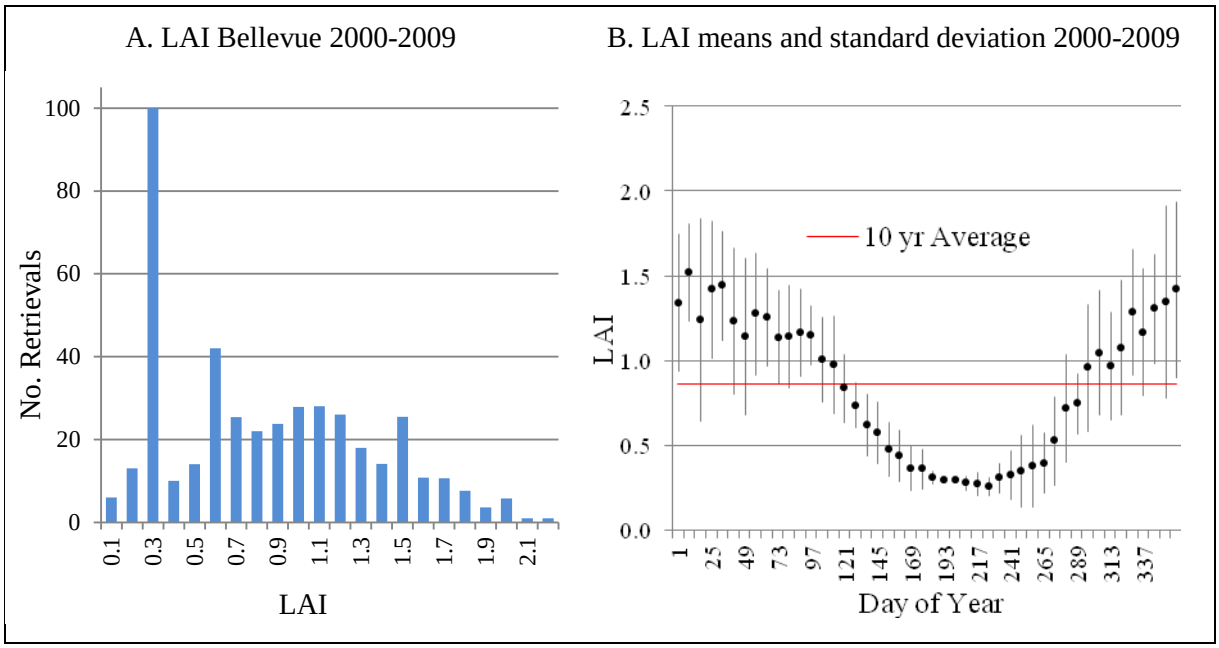

Figure 15: A) Histogram of the frequency distribution in MODIS LAI values, and B) means and standard deviation retrieved at the Bellevue site over the period 25 February 2000 to 31 December 2009.

LAI retrievals for the year 2004 at the Bellevue site are provided (Figure 16), including retrieval quality information derived from bits 5-7 of the FparLai_QC SDS (see Table 3, Chapter 2.7.1 for a definition of the FparLai_QC SDS and codes). With the exception of one 8-day composite spanning days 353-360 in 2003, all retrievals were performed using the main RT approach without saturation (FparLai_QC bits 5-7 = 0). The empirical backup algorithm was invoked over days 353-360 as a result of RT algorithm failure for reasons other than geometry (FparLai_QC bits 5-7 = 3). Maximum LAI returned in 2003 was 1.6, retrieved over days 25-32 using the main approach without saturation.

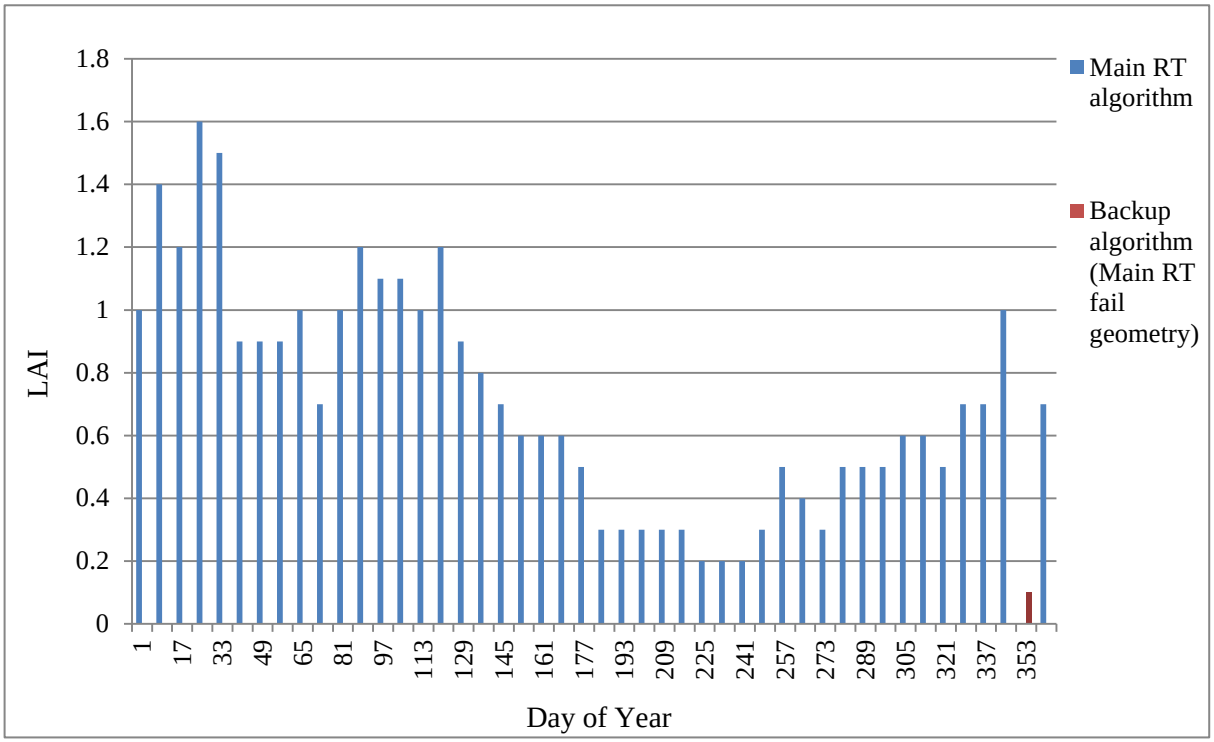

Figure 16: Composited LAI at the Bellevue site in 2003, indicating retrieval quality on each date.

As indicated earlier, climate data required to calculate ET_0 by (FAO-56 method) were recorded by Savage *et al.* (2004) for the same time period at the site in 2003. Class A-pan data were acquired from a nearby manual weather station (Faulklands) to fill gaps in the FAO-56 dataset where these occurred. There were concerns regarding the quality of the published FAO-56 data however, particularly after day 275 in 2003, where patterns of consistently recurring values were noted (Figure 20). Inaccurate ET_0 data would propagate errors in ET_{MODIS}, and it was considered preferable that these data be rejected from further analysis rather than risk compromising model performance.

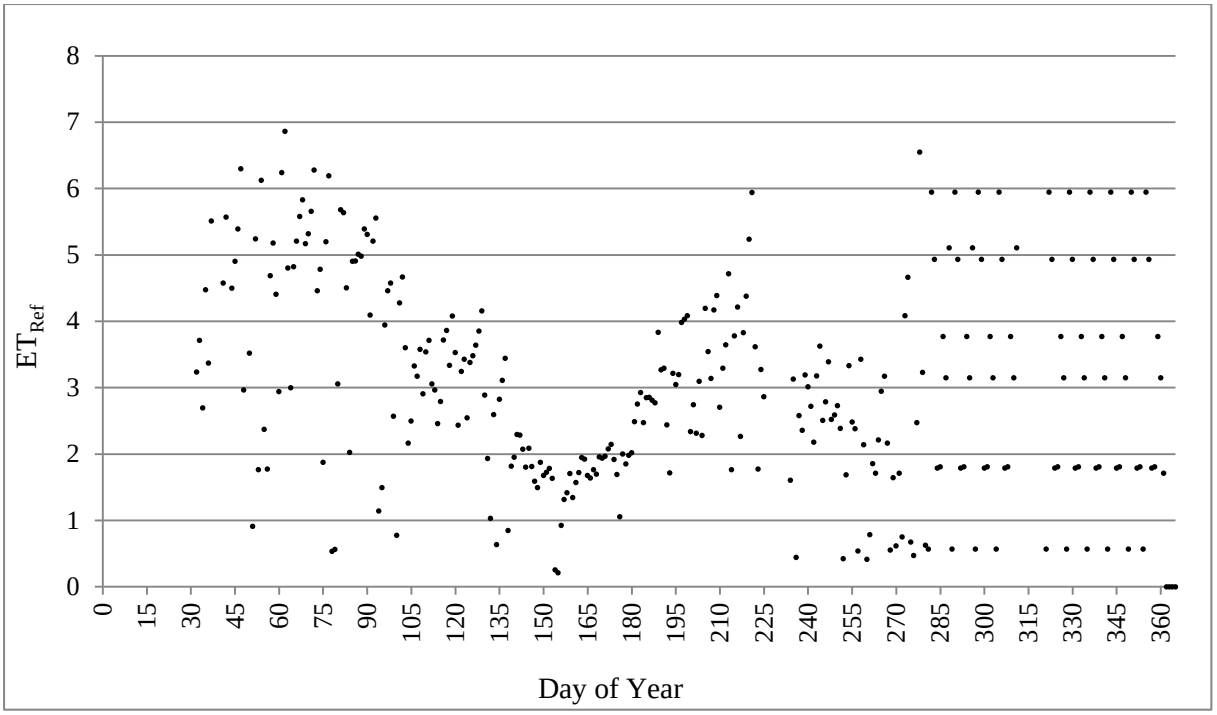

Figure 17: ET_0 (FAO-56) at the Bellevue site in 2003; suspect values are evident from approximately day 275 in 2003.

Daily ET for 275 days (days of year 1-275) in 2003 was modelled by applying ET_{MODIS} (Equation 20), parameterized using long-term MOD15A2 LAI_{max} (LAI_{max} = 2.2), 8-day MOD15A2 LAI, and daily ET_0 (FAO-56/A-pan) (Figure 18). Using this approach, a total of 320.0 mm ET was predicted for the 275 days for which reliable ET_0 (FAO-56/A-pan) data was available in 2003, relative to ET_0 of 867.9 mm, and rainfall of 344.5 mm for the same time period. ET_{ave} is plotted here for the purposes of comparison.

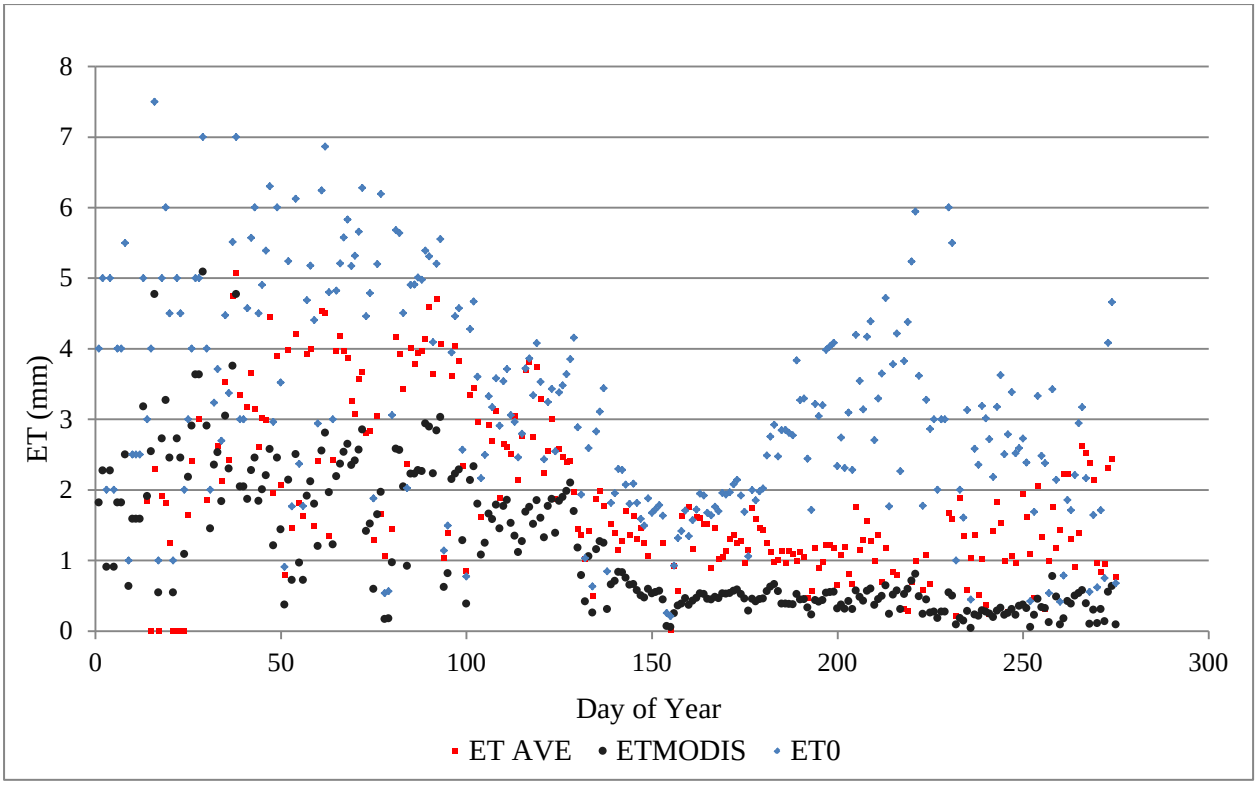

Figure 18: ET_{MODIS} vs. ET_0 (FAO-56/A-pan), ET_{ave} for day 1-275 of 2003, Bellevue.

A comparison of accumulated ET_{MODIS} and ET_{ave} was performed for the periods where both modelled and measured data were available, comprising a total of 235 days spanning both wet and dry seasons in 2003 (Figure 19). ET_{MODIS} over this period totalled 266.9 mm, while ET_{ave} for the same period totalled 460.2 mm, representing an underestimation of 42.0 % in modelled ET relative to measured ET.

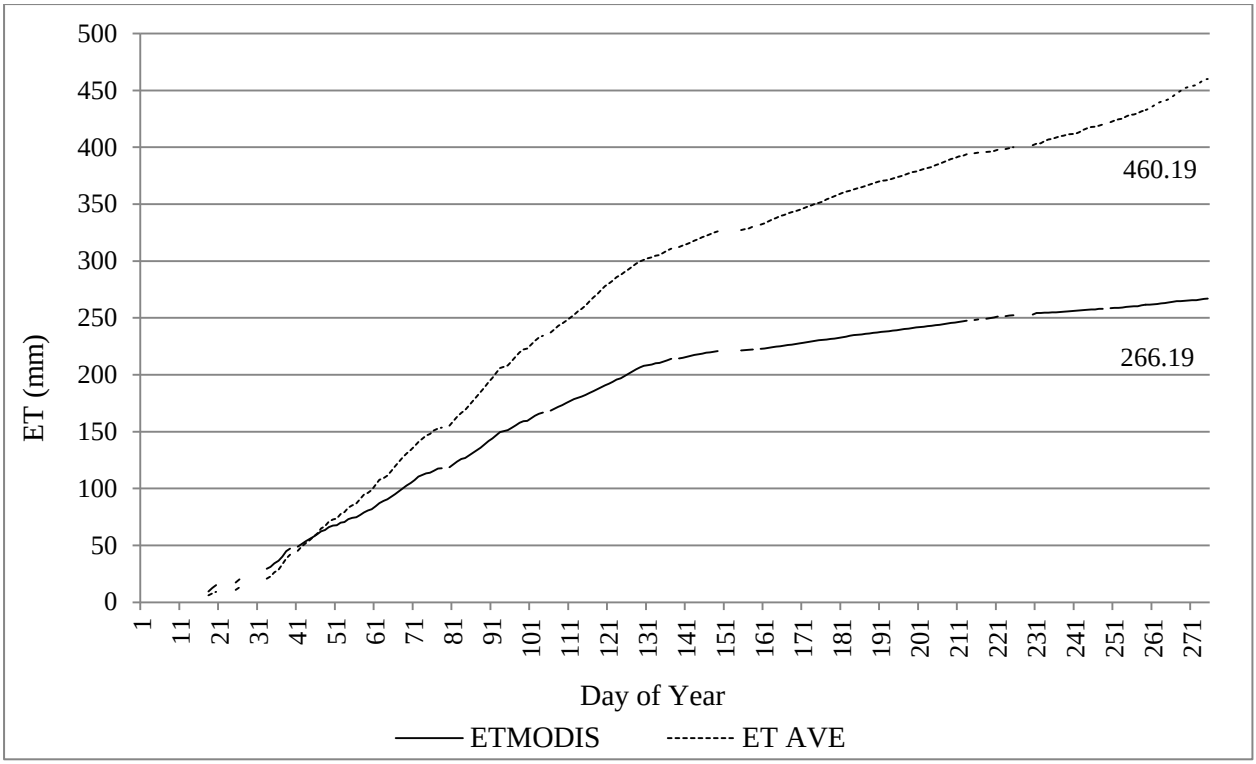

Figure 19: Accumulated ET_{MODIS} vs. ET_{ave} at the Bellevue site for 235 days of corresponding data spanning days 1-275 in 2003 (LAI_{max} = 2.2).

The relationship between ET_{ave} and ET_{MODIS} was evaluated by fitting a linear regression model where corresponding MOD15A2, ET_0 and ET_{ave} data were available, returning a r^2 value of 0.67 (Figure 20).

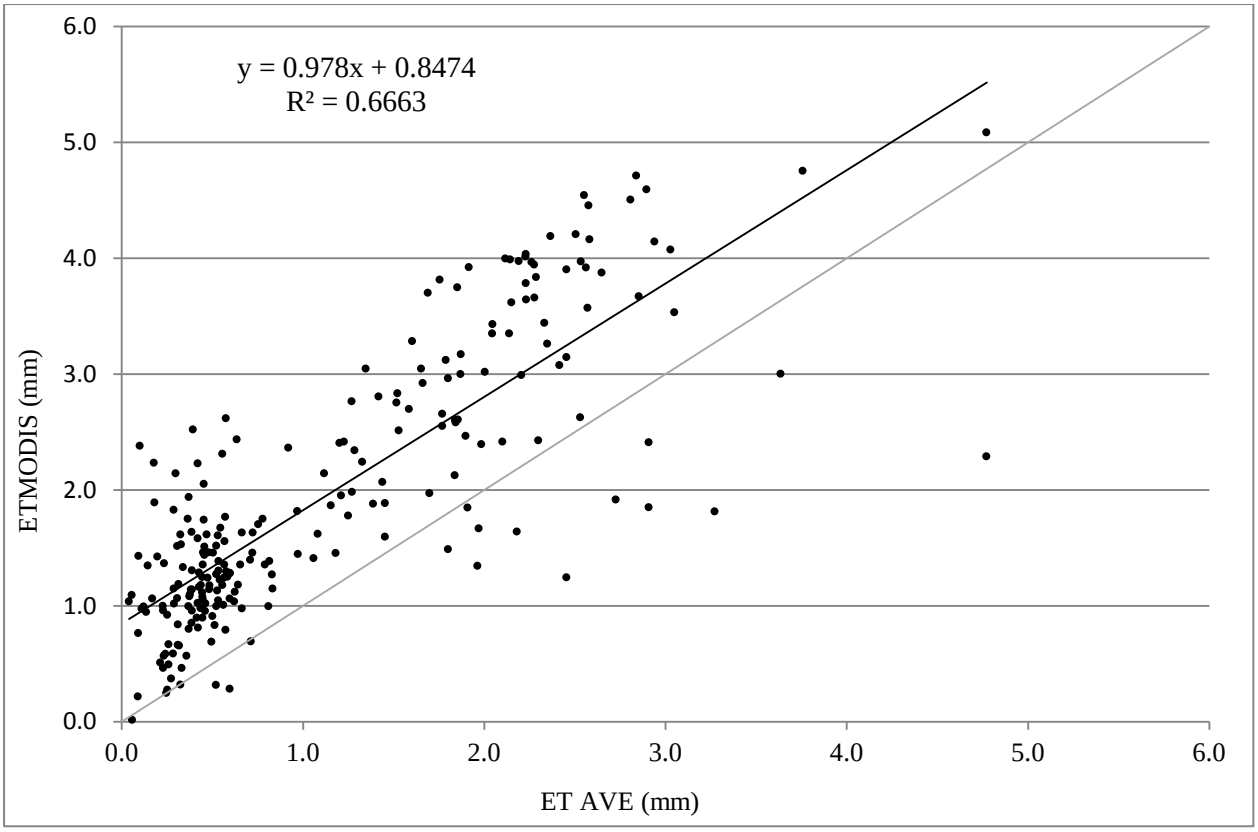

Figure 20: Linear regression model of the relationship between ET_{MODIS} and ET_{ave} over 235 days of corresponding data in 2003, Bellevue; 1:1 line shown in grey.

4.4 Groenkop mixed indigenous forest (George)

The frequency distribution in LAI observed at the Groenkop site for the period of data availability (25 February 2000-31 December 2009), comprising a total of 448 retrievals, is provided (Figure 21A). The LAI_{max} value observed over the 10-year period was 8.8, retrieved on a single occasion in 2001 (days 25 – 33), with a minimum of 0.5, also retrieved on a single occasion (days 137-145) in 2001, and the majority of retrievals in the range of ~ 4.8-6.3.

Means and standard deviation in annual LAI retrieved over the nearly 10-year period are provided (Figure 21B). In contrast to both the Skukuza and Bellevue sites, both of which experience a summer rainfall regime, the data suggest that most inter-annual variation in LAI at Groenkop occurs in the wetter winter period, with relatively less in the drier summer period. Consistent with what would be expected for this ecosystem, there is less pronounced seasonal variation in LAI across the year relative to the other sites used in this study, with an amplitude of 70 % (3.4 LAI) of the mean LAI for the 10-year period (4.9).

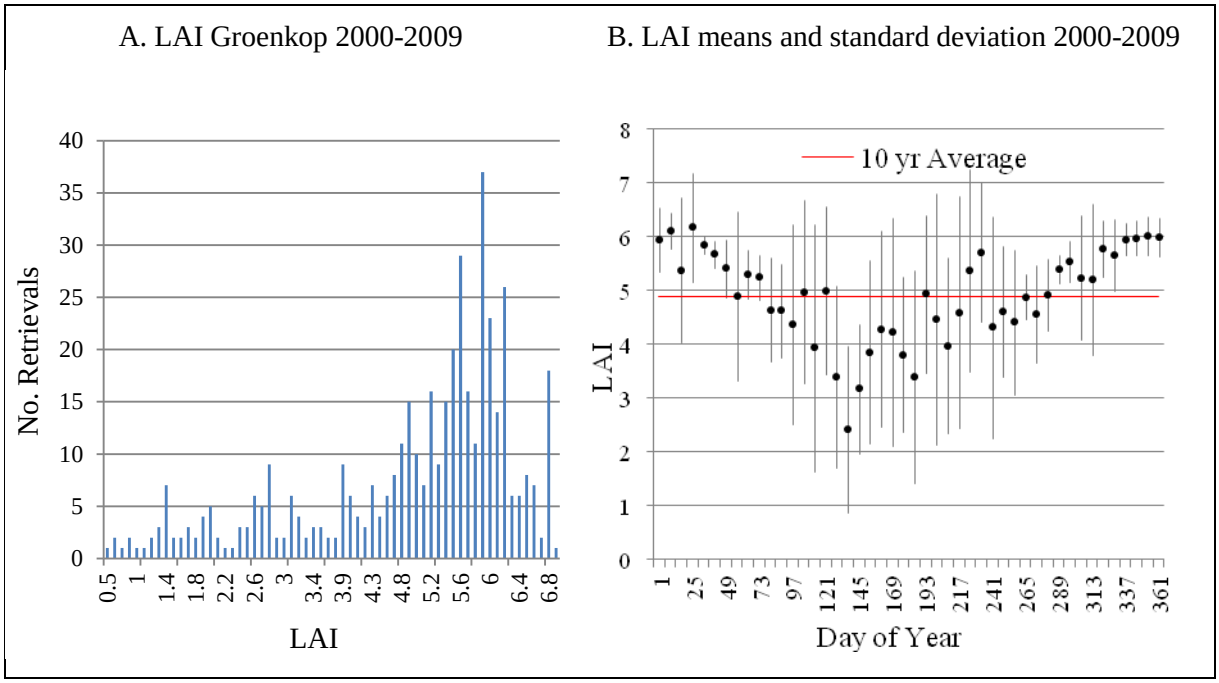

Figure 21: A) Histogram of the frequency distribution in LAI and B) mean and standard deviation retrieved at Groenkop over the period 25th February 2000 to 31 December 2009.

Figure 22 illustrates LAI retrievals for the year 2004 at Groenkop, indicating retrieval quality information extracted from bits 5-7 of the FparLai_QC SDS. Maximum LAI retrieved in 2004 was 6.8 (days 161-168), using the main approach with saturation (FparLai_QC SDS bits 5-7 = 1), with a minimum of 0.7 (days 185-192), retrieved using the main approach without saturation (FparLai_QC SDS bits 5-7 = 0).

Significantly fewer retrievals in 2004 were performed using the RT algorithm relative to other sites in this study. Only 54 % of retrievals in 2004 were performed using the RT algorithm with saturation (FparLai_QC bits 5-7 = 1), predominantly during the summer period (days 1-65 and 281-365); 33 % were performed using the RT algorithm without saturation (FparLai_QC bits 5-7 = 0), predominantly during autumn, winter and spring (days 65-273), and 13 % were performed using the backup algorithm (FparLai_QC bits 5-7 = 3), predominantly during winter (days 153-233).

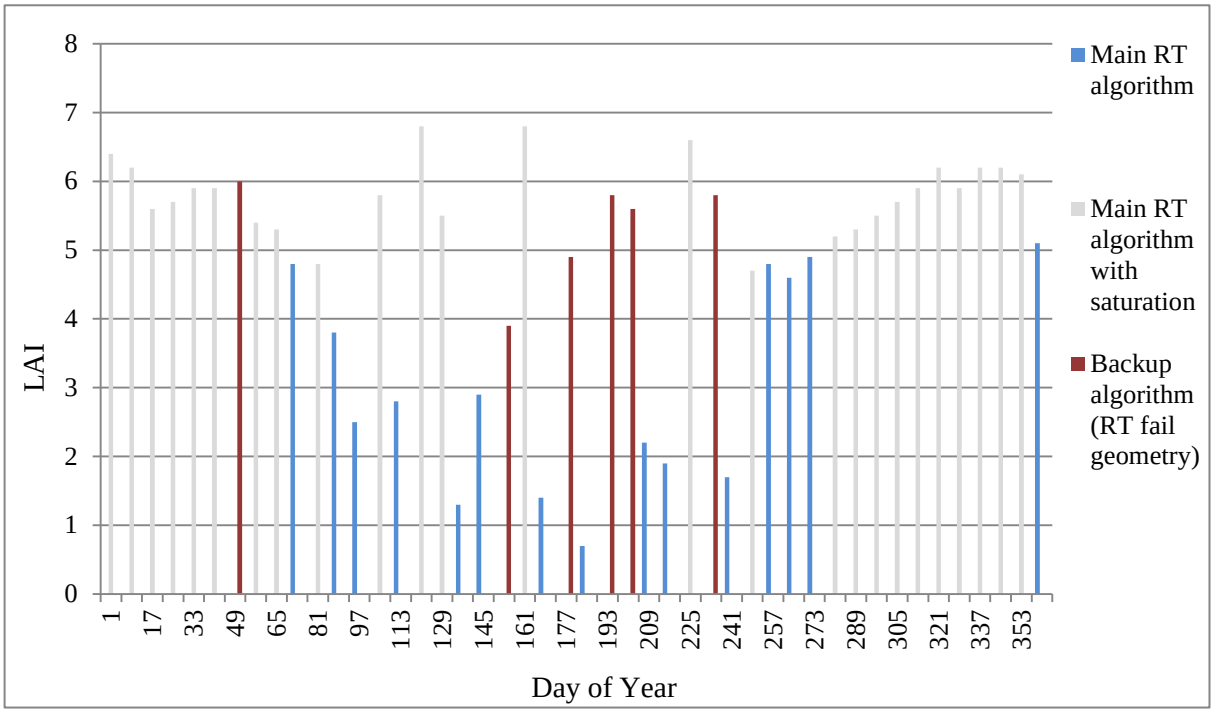

Figure 22: Composited LAI at the Groenkop LAS site in 2004, indicating retrieval quality on each date.

Daily ET for the entire year in 2004 was modelled by applying ET_{MODIS} (Equation 20), parameterized using long-term MOD15A2 LAI_{max} (LAI_{max} = 6.8), 8-day MOD15A2 LAI, and daily ET_0 (class A-pan; Outeniqua weather station) (Figure 23). By this approach, a total of 836.7 mm ET_a was predicted for 365 days in 2004, relative to total ET_0 (A-pan) of 1114.1 mm, and rainfall of 813.9 mm; ET_{LAS} is plotted here to provide comparison.

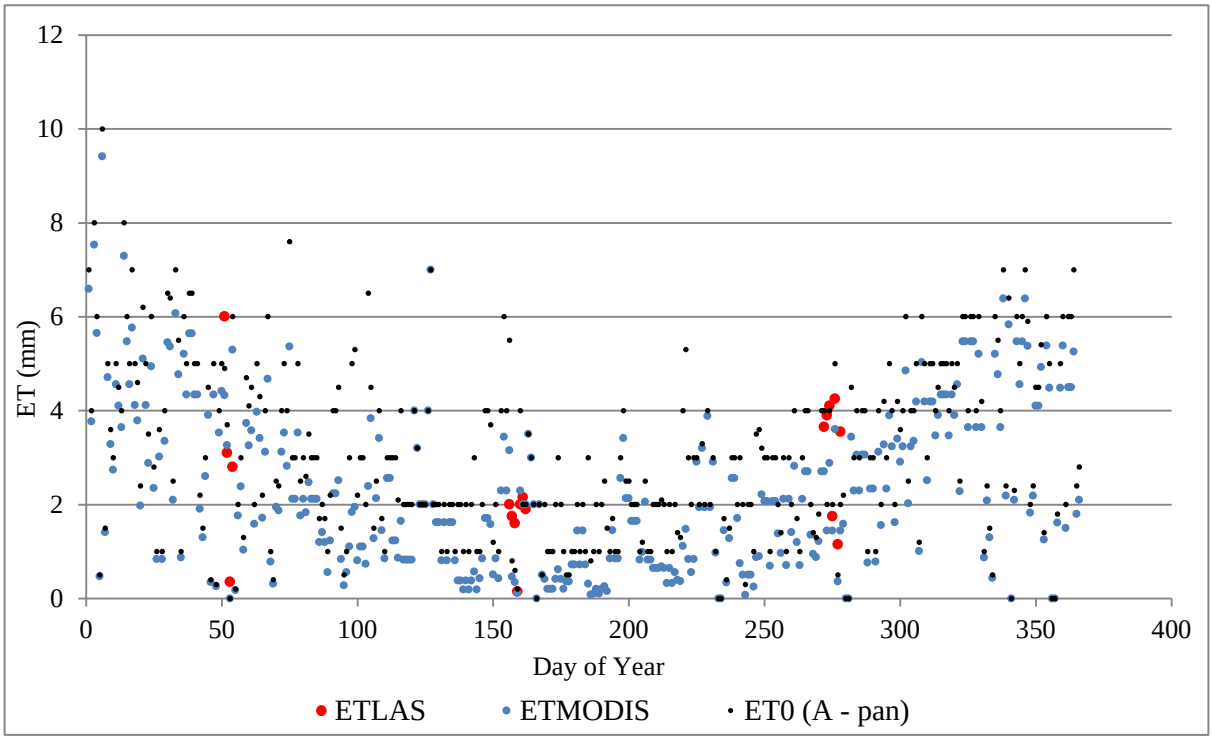

Figure 23: ET_{MODIS} vs. ET_0 (A-pan; Outeniqua), ET_{LAS} for 366 days in 2004, Groenkop.

ET_{MODIS} was evaluated at the Groenkop site using LAS data available on three separate occasions in 2004, comprising 4 days in February (days of year 51-54) (Figure 24A), 7 days in June (days of year 156-162) (Figure 25A), and 7 days in September/October (days of year 272-278) (Figure 26A), providing a total of 18 days. Dye *et al.* (2008) calculated ET_0 (FAO-56 method) for the periods corresponding with ET_{LAS} measurements, and these data replaced the class A-pan data in parameterizing ET_{MODIS}. The method used in retrieving LAI inputs for each ET_{MODIS} data point are also plotted, and provide an indication of confidence limits in the modelled data (extracted from bits 5-7 of the FparLai_QC dataset, where 1-3 plotted in figures 24-26 correspond with bit codes 0, 1 and 10, respectively; definitions provided in Table 3, Chapter 2.7.1).

The relationship between ET_{MODIS} and ET_{LAS} was evaluated by fitting a linear regression model in each case where corresponding data exists, returning r^2 values of 0.98 (days 51-54) (Figure 24B), 0.43 (days 156-162) (Figure 25B), and 0.80 (days 272-278) (Figure 26B).

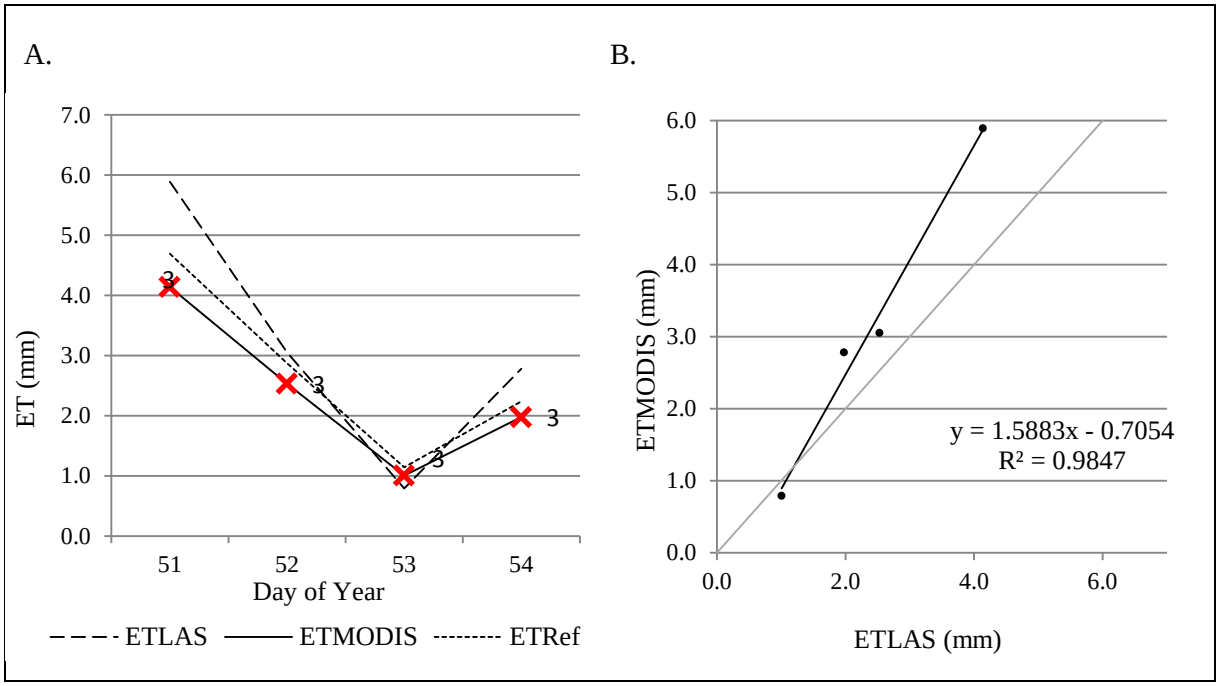

Figure 24: A) ET_{MODIS} vs. ET_0, ET_{LAS} for days 51-54 in February 2004, and (B) linear regression of modelled vs. measured data for the same period; 1:1 line shown in grey.

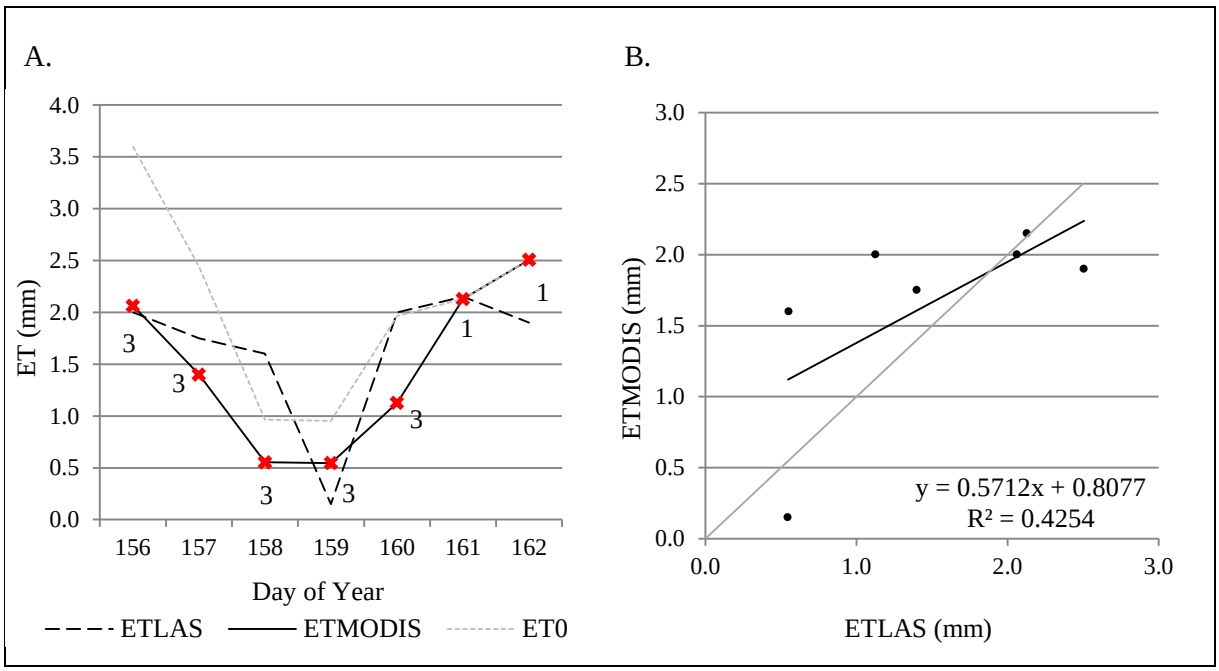

Figure 25: A) ET_{MODIS} vs. ET_0, ET_{LAS} for days 156-162 in June 2004 and B), linear regression of modelled vs. measured data for the same period; 1:1 line shown in grey.

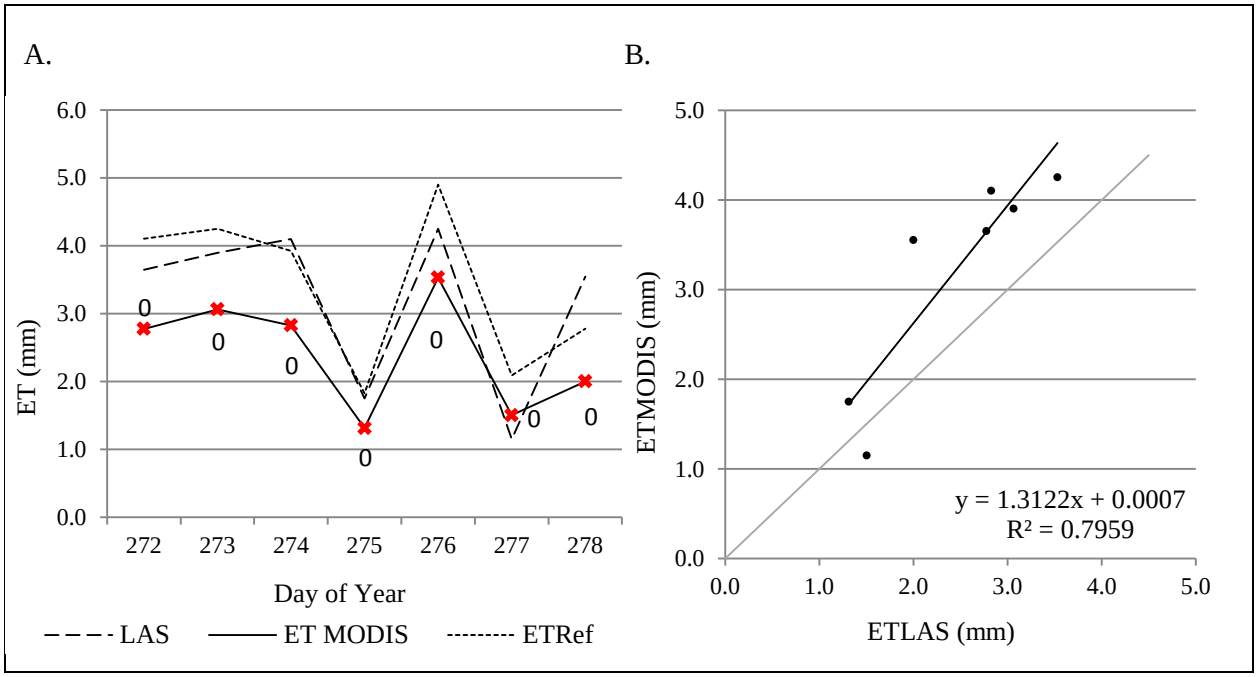

Figure 26: A) ET_{MODIS} vs. ET_0, ET_{LAS} for days 272-278 in September/October 2004 and B), linear regression of modelled vs. measured data for the same period; 1:1 line shown in grey.

ET_{MODIS} predicted 9.7 mm ET for the four days in February, relative to 12.5 mm ET_{LAS}, 10.3 mm for the seven days in June, relative to 11.6 mm ET_{LAS}, and 17.0 mm for the seven days in September / October, relative to 22.4 mm ET_{LAS}; these figures represent under-predictions in each case of 22.4 %, 11.2 % and 24.8 %, respectively Again, given the sparseness of data points available for validation, no comparison of annual accumulated ET was performed in this instance.

5. Discussion

5.1 Introduction

The discussion of results is structured as follows: first, a concise general summary and analysis of the key variables across the four validation sites is presented in Section 5.2, in terms of the following:

- ET_{MODIS} in relation to annual ET_0 and/or ET_p and precipitation for the year of validation; and

- ET_{MODIS} in relation to measured validation flux data specifically, and model performance.

This is followed by a detailed analysis in Section 5.3, addressing each site separately, and with reference to the literature where relevant, in respect of:

- long-term inter-annual and seasonal trends and patterns observed in remotely sensed LAI at each validation pixel;

- LAI trends and retrieval quality for the year in which ET_{MODIS} is applied at each pixel;

- Comparisons of modelled and measured water fluxes, a discussion of model performance and identification of uncertainties.

This is followed in Section 5.4 by a detailed analysis of model uncertainties; finally, opportunities and constraints of the approach as a means to derive continuous, spatially distributed estimates of evapotranspiration over wider areas of the South African land surface are assessed in Section 5.5.

5.2 General summary of key indicators

A general summary of the key indicators for each of the study sites, including ET_0 and/or ET_p, annual rainfall, modelled (ET_{MODIS}) and measured evapotranspiration (ET_a), fraction of annual precipitation evapotranspired, and regression equations including coefficients of determination (r^2 values), is reported in Table 5. Both annual data (for available dates within

respective years of study) and comparative data (*i.e.* only those dates where both validation ET_a data and ET_{MODIS} are available) are reported; a concise discussion of the data is presented on a site by site basis in Sections 5.2.1 to 5.2.4.

Table 5: Summary of results.

	Skukuza EC Site	**Skukuza LAS Site**		**Bellevue**	**Groenkop**		
	Annual 2007 (353 days)	Annual 2005 (365 days)		Annual 2003 (275 days)	Annual 2004 (366 days**)**		
ET_{MODIS} (mm)	408.4	435.2		320.0	836.7		
ET_0/ET_p (mm)	1420.5*	1451.7*		867.9†	1114.1‡		
Precipitation (mm)	530.8	229.0		344.5	813.9		
ET_{MODIS}/Precipitation (%)	76.9	190.0		92.9	102.8		
	Corresponding ET_{MODIS} / ET_a Data Periods						
	Annual 2007 (170 days)	Feb 2005 (7 days)	May 2005 (8 days)	Annual 2003 (235 days)	Feb 2004 (4 days)	Jun 2004 (7 days)	Sep / Oct 2004 (7 days)
ET_{MODIS} (mm)	194.8	27.4	6.7	266.9	9.7	10.3	17.0
ET_0/ET_p (mm)	662.1*	41.9*	27.84*	752.9†	10.9*	14.6*	23.9*
ET_a (mm)	147.9§	32.5+	8.2+	460.2ǂ	12.5+	11.6+	22.4+
% Error ET_{MODIS} vs. ET_a	+31.7	-15.7	-18.3	-42.0	-22.4	-11.2	-24.1
r^2 value	0.67	0.67	0.34	0.67	0.98	0.43	0.80
Equation	y = 0.811x + 0.444	y = 1.389x - 0.804	y = 1.158x + 0.045	y = 0.978x + 0.847	y = 1.588x - 0.705	y = 0.744x + 0.245	y = 1.312x + 0.000

* = FAO-56

† = FAO-56 + A-pan

‡ = A-pan

§ = EC

+ = LAS

ǂ = SLS

In Table 5, total measured evapotranspiration exceeds total modelled evapotranspiration in all cases, with the exception of the flux tower site at Skukuza, where evapotranspiration was overestimated by ET_{MODIS} by 31.7 % relative to measured (EC) values for the 170 days in 2007 where corresponding modelled and measured data were available (Fig. 8 and Table 5).

The most significant differences in measured versus predicted data, expressed as a percentage, were recorded at the Skukuza flux tower site in 2007 (31.7 % overestimate), and the Bellevue SLS flux site in 2003 (42 % underestimate). Coefficients of determination, a measure of the extent to which modelled data are able to explain observed data at validation periods, with just two exceptions (May 2005 at the Skukuza LAS site, where $r^2 = 0.34$, and June 2004 at Groenkop, where $r^2 = 0.43$), are within a range of 0.67 – 0.98.

5.2.1 Skukuza: EC flux tower site

Annual data

Total evapotranspiration (for 353 days of data availability) predicted at the flux tower site in 2007 was 408.4 mm, relative to ET_0 (FAO-56, Malekutu) of 1420.5 mm (Table 5); this represents a marked difference in modelled water use versus ET_0, which is unsurprising, given that conditions at the site diverge significantly from those assumed for the reference surface (relating to aerodynamic roughness, surface conductances and availability of water at the evaporating surface), and indicates that the system is significantly water limited, *i.e.* atmospheric evaporative demand exceeds available precipitation (Villegas, 2008). Total precipitation for 2007 was 530.8 mm (relative to MAP of 560 mm), suggesting that 76.9 % of precipitation was evapotranspired in that year, consistent with figures for other dryland systems reported in the literature (Wilcox, *et al*., 2003, Huxman, *et al*., 2004).

Validation periods

With specific reference to validation periods for which measured and modelled flux data coincide temporally, ET_{MODIS} predicted 194.8 mm evapotranspiration for 170 days of data availability at the flux tower near Skukuza in 2007, relative to 147.9 mm measured by the EC system, an overestimate of 31.7 % (Fig. 7 and Table 5); a coefficient of determination (r^2 value), a measure of how well the regression line fits the data, of 0.67 was returned (Fig. 9 and Table 5).

5.2.2 Skukuza: LAS site

Annual data

At the Skukuza LAS site, approximately 7.5 kilometres SE of the flux tower, similar conditions were observed in 2005, with ET_{MODIS} predicting 435.2 mm evapotranspiration for the 365 days (Table 5); ET_0 (FAO-56; Malekutu) was 1451.7 mm, marginally higher relative to 2007. Conditions appeared to be abnormally dry in 2005 however, with just 229.0 mm

precipitation recorded at Malekutu, less than half that measured at the same site in 2007, with modelled evapotranspiration representing almost double (190 %) this figure. Despite the significant difference in precipitation, modelled annual water fluxes were relatively similar in both years (435.2 mm in 2005 versus 408.4 in 2007). Because the FAO-56 submitted to ET_{MODIS} represents climatic conditions only (atmospheric evaporative demand, incorporating standard aerodynamic and surface resistance factors), similarities observed in ET_{MODIS} data between the sites in 2005 and 2007 are due to comparable LAI values, in spite of the marked differences in precipitation. Unless precipitation patterns at Malekutu differed substantially in these years relative to the flux tower and LAS sites some 40 kilometres away[2], these similarities in LAI, and therefore modelled evapotranspiration, would suggest that plants were either able to access deeper stored water in the drier conditions in 2005, or that soil moisture recharge may have originated externally, permitting photosynthesis (and associated spectral signatures) to continue at levels comparable to those in 2007 despite the arid conditions in 2005.

Validation periods

Validated over two discrete seven and eight day periods near the flux tower in February and May in 2005, ET_{MODIS} predicted 27.4 mm and 6.7 mm evapotranspiration respectively, relative to 32.5 and 8.2 mm measured by an LAS over the same periods (Fig. 12 and Table 5), underestimates of 15.7 % and 18.3 % in each case. Coefficients of determination for regressions fitted to respective datasets of 0.67 and 0.34 were returned for the February and May periods respectively (Figs. 13 and 14; Table 5).

5.2.3 Bellevue

Annual data

At the Bellevue site, ET_{MODIS} predicted 320.0 mm evapotranspiration for the 275 days of data availability in 2003 (Table 5). ET_0/ET_p (FAO-56 measured on site, patched with class A-pan data; Faulklands), was 867.9 mm for the same period, relative to precipitation of 344.5 mm (Table 5); the marked difference between atmospheric demand and precipitation indicates that, like the sites at Skukuza, this system was significantly water limited over the 275 days

[2] The significance of the distance of the Malekutu station from the flux sites is discussed in Section 5.4.5.

of data availability in 2003[3]. Based on modelled data, 92.9 % of precipitation was evapotranspired over 275 days, and suggests that nearly all available water, based on precipitation volumes recorded over this period, was harvested over this time in 2003.

Validation period

At the Bellevue site in 2003, ET_{MODIS} predicted 266.9 mm evapotranspiration over the 235 days for which corresponding modelled and measured data were available, relative to 460.2 mm measured using a SLS (patched with BR and EC data where missing or unreliable data occurred) (Fig. 18 and Table 5), representing an underestimate of 42 %; the coefficient of determination returned was 0.67 (Fig. 20 and Table 5).

5.2.4 Groenkop

Annual data

At the Groenkop site, ET_{MODIS} predicted 836.7 mm evapotranspiration for 366 days in 2004, relative to ET_p (class A-pan data; Outeniqua) of 1114.1 mm, and precipitation of 813.9 mm (Table 5), relative to long-term MAP of 860 mm. These data indicate that, while the system appears to be water limited according to the definition provided above, the difference between atmospheric demand and water availability over the year is significantly less pronounced relative to other sites in this study. Based on modelled data, all available water (102.8 %), as indicated by total precipitation recorded for that year, was evapotranspired in this system in 2004.

Validation periods

At the Groenkop site, where validation was performed over three discrete periods in February (four days), June (seven days) and September/October (seven days) in 2004, ET_{MODIS} predicted 9.7, 10.3 and 17.0 mm evapotranspiration, relative to 12.5, 11.6 and 22.4 mm respectively (Fig. 23 and Table 5), underestimates in each case of 22.4, 11.2 and 24.1 %. Coefficients of determination were 0.98, 0.43 and 0.80 respectively (Figs. 24 - 26).

[3] Total precipitation at the Bellevue site in 2003 was 478.9 mm, relative to long-term MAP of 724 mm; class A-pan data for the entire year, recorded at Faulklands station was 1118.8 mm, and confirms that the system is generally water limited.

5.3 Detailed analysis of results

5.3.1 Skukuza: EC flux tower site

MOD15A2 LAI and vegetation phenological dynamics

Dye, *et al*., (2008) describe this site near Skukuza in Mpumalanga Province as a semi-arid savanna system; it receives a MAP of 560 mm, predominantly in November and April (early Summer and Autumn), and is the most water limited (precipitation expressed as a fraction of atmospheric evaporative demand) of all the sites assessed in this study. Land cover at the site comprises a fairly homogenous mix of grass and shrubs, including a significant woody component across the validation pixel, with a complex, spatially discontinuous canopy structure; due to distinct differences in physiological activity of woody and herbaceous components, these characteristics of savanna systems present particular difficulties to remote observation (Privette & Roy, 2005), and modelling of evaporative fluxes (Dye, *et al*., 2008). Long-term (nearly 10-years) MOD15A2 LAI data retrieved at the flux tower location were interrogated both to assess the performance of the RT LAI algorithm in this system, as well as to characterize trends and seasonal patterns in vegetation phenology over this period, directly coupled to water use (Monteith, 1988) and a fundamental parameter in ET_{MODIS}.

Frequency distribution in remotely sensed LAI over the period 25 February to 31 December 2009 demonstrates that values are positively skewed. A predominance of values occur within the range of 0.3-1, with maximum and minimum values of 3.1 and 0.1, respectively (Fig. 5A). Pronounced seasonal variation in LAI is evident, with an amplitude of 113 % (LAI = 1.12) of the mean annual LAI (0.99) over the approximately 10 year period (Fig. 5B). Relatively high inter and intra-annual variation in LAI is apparent in the growing season (November to March), which is consistent with marked and rapid vegetation phenological responses to low and erratic rainfall and soil moisture distribution in these systems at this time of the year (Dye, *et al*., 2008); however, the extent to which these values may rather be an effect of inaccuracies in RT simulations and inputs is assessed in Section 5.4. High atmospheric evaporative demands and rapid declines in soil moisture at the end of the growing season (April/May) appear to force grasses and deciduous trees to decouple from the system (Palmer, *et al*., 2008), with a marked reduction in vegetation physiological activity, and inter and intra-annual variation in LAI values apparent; this appears to persist until around November with the onset of the growing season and replenishment of soil moisture levels (Fig. 5B).

LAI retrieval quality

Despite the challenges to remote sensing of vegetation characteristics in savanna systems described above, MODIS observations at this site appeared to generally realistically reflect seasonal vegetation phenological patterns, with LAI values retrieved by the algorithm within the bounds of those expected for these systems. Long-term average LAI maxima of approximately 1.8 were observed in the wet season, transitioning relatively smoothly to minima of approximately 0.5 in the winter dry season, when deciduous trees and shrubs decouple from the system (long-term maximum and minimum LAI returned was 3.1 and 0.1) (Figs. 5A and B). Although data appear generally credible, several seemingly non-physical spikes in values are evident in the summer wet seasons, both in long-term average data, over days 1-73 (Fig. 5B), and annual data in 2007, on day 361 (Fig. 6).

The MODIS LAI products are delivered with comprehensive uncertainty information contained in the FparLai_QC layer (described in Section 2.7.1), and these data were interrogated to establish algorithm performance at validation sites in this study. Extraction of the various bit fields comprising this dataset using the HEG tool is a relatively labour intensive process that cannot be automated, and for this reason it was not considered realistically feasible to interrogate the full 10 year data stack, and evaluation was restricted to the year in which validation was performed (2007); all 46 retrievals in 2007 were found to have been executed using the main RT algorithm without saturation (FparLai_QC layer bits 5–7 = 0), confirming best possible retrieval quality.

Comparison of modelled and measured water fluxes

ET_{MODIS} predicts a total of 194.8 mm evapotranspiration over the 170 day period of corresponding data availability system in 2007, relative to a total of 147.9 mm measured at the flux tower for the same period, representing an overestimation of 31.7 % (Fig. 8 and Table 5), and represents the second largest margin of error in modelled fluxes returned in this study. A regression model fitted to the data returned a r^2 value of 0.67 (Fig. 9 and Table 5), indicating that 59 % of the measured data is explained by ET_{MODIS}; this is within the mid range of values reported for several peer-reviewed remote sensing-based evapotranspiration models reviewed by Glenn, *et al*. (2010), which vary between $r^2 = 0.45$ to 0.96.

The slope of the regression line confirms that the model overpredicts evapotranspiration where EC values are low, and underpredicts where EC values are high. Accumulated

evapotranspiration for the 170 days over the full year in 2007 is plotted in Figure 8, revealing greatest divergence between modelled and measured values during the winter dry season, with greater convergence apparent during the summer growing season. Several possible causes of these errors were considered, including:

- potential inaccuracies in the EC flux measurements used to validate ET_{MODIS};
- possible differences in microclimate at flux sites and Malekutu weather station, used to calculate FAO-56 input to ET_{MODIS}; and
- potential overestimation of LAI by the RT algorithm at low spectral reflectance values (*i.e.* errors in RT simulations stored in LUTs for modelled versus observed surface reflectances).

These uncertainties are discussed in Section 5.4.

5.3.2 Skukuza: LAS site

MOD15A2 LAI and vegetation phenological dynamics

The complexities of remote observation and evapotranspiration modelling described at the flux tower site in Section 5.3.1 apply to the same extent at the LAS site used for model validation in 2005. Analysis of long-term remotely sensed LAI data was again undertaken to assess the performance of the LAI algorithm at this site, and identify and describe trends and seasonal patterns in vegetation phenology and water use. Unsurprisingly, given their proximity and comparable climatic and biophysical characteristics, very similar long-term phenological dynamics to those observed at the flux tower location, approximately 7.5 kilometres away, were observed at this site. No significant differences in terms of the range and frequency distribution of LAI values (Fig. 10A), seasonal amplitude, or intra and inter-annual variability in LAI (Fig. 10B) over the approximately 10 year data period were noted: maximum and minimum LAI at the site was 2.9 and 0.1 respectively (as opposed to 3.1 and 0.1 at the flux tower), with frequency distribution showing positively skewed values; seasonal amplitude was again 113 % of long-term average LAI, with the long-term average only slightly higher here in comparison to the flux tower site (1.02 as opposed to 0.99) (Figs. 5B and 10B).

While the similarity in long-term phenological dynamics at these sites is to be expected, their similarity in respective years of validation (Figs. 6 and 11) is somewhat surprising, given the marked differences in precipitation recorded in each year; total precipitation recorded at Malekutu station in 2005 was 229 mm, relative to 530.8 mm in 2007, and it would be reasonable to expect significant declines in vegetation physiological activity, signalled by lower LAI values across the year in 2005. This is not the case however, and phenological dynamics (Figs. 6 and 11), and therefore modelled vegetation water use (Figs. 7 and 12) appear largely similar in 2005 and 2007 at respective sites. Typically, these semi-arid systems are closely linked to rainfall and soil moisture, with rapid physiological responses to changes in its availability (Dye, *et al*., 2008); counter-intuitively, LAI data suggest that performance was largely unaffected by the reduced precipitation volumes in this year. These data appear to suggest that soil moisture storage in 2005 was adequate to support similar levels of vegetation physiological activity to that observed in 2007, despite significant differences in precipitation volumes between years; this is discussed further in Section 5.4.1.

LAI retrieval quality

Seasonal phenological patterns at the LAS site near Skukuza again appeared to be generally realistically modelled in MODIS observations, although with similar apparently non-physical spikes evident in mid to late summer in the long-term data (Fig. 10B) and annual data for 2005 (Fig. 11), in both early and late summer in the case of annual data. Retrieval quality, again only interrogated for the year of validation, was similarly high at the LAS site in 2005, with just one retrieval (day 361) performed by means of the back-up algorithm, based on the empirical relationship between NDVI and LAI (described in Section 2.7.1) (Fig. 11). Cloud and atmospheric contamination, which typically result in reflectances beyond the algorithm domain, is reported to be a major cause of RT algorithm failure (Shabanov, *et al*., 2005); information on cloud state is provided in bits 3-4 of the FparLai_QC layer, and although these data were not interrogated, given that the Lowveld region of South Africa experiences summer rainfall maxima and significant rainfall events at this time of year, it is considered probable that several consecutive days of cloud cover at Terra overpass times (the MOD15A2 product is composited at 8-day periods precisely to reduce the effect of cloud cover on retrievals) lead to algorithm failure in this single incidence in 2007. Despite the fact that retrievals by the backup algorithm are considered poor quality (Myneni, *et al*., 2007), the value returned on this occasion in 2005 appeared to be within realistic bounds (Fig. 11).

Comparison of modelled and measured water fluxes

ET_{MODIS}, applied at two seven and eight day periods in February and May of 2005, predicted a total of 27.4 and 6.7 mm evapotranspiration respectively (Table 5), relative to measured values of 32.5 and 8.2 mm; this represents an underestimation in modelled relative to measured values of 15.7 and 18.3 % respectively. Regression models fitted to respective datasets returned r^2 values of 0.67 in February and 0.34 in May, the latter representing the lowest returned for any of the sites assessed in this study.

While these results suggests a relatively small margin of error when expressed as a percentage in each case, r^2 values, with specific reference to the second validation period in May, demonstrate a poor fit of modelled to measured data, where just 34 % of measured data could be explained by ET_{MODIS}. Factors affecting model performance described for the EC site in Section 5.3.1, specifically distance of the climate station from the flux measurement site, and potential overestimation of LAI by the RT algorithm in the dry season, are equally of concern in this case, however of particular relevance, given the sparseness of data points available for validation, may have been the discrepancies in temporal scales of input data and model outputs. The MOD15A2 LAI product is produced as an 8-day composite, and there is a clear conflict in submitting these data to a daily time-step model, which becomes especially critical when the model is applied and/or validated over short periods. In the application of ET_{MODIS} at the LAS site in 2005, just one MOD15A2 composite overlapped temporally with the 7-day period in February (Figs. 13A and B), and two with the 8-day period in May (Figs. 14A and B). The coarseness of these data input to ET_{MODIS} configured to produce higher temporal resolution daily estimates inevitably propagate errors, which become statistically more significant when modelled over short periods of time. This is discussed in Section 5.4.

5.3.3 Bellevue

MOD15A2 LAI and vegetation phenological dynamics

Savage, *et al.,* (2004) describe Bellevue as a mixed community grassland system, which, in contrast to both Skukuza and Groenkop, is characterised by a relatively high degree of variation in land cover within the MODIS pixel footprint area, consisting of both natural and maintained grass cover, the former comprising a significant woody component, as well as a small proportion of built-up area and riparian vegetation (Figs. 3 and 28). Similar to the Skukuza sites, Bellevue, located on the eastern seaboard of KwaZulu-Natal, receives a majority of precipitation in summer, although MAP is higher in this region, with 724 mm

relative to 560 mm at Skukuza; given greater water availability, more productive systems characterized by higher standing plant biomass would be expected under natural conditions. Long-term MODIS data was again analyzed to assess algorithm performance in local conditions, and characterize trends and seasonal patterns in vegetation phenology.

Observations of long-term vegetation phenological patterns at Bellevue (Fig. 15B) were comparable to the Skukuza sites (Figs. 5B and 10B), with peaks of around 1.5 in the summer wet seasons, declining to minima of approximately 0.2-0.3 in the winter dry seasons; these maxima and minima, despite higher rainfall at Bellevue, are somewhat lower than the Skukuza sites however, with an average of 0.8, relative to 0.99 and 1.02 at Skukuza, and a lower seasonal amplitude (92 %, as opposed to 113 %). Visual comparison of both long-term and annual LAI at each site suggests that vegetation remains dormant for shorter periods over the dry season at Bellevue than Skukuza, with the latter demonstrating relatively more rapid declines and inclines between seasonal maxima and minima in each case.

A histogram of LAI values retrieved at the site indicates a maximum observed LAI of 2.2 and a minimum of 0.1 (Fig. 15A). Significantly, an abnormal distribution of values is evident, with a large predominance of retrievals of LAI = 0.3. On initial estimation, this could be considered to be attributable to the maintained grass surface at the park area to the north-west of the pixel (Fig. 28), which is mowed occasionally throughout the year (Savage, *et al*., 2004), and which would conceivably result in LAI values within a relatively consistent range across the year; this hypothesis is not supported by either the long-term or annual LAI values plotted in Figures 15B and 16, however. In this regard, it is also likely that higher biomass vegetation elements to the south and east of the pixel, accounting for the majority of the pixel by area, would dominate spectral signatures, and render this effect over a relatively small proportion of the total pixel area largely undetectable by the MODIS sensor, and there is the possibility that these values may rather be an artefact of inaccuracies in RT algorithm simulations and/or inputs (discussed in Section 5.4).

Again, there is relatively higher inter and intra-annual variation in LAI evident in the summer growth season at Bellevue relative to the winter dry season, with large variation about the mean evident at these times of the year (Fig. 15B); these erratic values may reflect rapid physiological responses to low and uneven precipitation and changes in soil moisture availability typical in water-limited systems (Dye *et al*. 2008), or, again, may instead be non-

physical values, an artefact of uncertainties in the RT algorithm. Interrogation of annual data retrieved at the site in 2003 demonstrate similarly erratic values in the wet season, particularly in January through to late March/early April, following which a relatively steep and consistent drop in values occurs until about day 225 (mid-August), as vegetation physiological activity declines in response to decreases in energy and water availability, and deciduous trees and shrubs decouple from the system (Fig. 16).

LAI retrieval quality

MODIS observations at the Bellevue site, with the exception of the predominance of retrievals of 0.3 LAI, and somewhat erratic values retrieved in the wet season, appeared to generally realistically reflect seasonal vegetation phenological patterns for the period of observation, with long-term average summer maxima of approximately 1.5 LAI transitioning relatively smoothly to average winter minima of approximately 0.2-0.3 LAI (Fig. 15B). The long-term maximum LAI value of 2.2 (Fig. 15A), which approaches the values observed at the Skukuza sites (Figs. 5A and 10A), probably exceeds that which could reasonably be expected for the maintained grass surface characterizing the validation site as described by Savage, *et al.* (2004) however, and suggests an effect of spectral dominance of higher biomass vegetation elements to the south and east of the pixel area (Fig. 28). This presents significant difficulties in terms of identifying the correct parameter value for LAI_{max} for this system, and seems to be a somewhat intractable problem for remote sensing approaches in complex landscapes, discussed later in this chapter.

Interrogation of the quality assessment data revealed a dominance of retrievals by the RT algorithm at the site in 2003, confirming best possible quality, with just one retrieval executed by the back-up algorithm (day 361) (Fig. 16). Again, no interrogation of the cause of the failure of the RT algorithm was performed, although the fact that it occurred in the summer rainfall season suggests that cloud cover would again have been responsible; in this case however, LAI returned by the back-up algorithm is clearly spurious, being significantly lower than both adjacent values retrieved by the RT algorithm.

Comparison of modelled and measured water fluxes

At the Bellevue site, ET_{MODIS} predicted a total of 266.2 mm evapotranspiration over the 235 days of corresponding data availability in 2003, relative to 460.19 mm measured evapotranspiration (measured using a SLS; missing data patched using EC and BR data) (Fig.

19 and Table 5), representing an underestimate of predicted versus measured evapotranspiration of 42 % (Table 5). This was the largest margin of error, expressed as a percentage of modelled versus measured evapotranspiration, encountered at any of the sites in this study. Despite this substantial underestimation, a regression analysis of modelled and measured data returned a r^2 value of 0.67 for the 235 day period (Fig. 20 and Table 5), and is within the mid range of values reported for several published models reviewed by Glenn, *et al.*, (2010).

Several uncertainties in model performance were identified at the Bellevue site, predominantly relating to:

- the high degree of variation in land cover within the MODIS pixel at the site, which introduces particular challenges to remote observation of vegetation characteristics and land cover, and radiative transfer modelling specifically (Garrigues, *et al*., 2008); and

- in relation to this, differences in footprint dimensions between micrometeorological instruments and satellite pixels, which leads to uncertainty in validation of modelled outputs in complex landscapes (Glenn, *et al*., 2007).

In particular, there were concerns regarding use of the LAI_{max} value 2.2, as it was considered unrealistically high for the surface comprising the SLS/EC/BR footprint; as alluded to above, this may have been an effect of higher biomass vegetation dominating spectral signatures at the pixel (*i.e.* high land cover variation in combination with differences in MODIS pixel size and flux footprint dimensions), although other possible errors, including uncertainties in RT modelling in mixed vegetation sites, and errors in land cover inputs to the RT algorithm, may have contributed, and are assessed in Section 5.4.

5.3.4 Groenkop

MOD15A2 LAI and vegetation phenological dynamics

Ecohydrologically, the Groenkop site is distinct from others assessed in this study; the system is characterized by significantly larger amounts of standing plant biomass, comprised of a largely homogenous and nearly closed canopy across the entire pixel area, which is reported to be phenologically relatively stable across the year (Dye, *et al*., 2008). The area receives

larger volumes of precipitation than both the Skukuza and Bellevue sites (with a MAP of 860 mm, relative to 560 and 724 mm at Skukuza and Bellevue, respectively), with peaks in March and October/November (autumn and early summer), although it is located on the eastern verge of the winter rainfall region of South Africa; this is significant in plant physiological terms in that, in contrast to the Skukuza and Bellevue sites, periods of high evaporative demand in summer and precipitation maxima do not entirely coincide. Long-term LAI was again analyzed to determine MODIS algorithm performance in this evergreen mixed indigenous forest system, and to characterize trends and patterns in vegetation phenology.

In contrast to the Skukuza and Bellevue sites, long term phenological patterns at Groenkop demonstrate significant inter and intra-annual variation in LAI in the winter months (as opposed to predominantly in the summer months in Skukuza and Bellevue, located in summer rainfall regions), with large variation about the mean at these times, and relatively consistent values in summer months (Fig. 21B). Long-term average maxima of approximately 6.1 LAI are noted in summer, with values in winter fluctuating erratically between approximately 2.4-5.9. Annual LAI for 2004 reflect long-term patterns described above, with highly erratic fluctuations in winter months, and relatively more consistent patterns in summer (Fig. 22).

Maximum and minimum LAI retrieved over the nearly 10-year period of data availability was 8.8 (retrieved on a single occasion), and 0.5 (retrieved on a single occasion), respectively, with frequency distribution demonstrating negatively skewed values and a predominance of retrievals between ~4.8-6.3 (Fig. 21A). Seasonal amplitude in LAI at this site was 70 % (LAI = 3.4) of the long-term average (4.9) which, although the lowest peak to trough difference for all the sites assessed in this study, is still considered high for this system relative to values reported at other evergreen broadleaf forest sites (Dye, *et al*., 2008; Myneni, *et al*., 2007). These data largely contradict the observations of Dye, *et al*. (2008), who suggest that Groenkop forest is characterized by generally stable canopy dynamics across the year, with a combined canopy and understory LAI of approximately 4.

LAI retrieval quality

Phenological patterns described by the algorithm at this site demonstrate a high proportion of erratic, apparently non-physical values, particularly in the winter months, as described above. Both LAI maxima and minima returned over the period of analysis, 8.8 and 0.5 respectively,

appeared to be beyond realistic bounds expected for this system, with long-term average LAI (4.9) exceeding that reported by Myneni, *et al*. (2007) for the Amazon forest (4.7), based on 5-years of data retrieved using the Collection 4 version of the RT algorithm. On this basis, it was concluded that MODIS was generally unable to realistically describe canopy phenological dynamics in this system, with particular inaccuracies evident during winter months.

Retrievals performed via respective execution branches of the algorithm in 2004 are plotted in Figure 22. Relatively high instances of retrievals performed by the backup algorithm (13 % of retrievals in 2004), considered low quality, and the RT algorithm with saturation (54 %), considered moderate quality, are evident (Yang, *et al*., 2006); the proportion of best quality retrievals successfully executed by the RT algorithm, just 33 % in 2004, was the lowest by a significant margin of all the sites assessed in this study.

Two factors explain the occurrence of retrievals by methods other than main RT approach in this instance: firstly, as described earlier, RT algorithm failure occurs in high cloud conditions and conditions of atmospheric contamination; the southern Cape region of South Africa experiences frequent frontal systems, associated with significant cloud cover, that pass over this region of the country during winter (Dye, *et al*., 2008), and would seem to explain observed RT algorithm failure almost exclusively at this time of the year. Secondly, retrievals over dense vegetation canopies, typically above 3.5 LAI, can result in saturation of the optical signal, where low sensitivities of LAI to surface reflectances occur, a condition described as saturation and which results in inaccuracies in modelled LAI (Shabanov, *et al*., 2005). Several improvements were implemented to the RT algorithm to address this issue, discussed in Section 5.4.4.

Comparison of modelled and measured water fluxes

ET_{MODIS} was evaluated over three discrete periods of four, seven and seven days in February, June, and September/October in 2004 (Figs. 24A, 25A and 26A). Modelled evapotranspiration for these periods was 9.7, 10.3 and 17.0 mm respectively, relative to measured evapotranspiration of 12.5, 11.6 and 22.4 mm (LAS system) (Table 5). These figures represent an underestimation of modelled versus measured evapotranspiration in each case of 22.4, 11.2 and 24.1 mm respectively (Table 5).

Linear regression models fitted to ET_{MODIS} and LAS data returned r^2 values of 0.98, 0.43 and 0.8 for the February, June and September/October validation datasets respectively (Figs. 24B, 25B, 26B and Table 5), with values in the winter validation periods representing the highest returned for any of the sites assessed in this study; conversely, the summer value represented the second lowest returned for any site. Given the high proportion of retrievals by execution branches other than the main RT algorithm at this site, each data point used in validation was labelled to indicate which retrieval approach was applied, thus contributing to establishing confidence limits in the data, where 0 = main RT algorithm (best possible quality), 1 = RT with saturation (moderate quality), and 3 = backup algorithm (poor quality). Modelled data clearly demonstrate better agreement with measured data during summer (r^2 = 0.98 and 0.8 in February and September/October, respectively), with significantly poorer agreement during winter (r^2 = 0.43 in June). This is despite the fact that the single retrieval used in validation in February was performed using the backup algorithm, reportedly of low quality. Two retrievals used in the September/October validation period were both performed using the main RT approach, while two retrievals used in the June validation period were performed using the backup approach and RT approach with saturation, respectively; this would in part explain the poor agreement observed in the data in June.

There were significant uncertainties and potential sources of error identified in model application at the Groenkop site, relating predominantly to the apparent unreliability of LAI retrievals by the RT and backup algorithms, particularly in winter, submitted to ET_{MODIS}; to a lesser extent, similar to the LAS site at Skukuza, the small number of data points available for validation and effects of discrepancies in temporal scales of input LAI data and modelled outputs, were also of concern, and would have been a factor despite high r^2 values in summer validation periods.

5.4 Uncertainties in ET_{MODIS} and measured flux data

Several potential sources of error and uncertainty were identified in model performance and evaluation, discussed in Sections 5.3.1 to 5.3.4, which have implications either for model performance directly (*i.e.* model accuracy), or validation (*i.e.* the measure of model performance); the former imply errors in ET_{MODIS}, while the latter imply errors or uncertainties in the approach to evaluation of ET_{MODIS}. Five broad types of error and uncertainty are identified:

1. uncertainties in measured evapotranspiration data from ground-based instrumentation used in validation in each case;

2. differences in the flux components being evaluated;

3. differences in flux footprint dimensions of ground-based instrumentation and MODIS pixels in complex landscapes, and uncertainties related to scaling up;

4. uncertainties in the RT algorithm and inputs, and ultimately MOD15A2 LAI submitted to ET_{MODIS}; and

5. uncertainties in ET_{MODIS}, including assumptions and parameterization.

These are discussed in the following sections.

5.4.1 Uncertainties in measured flux data and limits of instrument accuracy

Micrometeorological instruments have generally been shown to be capable of delivering high quality estimates of surface fluxes in most ecosystems, assuming rather extensive criteria regarding instrument set-up (including minimum fetch requirements and sensor configurations) and data analysis and processing are met (Savage, *et al*., 2004; Glenn, *et al*., 2007; Zeweldi, *et al*., 2009). They remain subject to several sources of error and uncertainty however (Glenn, *et al.*, 2007), which may ultimately yield inaccuracies in validation of modelled outputs. Glenn, *et al*., (2007) review several studies assessing the performance of EC systems in a range of conditions, concluding that flux estimates from these systems are associated with errors in the order of 20-30 %, as validated by independent techniques; errors may be systematic (*i.e.* apply consistently to all or parts of the daily cycle) or random (Moncreiff, *et al*., 1996). They report a similar spread in values (20 %) for estimates obtained in experiments using the BR technique. While any errors or inaccuracies in measured flux data used for validation in this study could not be quantified, there were some concerns regarding certain datasets in particular, which demonstrated a number of apparent anomalies; these included EC data from the flux tower at Skukuza, and SLS data from Bellevue.

Cursory observation of EC (Fig. 7) and LAS (Fig. 12) data at the Skukuza sites revealed marked differences in the magnitude of evaporative fluxes registered at respective sites and

years, where EC data demonstrate consistently lower values than the LAS instrument where datasets overlap (Figs. 7 and 12; the same data are plotted in Figure 27 for comparison). While any comparison of these data must be done with caution, and cognisant of specific, variable microclimatic conditions driving evapotranspiration at each site between years, it may nevertheless be reasonable to expect some level of agreement between the data, given the proximity of the sites, and similarity in biophysical conditions and MODIS LAI values observed in each case (Figs. 6 and 11). Despite the large discrepancies in precipitation between years at Skukuza however, where approximately double the amount of precipitation in 2005 was recorded in 2007, evapotranspiration recorded by the LAS in 2005 over two discrete periods was markedly higher than that recorded by the EC in 2007 (Fig. 28). Observation of cumulative rainfall for respective periods reveals that greater volumes of precipitation fell in the first months of 2005 relative to 2007 (Fig. 27), however; in combination with the possibility of higher levels of soil moisture storage in 2005 at the LAS site, this may to some extent explain this phenomenon. Nevertheless, other than to note these apparent discrepancies, without additional field measurements it is difficult to make any conclusions regarding the accuracy of respective datasets however.

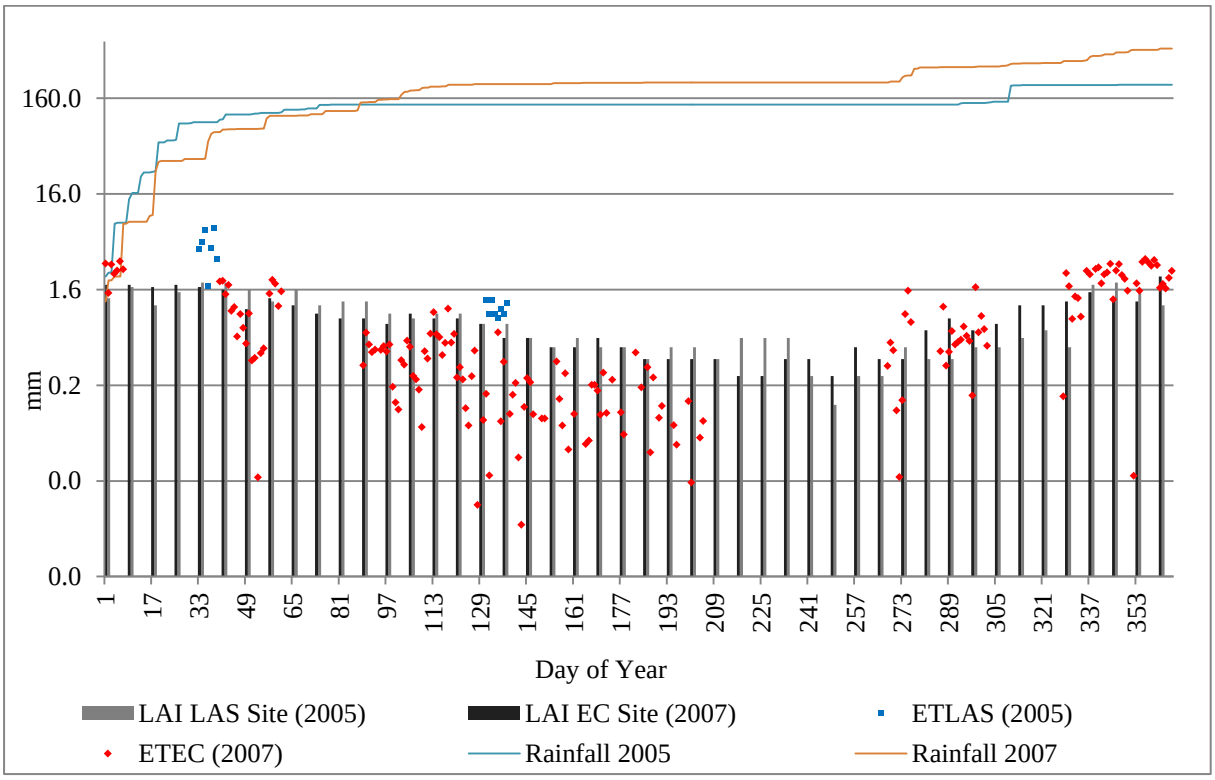

Figure 27: Comparison of EC and LAS data for Skukuza sites in 2005 and 2007 respectively, indicating LAI for both years (y axis is logarithmic).

The other instance where concerns regarding measured flux data emerged was Bellevue, where seemingly high rates of evapotranspiration were recorded by the SLS (patched with BR and EC data) instrument deployed at the site in 2003. For 365 days in 2003, 634.6 mm evapotranspiration was recorded by Savage, *et al*., (2004), which exceeded rainfall of 478.9 mm for the same period. Evapotranspiration may exceed precipitation in certain cases where plants are able to access stored soil moisture, or where soil moisture is augmented, for example by fog drip or lateral water flows in the soil profile (Dye, *et al*., 2008), and has been noted to occur in the KwaZulu-Natal midlands area where significant mist events may occur (Clulow, 2007). Significant disagreement between ET_{MODIS} and ET_a in this instance (evapotranspiration was under-predicted by 42 %) however, in combination with the fact that annual ET_a exceeded precipitation, perhaps suggest that closer examination of validation data at this site may be required.

5.4.2 Differences in flux components being evaluated

A second contributing factor to the observed differences in modelled and measured data may be attributable to differences in the flux component/components being evaluated in respective approaches; ground-based micrometeorological instruments measure total moisture flux, *i.e.* evaporation from soil and canopy surfaces, and transpiration from vegetation, within the flux footprint, whereas ET_{MODIS}, being based entirely on the FAO-56 equation (which calculates ET_0 for a fully vegetated surface) and LAI, effectively provides an estimate of transpiration only. Because transpiration dominates evaporative fluxes in most systems (Williams, *et al*., 2004), potential error introduced into modelled evapotranspiration in this way is probably negligible, however, may theoretically become significant where vegetation cover is very low and soil evaporation represents a larger component of total evapotranspiration; this is difficult to account for given that there is no easy way to differentially measure evaporation and transpiration simultaneously.

Both Bellevue and Groenkop sites almost certainly comprised full, actively photosynthesizing vegetation cover throughout periods of validation, and evaporation is likely to have comprised a negligible proportion of total moisture flux; however, during the dry season in Skukuza, when much of the vegetation becomes dormant, evaporation from soil surfaces may have represented a significant fraction of total evapotranspiration, and the inability of ET_{MODIS} to account for these fluxes could potentially have introduced measurable error. The 15.7 % underestimate of evapotranspiration by ET_{MODIS} relative to the LAS in

2005 would support this reasoning (Table 5); in contrast however, the 31.7 % overestimate of evapotranspiration relative to flux tower measurements in 2007 suggests that any error introduced by neglecting soil evaporation by the model was, in this instance, relatively insignificant.

5.4.3 Differences in MODIS pixel size and ground-based flux footprint dimensions in complex landscapes

Differences in the dimensions of the MODIS pixel and flux footprints of micrometeorological instruments introduces significant uncertainty into validation, given that it is difficult to determine to what extent ground-based flux measurements are representative of conditions within the satellite pixel; this uncertainty is compounded in complex landscapes and where differences in pixel/footprint dimensions are large (Glenn, *et al*., 2007). Validation sites for this study were specifically selected to limit landscape complexity to the extent possible, however, there were concerns at the Bellevue site, where large differences in micrometeorological flux measurement footprint and MODIS pixel area occurred, in combination with a high degree of surface heterogeneity (Figs. 3 and 28). Fetches reported by Savage, *et al*., (2004) for the SLS and EC instruments were 90 and 138 m for transmitter and receiver respectively in prevailing north westerly winds (SLS), and 135 m for the portable EC instrument, significantly smaller than the 1 km^2 MODIS pixel area (Fig. 28).

Figure 28: Aerial image of the Bellevue site (MODIS pixel footprint in white outline) indicating the SLS path to the NW; high land cover variation is evident, with high plant biomass loads visible to the south and east of the SLS flux footprint.

In this case, it would be expected that natural grassland/woody savanna areas and riparian vegetation components to the south and east of the pixel would typically dominate spectral reflectances in the MODIS pixel, resulting in LAI observations unrepresentative of spectrally weaker areas (such as would be expected for the flux footprint area of micrometeorological instrumentation) and the pixel as a whole, ultimately introducing error into modelled data, and disagreement with measured fluxes.

Both Groenkop and Skukuza sites (EC flux tower and LAS) on the other hand demonstrated little or no visible land cover variation within the MODIS pixels used in validation (Figs. 2 and 4), largely eliminating any uncertainty in this regard. In addition, the flux footprint of the LAS instruments used at Skukuza in 2005 and Groenkop, given its capability for longer beam path lengths (4250 and 3200 m respectively), is better representative of the 1 km^2 MODIS pixel area than both the SLS instrument, as well as the EC flux tower, with a fetch of 600 m in the prevailing wind direction at Skukuza.

In addition to these uncertainties, land cover variation also presents several complex challenges to remote observation of vegetation characteristics, as well as the radiative transfer

algorithm and remotely-sensed inputs specifically (Privette & Roy, 2005; Garrigues, *et al*., 2008), introducing further uncertainty into model validation. With regards to the former, mixed vegetation types and vegetation clumping at sub-pixel scales are generally not well described by global radiative transfer models (Garrigues, et al., 2008), and present particular difficulties to remotely-sensed land cover classification, which is a key input to the MODIS RT algorithm (discussed in Section 2.7.1); these uncertainties are addressed in the following section.

5.4.4 Uncertainties in LAI RT algorithm, and algorithm inputs

Remotely-sensed LAI is a key input to ET_{MODIS}, and although no rigorous sensitivity analysis was conducted in this study, model performance is recognised to be highly sensitive to LAI estimates provided by the MODIS RT algorithm. Generally, the quality of LAI modelled using the RT algorithm is determined by two main factors:

1. uncertainties in algorithm inputs (surface reflectances retrieved by the MODIS instrument and land cover inputs derived from the MOD12Q1 product); and

2. model uncertainties, or the consistency between RT simulations stored in the algorithm LUTs, and corresponding MODIS surface reflectances (Shabanov, *et al*., 2005).

While it was not possible to assess uncertainties relating to MODIS surface reflectances and inconsistencies with LUT simulations stored in the algorithm directly, published literature dealing with validation of the LAI product was reviewed to establish algorithm performance in the systems encountered in this study, particularly broadleaf forests, given the high proportion of low quality retrievals observed in this study. A large number of publications are available that address the issues of validation and uncertainty in the LAI products (for example, Privette, *et al*., 2002, Shabanov, *et al*., 2005; Heinsch *et al.,* 2006; Garrigues, *et al*., 2008).

Algorithm failure and overestimation of LAI in broadleaf forests, specifically in earlier versions of the product, were discovered to be due to inaccurate radiative transfer parameters (specifically leaf albedo), the fact that no distinction was made between evergreen and deciduous broadleaf classes, and a high sensitivity of the algorithm to noise in surface reflectances for high LAI in the saturation domain. Several improvements were introduced to

the most recent version of the algorithm, termed Collection 5 (utilized in this study) to address these issues. Key improvements include an eight biome land cover classification system (as opposed to the six biome system incorporated into Collection 3, and earlier versions of the algorithm), where broadleaf and needle leaf forest classes are divided into evergreen and deciduous sub-classes, and improvements in RT simulations in the saturation domain (a new stochastic radiative transfer model was applied, allowing better representation of canopy structure and spatial heterogeneity typical of woody biomes, and to achieve improved radiometric consistency between simulated and MODIS reflectance values) (Shabanov, *et al*., 2005). Recalculations by the new stochastic RT model resulted in an increase of 10-15 % in the proportion of global retrievals performed by the best quality main algorithm in forest biomes, and Collection 4 anomalies over deciduous broadleaf forests (overestimation through the year and failure in summer) and evergreen needleleaf forests (overestimation of seasonal peak) were significantly reduced (Yang, *et al*., 2006). Despite these improvements in the algorithm, the accuracy of retrievals is, however, ultimately limited by the accuracy of MODIS surface reflectance inputs.

Several steps have been introduced in an attempt to reduce error in this regard, including compositing to limit the effect of cloud and aerosol contamination (Knyazikhin, *et al*., 1999), utilizing data retrieved at different overpass times (either from Terra, which retrieves data in the morning, or Aqua, which retrieves in afternoon), and the combination of reflectance data from both Terra and Aqua to ensure that best available data is used (Mùnch, *et al*., In Press). Recent LAI products from the Aqua satellite, and combined Terra/Aqua products, are discussed later in this thesis.

Land cover classification uncertainties

With regards to uncertainties relating to land cover inputs specifically, these may be relatively easily evaluated by interrogating the MOD12Q1 land cover dataset submitted to the RT algorithm in the MOD15A2 product. Land cover, in combination with MODIS spectral information, is a key input into the RT algorithm affecting retrieval quality (Shabanov, *et al*., 2005). It determines unique model configurations and fixed parameter values appropriate to each biome that yield information on vegetation architecture and radiative transfer regimes (Privette, *et al*., 2002; Kauwe, *et al*., 2011). Land cover classification utilized in the Collection 5 RT algorithm is based on the IGBP system, comprising eight classes differentiated according to grasses and cereal crops, shrubs, broadleaf crops, savannas,

broadleaf forests (with evergreen and deciduous subclasses), and coniferous forests (with evergreen and deciduous subclasses).

The MOD12Q1 land cover classification for each of the MOD15A2 pixels assessed was interrogated to establish confidence limits in algorithm performance; the analysis confirmed correct classification in all cases with the exception of the Bellevue site, which was incorrectly classified as “urban and built up” (Fig. 29B). The extent to which erroneous land cover classification may have forced errors in LAI values modelled by the RT algorithm (and ultimately propagating into errors in ET_{MODIS}) is not quantified, although non-physical values would be anticipated. Land cover classification errors would seem to present a somewhat intractable problem in global remote sensing approaches of this nature, particularly in highly complex and dynamic landscapes, where classification based on spectral information is inherently more challenging; this is amplified in moderate resolution products such as MODIS, where large variation in land cover may occur within individual pixels footprints, in this case 1 km^2.

A.

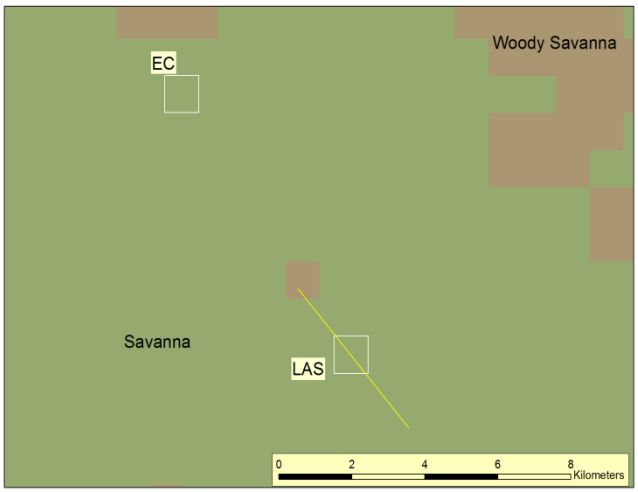

B.

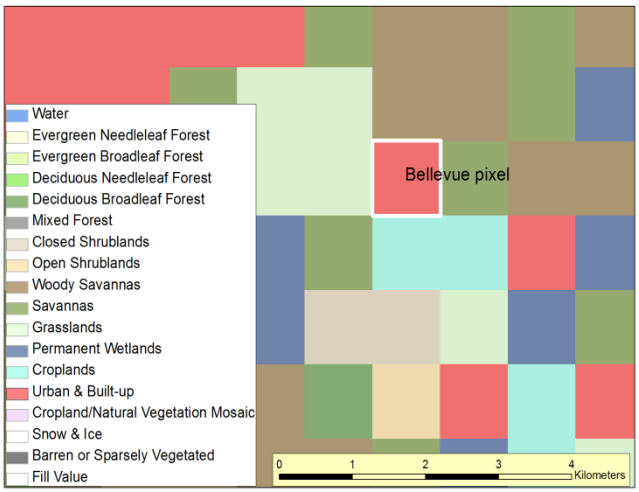

C.

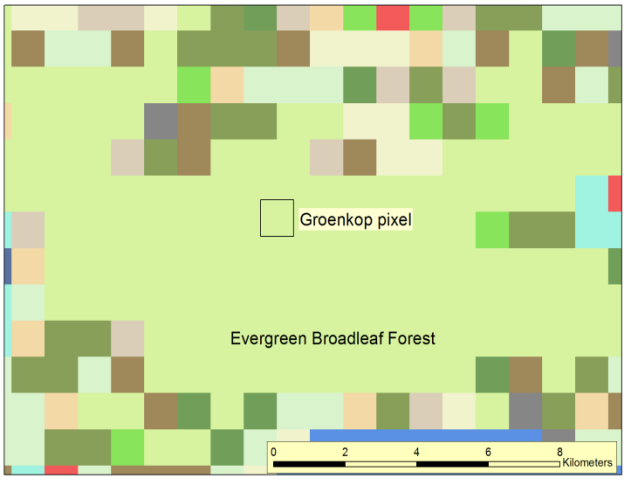

Figure 29: MOD12Q1 Land cover classification for A. Skukuza, B. Bellevue, and C. Groenkop sites.

5.4.5 Uncertainties in ET_{MODIS}, and parameterization of terms:

The fifth type of uncertainty relates to ET_{MODIS}, including its theoretical basis and assumptions, as well as specific uncertainties related to parameterization of input variables, including the following:

- the assumption that ET_a never exceeds ET_0;
- uncertainties associated with identification of pixel LAI_{max} input to ET_{MODIS};
- uncertainties associated with potential microclimatic differences at weather stations used to calculate FAO-56 input to ET_{MODIS}, and flux measurement sites;

- conflicts in temporal resolution of input MODIS LAI data, and modelled daily evapotranspiration outputs; and
- uncertainties associated with the use of class A-pan data to parameterize ET_{MODIS} in the absence of suitable FAO-56 data.

These points are discussed below.

Model assumptions:

A key assumption of ET_{MODIS} is that ET_a never exceeds ET_0, assumed to occur when LAI = LAI_{max} (Equation 20); this relationship determines the scaling of ET_a from ET_0, and therefore has fundamental implications for model performance. However, this assumption may not always hold, specifically in systems characterized by very high LAI, such as forests; the FAO definition of a reference surface is defined as a grass surface of uniform height in full physiological activity, where surface resistance is 70 s m^{-1} with an assumed (active) LAI of half actual LAI, where LAI is assumed to be 24 x vegetation height (0.12), resulting in active LAI of 1.44 (Equations 16 and 17, Chapter 2) (Allen, et al., 1998). Dye, *et al.*, (2008) reported that reference evapotranspiration as calculated by the FAO-56 method underestimated measured fluxes (LAS) at Groenkop forest when ET was high, and overestimated fluxes at low ET, which they suggest is due to the assumption of a constant surface resistance in the FAO-56.

Although the relationship between LAI and canopy conductances appears to be non-linear and variable due to changes in leaf-level stomatal conductance rates in response to external stimuli, given the large difference in the LAI of these surfaces (maximum LAI retrieved at Groenkop was 6.8; Fig. 21A), it would be reasonable to assume that these systems are capable of higher rates of evapotranspiration than the FAO reference surface, borne out by the results of Dye, et al. (2008). This would suggest that the range of systems within which ET_{MODIS} may confidently be applied should be restricted to those with LAI values that at least approach those assumed for the reference surface.

Uncertainties regarding identification of pixel LAI_{max}

The maximum LAI parameter value submitted to ET_{MODIS} (LAI_{max}) has significant implications for model performance. The approach assumes that optimal levels of

productivity are achieved in the system within the approximately 10-year time-span of MODIS data (represented by the LAI_{max} value returned for some 460 retrievals), thus establishing the upper bound against which system performance and water use is scaled in ET_{MODIS}. However, given that remotely sensed data are by nature prone to multiple sources of uncertainty, some difficulty was encountered in attempting to solve LAI_{max} in an objective manner in certain cases. At the Bellevue and Groenkop sites in particular, several seemingly anomalous LAI values were returned over the 10-year period of analysis; in combination with relatively high incidences of low quality retrievals performed with the backup algorithm at Groenkop, and the RT algorithm with saturation, significant uncertainty was introduced into parameter selection at these sites.

Maximum LAI values retrieved by MODIS, and submitted to ET_{MODIS}, at Groenkop over the approximately 10-year period of analysis was 6.8, and 2.2 at Bellevue (Figs. 15A and 21A respectively), both of which are considered uncharacteristically high for these systems (Asner, *et al*., 2003; Dye, *et al*., 2008; Myneni, *et al*., 2007) (see Sections 5.3.3 and 5.3.4 for a discussion of retrieval uncertainties at these sites). To evaluate the effect of non-physical LAI_{max} values submitted to ET_{MODIS} on model results, the model was run using a parameter value of 1.7, the average LAI for grasslands based on the results of 28 studies using various destructive and non-destructive approaches, and synthesized by Asner, *et al.,* (2003). Based on this value, ET_{MODIS} predicted 344.65 mm evapotranspiration for the 235 days of flux data availability relative to ET_{AVE} of 460.19, representing an underestimate of 25.1 %, as opposed to 42.0 % using the 2.2 LAI_{max} parameter value (the coefficient of determination obviously remains unchanged). This demonstrates the sensitivity of ET_{MODIS} to LAI_{max}, where an inverse relationship between LAI_{max} and modelled evapotranspiration exists.

Proximity of weather stations used to calculate FAO-56 inputs to ET_{MODIS} to flux measurement sites

FAO-56 calculations used to derive ET_{MODIS} are in most instances based on micrometeorological data recorded at the nearest operational automatic weather station (where indicated, however, class A-pan data were submitted due to an absence of operational automatic weather stations within reasonable proximity to validation sites), which vary in proximity to respective validation sites. Differences in micrometeorological conditions measured at weather stations, determining the ET_0 component of $ET_{MODIS,}$ were assumed to be negligible, and the effect of distance has largely been ignored; differences in

micrometeorological conditions may conceivably become a factor where larger distances, or significant differences in altitude occur, however.

Application of ET_{MODIS} at both Groenkop and Bellevue utilized FAO-56 inputs calculated based on data recorded at the sites themselves at validation periods, and A-pan data for remaining periods, measured at distances no further than 12 – 13 kilometres away. While variations in micrometeorological conditions were likely negligible in these instances, the distances between flux measurement sites at Skukuza and the location of Malekutu weather station used in calculating the FAO-56 input were significantly larger, approximately 42 kilometres in each case, although the altitudinal difference was relatively small: 538 m at Malekutu and 365 m at the flux measurement site. To establish whether micrometeorological differences may have been a factor in model performance, ET_0 calculations from an earlier time period, recorded at the nearby Skukuza weather station[4] located some 11.5 kilometres from the flux measurement sites, were compared to calculations from the Malekutu station for the same period; little discernible difference was noted between the datasets, and it was concluded that differences in micrometeorological conditions were unimportant despite the relatively large distance separating measurement sites in this instance.

Conflicts in temporal resolution of input LAI data and modelled daily evapotranspiration

The MOD15A2 LAI products are produced as 8-day composites, where the highest LAI value observed over the composting period is returned (Knyazikhin, *et al*., 1999); there is a clear conflict in using temporally coarse data to produce higher resolution modelled outputs, in this case at daily time-steps. Where estimates of water use are required over shorter time periods, these discrepancies in temporal resolution of model inputs may result in potentially significant inaccuracies in evapotranspiration estimates by ET_{MODIS}, particularly where daily variation in LAI is high; this may to some extent have explained the poor agreement between modelled and measured fluxes observed in June 2005 at Skukuza, where a coefficient of determination of 0.36 was returned over a period of 8-days (Fig. 14B and Table 5).

Model errors introduced through the submission of course resolution inputs can be resolved by increasing the temporal resolution of inputs, or degrading the resolution of modelled outputs; for water resource management applications, estimates of water use at daily time-

[4] Skukuza meteorological station (SANParks) is located in close proximity to the flux tower and LAS sites, however no microclimatic data were available for periods corresponding with validation in this study.

steps are desirable, and it is therefore preferable to increase the temporal resolution of LAI data submitted to the model, rather than degrade the resolution of model outputs. A combined LAI product (*i.e.* incorporating spectral information from both Terra and Aqua satellites) (MCD15A3) with a shorter 4-day compositing period became operationally available during the course of this research, and provides an opportunity to better match data input and output resolution. Its use within an FAO-56 formulation presents an opportunity for future investigation.

Use of FAO-56 with class A-pan data

In several instances, particularly in long-term (annual) applications of ET_{MODIS}, it was necessary to rely on class A-pan data to parameterize ET_{MODIS} where FAO-56 data were absent; as class A-pan provides a measure of evaporative demand of the atmosphere only, without accounting for vegetation controls on moisture fluxes, use of these data would inevitably introduce errors into ET_{MODIS}, although were not quantified in this study. In nearly all cases, validation was performed using model outputs based on the FAO-56; however, A-pan data was used at Bellevue, and would be expected to have influenced model performance at this site. Gaps in data availability are a recurring problem in applications of this nature, and class A-pan data were applied in this study to demonstrate the potential for secondary data sources where circumstances dictate.

5.5 ET_{MODIS} - opportunities and constraints to general application for water resource management objectives

Scientifically rigorous, rule-based approaches to dealing with several key aspects of uncertainty would need to be developed in any attempt to operationalize ET_{MODIS} for application over wider areas in South Africa; leading on from the points discussed in Section 5.4.6, these relate to the following issues:

- Selection of LAI_{max} value submitted to ET_{MODIS}

The difficulties relating to objective selection of appropriate LAI_{max} values for input to ET_{MODIS}, and the implications of variations in the LAI_{max} value for model performance, have been demonstrated in Section 5.4.6; MODIS pixel-level quality assessment information supplied with each image tile provides a useful first approach to evaluating reliability of retrievals, although significant uncertainty remains that is not described, particularly where complex land cover types are encountered (discussed below). A consistent, defensible

approach to identifying LAI_{max} values for input to ET_{MODIS} for the range of landscapes assessed would therefore be needed, and represents a significant challenge to operationalizing the approach over wider areas.

- Model application in complex landscapes, and resulting uncertainty

Related to the first point, landscape complexity presents particular difficulties in terms of remote observation of vegetation characteristics, including radiative transfer modelling, and land cover classification; issues relating to mixed pixels where spectral signatures may be dominated by spatially unrepresentative but high biomass vegetation types has been discussed in Section 5.4.6, as have the complexities of accurate land cover classification, particularly by moderate resolution sensors in these conditions.

Several errors in land cover classification in the MOD12Q1 product (submitted to the RT algorithm) were encountered in the approach to this study, particularly in the Bellevue area, assumed to be attributable to the high variation of land cover in the region (Figs. 3 and 29B). Heterogeneous commercial and subsistence production landscapes characterize much of South Africa's higher rainfall areas, and are often where information on evapotranspiration is especially needed, coinciding with areas where uncertainties in terms of remotely LAI inputs are likely to be highest. In this context, the quality of water use estimates required will set limits with respect to the degree of catchment land cover heterogeneity within which the model could confidently be applied (*i.e.* defining acceptable levels of uncertainty), where a need for high confidence estimates would effectively exclude heterogeneous catchments.

- Representivity of climate data used to calculate ET_0 input to ET_{MODIS}

In any application of ET_{MODIS} at landscape scales, the footprint of flux estimation, ultimately at the level of the individual MODIS pixel, will with few exceptions be separated in space from the localities of ground-based weather stations at which weather data required to calculate the ET_0 component of ET_{MODIS} must be acquired. Given the uncertainty that potential differences in microclimate introduces to modelled outputs, rules would be required describing the acceptable range (in terms of distance; altitude) within which these data remain representative with respect to pixel (LAI) locations.

- Algorithm performance in forest biomes

Despite the improvements to the RT algorithm implemented in Collection 5 MOD15A2 data to address high incidences of algorithm failure reported in earlier versions in broad-leaf forests (Shabanov, *et al*., 2005; Garrigues, *et al*., 2008), in the approach to this study, LAI retrievals were found to be highly erratic and generally unrealistic in this biome, particularly in winter, and specifically in indigenous broadleaf forests; interrogation of quality assessment data at Groenkop in 2004 revealed high proportion of retrievals by the backup algorithm (in winter), and main approach with saturation (throughout the year). Although information on cloud state, provided with the MOD15A2 data, was not interrogated, this is expected to be the cause of algorithm failure in these instances.

In addition to the Groenkop site reported in this study, it is noted that similar results were obtained at several other forest sites not reported here. Based on these results, MODIS LAI retrievals over forests in South Africa appear to be associated with unacceptable levels of uncertainty, and given the unreliability of LAI inputs, ET_{MODIS} is probably unsuitable as an approach for estimating continuous vegetation water use in these systems.

6. Summary & Conclusions

With growing human pressures on land and water in this century, it is widely acknowledged that integrated approaches to water resource management, in which explicit recognition is given to the connectivity of the hydrological cycle and the role of vegetation in water balance partitioning, are key to sustaining the country´s future water requirements. Post-Apartheid water legislation and policy, which strongly embraces the ideals of Integrated Water Resource Management (IWRM), provides a clear mandate to accomplish this, recognising that land use activities may have significant impacts on the hydrological cycle and should be regulated in terms of consequences for water resources. A major obstacle to achieving integration of land and water resource management to any real extent however, has been the technical difficulty of measuring the water use of land-based activities at appropriate time and spatial scales. Currently, satellite remote sensing is the only method by which criteria in respect of data continuity and spatial and temporal resolution can be met (Glenn, *et al*. 2007).

In this thesis, a novel evidence-based approach for deriving continuous, spatially distributed estimates of evapotranspiration at daily time-steps and 1-kilometre spatial resolution is

described, based on functional convergence theory (Field 1991), and using the standard 8-day MODIS LAI product to adjust the FAO-56 Penman-Monteith equation according to vegetation physiological status. The approach responds to the need for simple, yet theoretically robust satellite-based techniques for the estimation of actual evapotranspiration over large landscape areas in South Africa, which typically demands relatively complex methodologies requiring extensive parameterization procedures (Gibson, *et al.*, 2009; Mùnch, *et al*., In Press). ET_{MODIS} was tested at four sites located within three different ecosystems in South Africa, using validation flux data measured in earlier studies by means of EC and BR systems, and both large aperture and surface layer scintillometers; with two exceptions, ET_{MODIS} was able to produce estimates of vegetation water use to within11.2– 24.1 % of measured fluxes, applied over a wide range of time periods (4 – 235 days) (Table 5). Coefficients of determination, describing the extent to which observed fluxes are explained by the model, again with two exceptions, ranged between 0.67 – 0.98, and are within the range of values reported for several published satellite-based evapotranspiration models reviewed by Glenn, *et al*., (2010). While the outliers cannot be ignored, potential causal factors with respect to these four instances where relatively large discrepancies in flux volumes and poor agreement between modelled and measured data were observed are comprehensively examined.

Analysis of the possible causes of errors of uncertainty highlighted a variety of potential underlying causes for biases observed between modelled and measured data; broadly, these relate to:

- uncertainties and potential error in measured data used in model evaluation, which have implications for model performance measures (*i.e*. errors in validation);

- uncertainties and error in MODIS LAI input to ET_{MODIS}, which have direct implications for model accuracy; and

- uncertainties and error in ET_{MODIS} itself, including model assumptions and parameterization.

Of these, probably the most significant source of uncertainty relates to model application in complex landscapes. Landscape heterogeneity presents particular difficulties to remote observation of land cover and vegetation characteristics, including LAI, particularly over the larger spatial scales of the moderate resolution sensors. Due to the sensitivity of the ET_{MODIS} to LAI inputs, inaccuracies in this term yield potentially significant errors in modelled outputs; this is problematic given that much of South Africa's higher rainfall catchments, where estimates of vegetation water use are often particularly needed, are characterized by heterogeneous commercial and subsistence production landscapes.

Also of concern is the assumption by ET_{MODIS} that ET_a never exceeds ET_0 (given that ET_0 is based on a hypothetical surface in full physiological activity and never water limited) and that $ET_a = ET_0$ when $LAI = LAI_{max}$. Earlier studies indicate that evapotranspiration in highly productive ecosystems does in fact exceed rates calculated for the FAO reference surface. Although the relationship between LAI and canopy conductance is non-linear and varies due to stomatal responses to environmental stimuli (Dye, *et al*., 2008), given that stomatal conductance is unknown, higher LAI must be assumed to equate with higher canopy level conductance; this would suggest that model application should strictly be limited to systems where LAI approximates that of the reference surface. Allen, *et al*., (1998) calculate photosynthetically active leaf area as half total leaf area, where leaf area = 24 x vegetation height (0.12 m), resulting in active LAI of 1.44, and total LAI of 2.9.

With respect to the opportunities and constraints of ET_{MODIS} as a viable approach for addressing queries regarding water use of land-based activities on an operational basis in South Africa, key issues relate to spatial and temporal scales required, and acceptable levels of uncertainty in modelled outputs. With regards to the former, spatial resolution of flux estimates by the model are ultimately determined by MODIS pixel resolution, which for all global LAI products currently available is 1 km^2; MODIS products were developed for application at global scales, however, at landscape and catchment scales, most relevant to water resource management objectives, particularly in complex landscapes, the lack of resolution of land cover heterogeneity at 1-km becomes increasingly significant. For practical purposes, this effectively limits the use of the approach to relatively homogenous landscapes, where the "minimum mappable unit" is 1 km^2. Application of the technique in complex landscapes is associated with a high level of uncertainty, increasing with the degree of heterogeneity, discussed in Section 5.4.

Regarding temporal resolution, the standard MOD15A2 product is delivered as an 8-day composite to reduce impacts of cloud and atmospheric contamination on retrievals, where the highest LAI value observed over the 8-day period is returned. Although MOD15A2 LAI is used to produce flux estimates at daily time-steps in this approach, this inevitably propagates error in modelled data, the significance of which is inversely proportional to the duration of observation. Essentially, therefore, confidence limits in daily time-step data are relatively lower, being optimal at 8-day time-steps. For water resource management purposes, where longer-term changes in water balance components are of interest, this may be adequate, however it presents a problem in ecohydrological research-related applications, where high levels of detail, and certainty, regarding fluctuations in vegetation water use are typically needed.

Finally in this respect, and related to these issues, a key factor in considering potential areas of application of ET_{MODIS} is the degree of certainty required in modelled outputs. The strength of the technique is its ability to offer continuous, spatially and temporally resolved estimates of vegetation water use at near-real time, the value of which lies in the high quality, validated remotely sensed LAI data, and its basis in sound, well-established physical theory, *i.e.* the FAO-56 Penman-Monteith equation. The simplicity of the approach may be perceived as both a strength and a weakness however, in that on one hand, parameterization requirements are low, reducing uncertainty and allowing widespread application, while on the other, important physical processes are neglected, for example soil and canopy evaporation, or changes in leaf-level stomatal conductances to ambient conditions, for example. Nevertheless, validation of model performance in this study suggests that it is in most cases able to produce flux estimates to within relatively close approximations of micrometeorological measurements. In this context, ET_{MODIS} offers a useful means to assess vegetation water use over wide areas and across time, where alternatives are to a large extent unavailable, although it remains experimental and confidence limits should be set on the basis of further testing.

6.1 Recommendations for further research

Several potential avenues of future research directed at improving the performance of the basic approach described in this study are evident, discussed below.

- Testing uncertainties

Primarily, such research would comprise further application of the model in a range of different ecosystems, and additional examples from the same ecosystems, towards testing the analyses of uncertainties presented in this thesis. This demands high quality validation data at scales which at least partially correspond with satellite pixel footprints, typically from micrometeorological instruments (and particularly the LAS instrument, given its capability for long path lengths, and therefore larger flux footprints), which are likely to become increasingly widely available in the near future as technologies become more accessible and affordable. This would contribute to describing the uncertainty in the model in its current form.

- New global MODIS LAI products

Since the release of the MOD15A2 8-day LAI product from the Terra satellite, and subsequent to the initiation of this study, additional Terra and Aqua, and combined Terra/Aqua four and eight day LAI products have become operationally available, including:

~ the 8-day MYD15A2 product from the Aqua satellite;

~ the Terra/Aqua combined 8-day MCD15A2 product; and

~ the combined Terra/Aqua 4-day MCD15A3 product.

The potential advantages of the Aqua/MYD15A2 and combined MCD15A2 products are associated with the different overpass times of the respective satellites (Terra captures images in the morning, and Aqua in the afternoon), which has important implications for spectral reflectances measured at the surface (Münch, *et al*., In Press). The potential implications for LAI and ET_{MODIS} would need to be determined.

The MCD15A3 product offers the opportunity to improve the temporal resolution of LAI inputs to ET_{MODIS}, and increase the confidence in modelled outputs at high time-steps. Evaluation would need to consider the potential compromise in quality of LAI given shorter

compositing periods however, in combination with the disadvantage of higher data processing requirements.

- MOD16 global ET product

At the time of preparation of this thesis, a global evapotranspiration product was newly released on an operational basis by the MODLAND team, based on the algorithm developed by Mu, *et al*., (2011), which uses the Penman-Monteith (Monteith, 1964) logic (as described in Section 2.6.4). Essentially, the MOD16 ET algorithm relies on gridded meteorological data and information on surface resistance, derived using the MOD15A2 LAI product to relate stomatal to canopy scale conductance, to produce 8-day, monthly and annual estimates of evapotranspiration at 1-km^2 spatial resolution. No comparison of MOD16 ET and ET_{MODIS} was performed during this study, however it would be interesting to evaluate the extent to which respective approaches demonstrate agreement. While the MOD16 ET product is based on advanced technique and physical theory, its designation as a global product inevitably implies certain trade-offs with respect to quality and precision of data inputs. ET_{MODIS} represents a significantly more simple approach than Mu, *et al*., (2011), however has the advantage of being based on local, real-time microclimatic data.

7. References

Allen RG, Pereira LS, Raes D, Smith M. 1998. *Crop evapotranspiration - Guidelines for computing crop water requirements.* Rome: FAO - Food and Agriculture Organization of the United Nations.

Allen RG, Clemmens AJ, Burt CM, Solomon K, O'Halloran T. 2005a. Prediction accuracy for projectwide evapotranspiration using crop coefficients and reference evapotranspiration. *Journal of Irrigation and Drainage Engineering-Asce* 131:24-36. 10.1061/(asce)0733-9437.

Allen RG, Pereira LS, Smith M, Raes D, Wright JL. 2005b. FAO-56 dual crop coefficient method for estimating evaporation from soil and application extensions. *Journal of Irrigation and Drainage Engineering-Asce*131:2-13. 10.1061/(asce)0733-9437.

Allen RG, Pereira LS, Howell TA, Jensen ME. 2011. Evapotranspiration information reporting: I. Factors governing measurement accuracy. *Agricultural Water Management* 98(6): 899-920.

Archibald SA, Kirton A, van der Merwe MR, Scholes RJ, Williams CA, Hanan N. 2009. Drivers of inter-annual variability in Net Ecosystem Exchange in a semi-arid savanna ecosystem, South Africa. *Biogeosciences* 6(2): 251-266.

Ashton, P. 2000. *Integrated Catchment Management: Balancing Resource Utilization and Conservation.* AWIRU Occasional Paper No. 5. African Water Issues Research Unit, Pretoria University. Available from Website http://www.up.ac.za/academic/libarts/polsci/awiru.

Ashton PJ, Hardwick D. Breen C. 2008. 'Changes in Water Availability and Demand within South Africa's Shared River Basins as Determinants of Regional Social and Ecological Resilience'. In Burns, MJ, Weaver AVB (eds), *Exploring Sustainability Science: A Southern African Perspective.* Stellenbosch: Stellenbosch University Press.

Asner GP, Scurlock JMO, Hicke JA. 2003. Global synthesis of leaf area index observations: Implications for ecological and remote sensing studies. *Global Ecology and Biogeography* 12: 191–205.

Ayra SP. 2001. Introduction to Micrometeorology. California: Academic Press.

Badenhorst JW, de Lange M, Mokwena ME, & Rutherfoord RJ, 2002. Water Conservation and Water Demand Management in Agriculture: Development of Water Management Plans by Irrigation Water Suppliers in South Africa. *ICID 18th Congress.* Montreal, Canada.

Baker J. 2008. Challenges and Cautions in Measuring Evapotranspiration. *Southwest Hydrology* 7(1): 24 - 33.

Baldocchi D. 2001. Assessing Ecosystem Carbon Balance: Problems and Prospects of the Eddy Covariance Technique. *Annual Review of Ecology and Systematics* 33: 1-33.

Bastiaanssen WG, Menenti M, Feddes RA, Holtslag AA. 1998a. A remote sensing surface energy balance algorithm for Land (SEBAL): Part 1. Formulation. *Journal of Hydrology*

Bastiaanssen WG, Pelgrum H, Wang J, Ma Y, Moreno J, Roerink R. 1998b. A remote sensing surface energy balance algorithm for land (SEBAL). Part 2: Validation. *Journal of Hydrology* 212 - 213:213 - 229. 10.1016/s0022-1694(98)00254-6.

Blaney H, Criddle W. 1950. Determining Consumption Use and Irrigation Water Requirements. Washington, D.C.

Blight, JJ, Gush, MB, Le Maitre, D and Jewitt, GPW. 2005. Impacts of afforestation on low flows: Paired catchment data revisited. *12th South African National Hydrology Symposium*, ESKOM Convention Centre, Midrand, South Africa. September 2005, pp 10.

Blignaut, JN, Marais C, Turpie JK. 2007. Determining a charge for the clearing of invasive alien plant species (IAPs) to augment water supply in South Africa. *Water SA* 33:27-34.

Bosch JM. 1979 Treatment effects on annual and dry period streamflow at Cathedral Peak. *South Africa Forestry Journal*, 108: 29-38.

Bosch JM, Hewlett JD. 1982. A review of catchment experiments to determine the effect of vegetation changes on water yield and evapo-transpiration. *Journal of Hydrology* 55(1-4): 3-23.

Bowen I. 1926. The ratio of heat losses by conduction and by evaporation from any water surface. *Physics Review* 27:779-787.

Burt CM, Mutziger AJ, Allen RG, Howell TA. 2005. Evaporation research: Review and interpretation. *Journal of Irrigation and Drainage Engineering-Asce* 131:37-58. 10.1061/(asce)0733-9437(2005)131:1(37).

Calder I. 1998. Water-Resource and Land-Use Issues. SWIM Paper 3. Colombo, Sri Lanka: International Water Management Institute.

Calder IR. 2005.*The Blue Revolution, Land Use and Integrated Water Resources Management* (Second edition). Earthscan, London.

Calder IR, Dye P. 2001. Hydrological impacts of invasive alien plants. *Land Use and Water Resources* 1:1-12.

Carlson TN, Buffum MJ. 1989. On estimating total daily evapotranspiration from remote surface-temperature measurements. *Remote Sensing of Environment* 29(2): 197-207.

Cleugh HA, Leuning R, Mu Q, Running SW. 2007. Regional evaporation estimates from flux tower and MODIS satellite data. *Remote Sensing of Environment* 106:285-304. doi:10.1016/j.rse.2006.07.007.

Clulow AD. 2007. The long-term measurement of total evaporation over *Acacia mearnsii* using large aperture scintillometry. M.Sc. Thesis. University of KwaZulu-Natal: South Africa.

Clulow AD, Everson CS, Mengistu MG, Jarmain C, Jewitt GPW, Price JS, Grundling PL. 2012. Measurement and modelling of evaporation from a coastal wetland in Maputaland, South Africa. *Hydrological and Earth Systems Science Discussions* 9: 1741–1782.doi:10.5194/hessd-9-1741-2012.

Consoli S. 2011. Evapotranspiration Estimation Using Micrometerological Techniques. Pages 17-42 *in* G. Gerosa, editor. *Evapotranspiration - From Measurements to Agricultural and Environmental Applications*. Intech, Rijeka, Croatia.

D'Urso G. 2001. Simulation and management of on-demand irrigation systems. A combined agrohydrological and remote sensing approach. Wageningen University, Wageningen, Netherlands.

Darvishzadeh R, Skidmore A, Schlerf M, Atzberger C, Corsi F, Cho M. 2008. LAI and chlorophyll estimation for a heterogeneous grassland using hyperspectral measurements. *ISPRS Journal of photogrammetry and Remote Sensing* 63: 409-426.

De Bruin H. 2002. Introduction: Renaissance of scintillometry. *Boundary-Layer Meteorology* 105(1): 1-4.

Dixon HH, Joly J. 1984. On the Ascent of Sap. *Philosphical Transactions of the Royal Society of London*. 186: 563-576.

Doorenbos J, Pruitt WO. 1977. Crop water requirements. Irrigation and Drainage Paper No. 24, (rev.) FAO, Rome, Italy, 144 pp.

Drexler JZ, Snyder RL, Spano D, Paw KTU. 2004. A review of models and micrometeorological methods used to estimate wetland evapotranspiration. *Hydrological Processes* 18(11): 2071-2101.

DWAF. 1997. *White Paper on a National Water Policy for South Africa.* Pretoria: Department of Water Affairs and Forestry.

Dye P, Versfeld D. 2007. Managing the hydrological impacts of South African plantation forests: An overview. *Forest Ecology and Management* 251(1-2): 121-128.

Dye PJ, Gush MB, Everson CS, Jarmain C, Clulow A, Mengistu M, Geldenhuys CJ, Wise R, Scholes RJ, Archibald S, Savage MJ. 2008. Water-use in relation to biomass of

indigenous tree species in woodland, forest and/or plantation conditions. Water Research Commission, Pretoria.

Eugster W. and Zeeman M. 2006. Micrometeorological techniques to measure ecosystem-scale greenhouse gas fluxes for model validation and improvement. *International Congress Series*1293: 66-75.

Everson CS, Dye PJ, Gush MB, Everson TM. 2011. Water use of grasslands, agroforestry systems and indigenous forests. *Water SA* 37(5): 781-788.

Falge E, Baldocchi DD, Olsen R, Anthoni PM, Aubinet M, Bernhofer C. 2001. Gap filling strategies for defensible annual sums of net ecosystem exchange. *Agricultural and Forest Meteorology* 107:43 - 69.

Farahani HJ, Howell TA, Shuttleworth WJ, Bausch WC. 2007. Evapotranspiration: Progress in measurement and modelling in agriculture. *American Society of Agricultural and Biological Engineers* 50(5): 1627-1638.

Field CB. 1991. Ecological scaling of carbon gain to stress and resource availability. In: Mooney H, Winner S, Pell E(eds), *Integrated Responses of Plants to Stress*. San Diego, CA: Academic Press, 35-65.

Fuentes S, Palmer AR, Taylor D, Zeppel M, Whitley R, Eamus D. 2008. An automated procedure for estimating the leaf area index (LAI) of woodland ecosystems using digital imagery, MATLAB programming and its application to an examination of the relationship between remotely sensed and field measurements of LAI. *Functional Plant Biology*35:1070-1079. doi:10.1071/FP08045

Garrigues S, Lacaze R, Baret F, Morisette JT, Weiss M, Nickeson JE, Fernandes R, Plummer S, Shabanov NV, Myneni RB, Knyazikhin Y, Yang W. 2008. Validation and intercomparison of global Leaf Area Index products derived from remote sensing data. *Journal of Geophysical Research*113, G02028, doi:10.1029/2007JG000635.

Geldenhuys CJ. 1982. The management of the southern Cape forests. *South African Forestry Journal* 121: 1-7.

Geldenhuys CJ. 1993. Observations of the effects of drought on evergreen and deciduous species in the Eastern Cape forests. *South African Journal of Botany* 59(5): 522-534.

Geldenhuys, C.J. 1998. Long-term monitoring plots show trends in the composition, growth and mortality of mixed evergreen forest in South Africa. In: F. Dallmeier & J.A. Comiskey (eds). *Forest Biodiversity Research, Monitoring and Modeling: Conceptual background and Old World Case Studies. Man and the Biosphere Series*, Volume 20. UNESCO, Paris & Parthenon Publishing. p.457-479.

Gibson LA, Munch Z, Engelbrecht J, Petersen N, Conrad JE. 2009. Remote sensing as a tool towards resource assessment and determination of the legal compliance of surface and groundwater use. WRC Project K5/1690. Water Research Commission, Pretoria

Gibson LA, Mùnch Z, & Engelbrecht J. 2011. Particular uncertainties encountered in using a pre-packaged SEBS model to derive evapotranspiration in a heterogeneous study area in South Africa. *Hydrological Earth System Science* 15: 295–310. doi:10.5194/hess-15-295-2011.

Gillies RR, Carlson TN. 1995. Thermal remote-sensing of surface soil-water content with partial vegetation cover for incorporation into climate-models. *Journal of Applied Meteorology* 34(4): 745-756.

Glenn EP, Huete AR, Nagler PL, Hirschboeck KK, Brown P. 2007. Integrating remote sensing and ground methods to estimate evapotranspiration. *Critical Reviews in Plant Sciences*26:139-168. 10.1080/07352680701402503.

Glenn EP, Nagler PL, Heute AR. 2010. Vegetation Index Methods for Estimating Evapotranspiration by Remote Sensing. *Surveys in Geophysics* 31 (6):531–555.DOI 10.1007/s10712-010-9102-2.

Glenn EP, Doody TM, Guerschman JP, Huete AR, King EA, McVicar TR, Van Dijk A, Van Niel TG, Yebra M, and Zhang YQ. 2011. Actual evapotranspiration estimation by ground and remote sensing methods: the Australian experience. *Hydrological Processes*25:4103-4116. 10.1002/hyp.8391.

Global Water Partnership. 2000 *Integrated Water Resource Management*. Global Water Partnership Technical Advisory Committee, *Background Paper* no.4. Stockholm, Sweden.

Goetz, S. J., & Prince, S. D. 1999. Modelling terrestrial carbon exchange and storage: evidence and implications of functional convergence in light-use efficiency. *Advances in ecological research* 28: 57-92.

Görgens AHM, van Wilgen BW. 2004. Invasive alien plants and water resources in South Africa: current understanding, predictive ability and research challenges. *South African Journal of Science* 100(1): 27-33.

Granger RJ. 2000. Satellite-derived estimates of evapotranspiration in the Gediz basin. *Journal of Hydrology* 229: 70–76.

Gush MB, Scott DF, Jewitt GP, Schulze RE, Lumsden TG, Hallowes LA, and Görgens AHM. 2002. *Estimation of Streamflow Reduction Resulting from Commercial*

Afforestation in South Africa.WRC Report No. TT 173/02. Water Research Commission, South Africa.

Hamon WR. (1963). Computation of Direct Runoff Amounts from Storm Rainfall. *Int. Assoc. Sci. Hydrol. Pub.* 63: 52-62.

Hargreaves GH & Samani ZA. 1985. Reference Crop Evapotranspiration from Temperature. *Applied Eng. in Agric*. 1(2): 96-99.

Heinsch FA, Zhao MS, Running SW, Kimball JS, Nemani RR, Davis KJ, Bolstad PV, Cook BD, Desai AR, Ricciuto DM, Law BE, Oechel WC, Kwon H, Luo HY, Wofsy SC, Dunn AL, Munger JW, Baldocchi DD, Xu LK, Hollinger DY, Richardson AD, Stoy PC, Siqueira MBS, Monson RK, Burns SP, Flanagan LB. 2006. Evaluation of remote sensing based terrestrial productivity from MODIS using regional tower eddy flux network observations. *IEEE Transactions on Geoscience and Remote Sensing* 44:1908-1925. 10.1109/tgrs.2005.853936

Hill MJ, Senarath U, Lee A, Zeppel M, Nightingale JM, Williams RDJ, McVicar TR. 2006. Assessment of the MODIS LAI product for Australian ecosystems. *Remote Sensing of Environment* 101:495-518.

Howell TA, Evett SR. 2004. The Penman-Monteith Method. Section3 in Evapotranspiration: Determination of Consumptive Use in Water Rights Proceedings. Continuing Legal Education in Colorado, Inc. Denver, CO.

Hughes DA. 2004. Three decades of hydrological modelling research in South Africa. *South African Journal of Science* 100(11-12): 638-642.

Huxman TE, Snyder KA, Tissue D, Leffler AJ, Ogle K, Pockman WT, *et al*. 2004. Precipitation pulses and carbon fluxes in semiarid and arid ecosystems. *Oecologia* 141(2): 254-268.

Jackson RD, Reginato RJ, Idso SB. 1977. Wheat canopy temperature: a practical tool for revaluating water requirements. *Water Resources Research* 13: 651-656.

Jarmain C, Bastiaanssen W, Mengistu MG, Jewitt G, Kongo V. 2009. *A Methodology for Near-Real Time Spatial Estimation of Evaporation.* 1751/1/09. Water Research Commission, Pretoria.

Jarmain C, Everson CS, Savage MJ, Mengistu M, Clulow AD. 2009. *Refining Tools For Evaporation Monitoring In Support Of Water Resources Management*. K5/1567/08, Water Research Commission, Pretoria.

Jensen ME, Haise HR. 1963. Estimating evapotranspiration from solar radiation. *J. Irrig. Drainage Div. ASCE* 89: 15-41.

Jensen KH, Illangasekare TH. 2011. HOBE: A Hydrological Observatory. *Vadose Zone Journal* 10: 1-7.

Jewitt G. 2006. Integrating blue and green water flows for water resources management and planning. *Physics and Chemistry of the Earth* 31: 753–762.

Jobaggy EG, Fernandez RJ, Nosetto MD, Santoni CS, Marchesini VA. 2011. The role of rangelands as hydrological regulators in the Pampas and Chaco., IXth International Rangelands Congress: Diverse Rangelands for a Sustainable Society. IXth International Rangelands Congress, Rosario, Argentina, pp. 39 – 43.

Jonker, L. 2007. Integrated water resources management: The theory praxis nexus, a South African perspective. *Physics and Chemistry of the Earth* 31 (15-18): 1257-1263.

Jovanovic, N and Israel, S. 2012. Critical review of methods for the estimation of actual evapotranspiration in hydrological models. Evapotranspiration: Remote Sensing and Modeling. InTech Open, CSIR, Pretoria.

Justice CO, Townshend JRG, Vermote EF, Masuoka E, Wolfe RE, Saleous N, Roy DP, Morisette JT. 2002. An overview of MODIS Land data processing and product status. *Remote Sensing of Environment* 83: 3-15.

Kalma JD, Jupp DLB. 1990. Estimating evaporation from pasture using infrared thermometry - evaluation of a one-layer resistance model. *Agricultural and Forest Meteorology* 51: 223-246. 10.1016/0168-1923(90)90110-r.

De Kauwe MG, Disney MI, Quaife T, Lewis P, Williams M. 2011. An assessment of the MODIS collection 5 leaf area index product for a region of mixed coniferous forest. Remote Sensing of Environment 115:767–780.

Kelliher FM, Leuning R, Raupach MR, Schulze ED. 1995. Maximum conductances for evaporation from global vegetation types *Agricultural and Forest Meteorology* 73: 1-16.

Knyazikhin Y, Martonchik JV, Diner DJ, Myneni RB, Verstraete M, Pinty B, *et al*. 1998. Estimation of vegetation canopy leaf area index and fraction of absorbed photosynthetically active radiation from atmosphere-corrected MISR data. *Journal of Geophysical Research-Atmospheres*103 (D24): 32239-32256.

Knyazikhin Y, Martonchik JV, Myneni RB, Diner DJ, Running SW. 1998. Synergistic algorithm for estimating vegetation canopy leaf area index and fraction of absorbed photosynthetically active radiation from MODIS and MISR data. *Journal of Geophysical Research-Atmospheres*103 (D24): 32257-32275.

Knyazikhin Y, Glassy J, Privette JL, Tian Y, Lotsch A, Zhang Y, Wang Y, Morisette JT, Votava P, Myneni RB, Nemani RR, Running SW. 1999. MODIS Leaf Area Index (LAI)

and Fraction of Photosynthetically Active RadiationAbsorbed by Vegetation (FPAR) Product (MOD15). Algorithm Theoretical Basis Document. (*http://eospso.gsfc.nasa.gov/atbd/modistables.html).*

Knyazikhin Y, Martonchik JV, Myneni RB, Diner DJ, Running SW. 1998. Synergistic algorithm for estimating vegetation canopy leaf area index and fraction of absorbed photosynthetically active radiation from MODIS and MISR data. *Journal of Geophysical Research-Atmospheres* 103:32257-32275.

Kustas WP, Norman JM. 1997. A two-source approach for estimating turbulent fluxes using multiple angle thermal infrared observations. *Water Resources Research*33(6): 1495-1508.

Kustas WP, Norman JM. 1999. Reply to comments about the basic equations of dual-source vegetation-atmosphere transfer models. *Agricultural and Forest Meteorology* 94(3-4): 275-278.

Kustas WP, Norman JM. 1999. Evaluation of soil and vegetation heat flux predictions using a simple two-source model with radiometric temperatures for partial canopy cover. *Agricultural and Forest Meteorology* 94(1): 13-29.

Leuning R, Zhang YQ, Rajaud A, Cleugh H, Tu K. 2009. A simple surface conductance model to estimate regional evaporation using MODIS leaf area index and the Penman-Monteith equation (vol 45, W10419, 2008). *Water Resources Research* 44, W10419, doi 10.1029/2007WR006562.

Lhomme JP. 1997. Towards a rational definition of potential evaporation. *Hydrology and Earth System Sciences* 1(2): 257-264.

Makkink GF. 1957. Testing the Penman Formula by Means of Lysimeters. *J. Inst. of Water Eng.* 11: 277-288.

Mauser W, Schadlich S. 1998. Modelling the spatial distribution of evapotranspiration on different scales using remote sensing data. *Journal of Hydrology* 212-213: 250-267.

McClenahan K, Macinnis-Ng C and Eamus D. 2004.Hydraulic architecture and water relations of several species at diverse sites around Sydney. *Australian Journal of Botany* 52(4): 509-518.

McVicar TR, Jupp DLB. 1999. Estimating one-time-of-day meteorological data from standard daily data as inputs to thermal remote sensing based energy balance models. *Agricultural and Forest Meteorology* 96(4): 219-238.

Meijninger WM, Hartogenesis OK, Kohsiek W, Hoedjes JC, Zuurbier RM, De Bruin HA. 2002. Determination of Area - Averaged Sensible Heat Fluxes with a Large Aperture

Scintillometer Over a Heterogeneous Surface - Flevoland Field Experiment. *Boundary-Layer Meteorology* 105:37-62. 10.1023/A: 1019647732027.

Monteith JL. 1965. *Evaporation and the Environment, The State and Movement of Water in Living Organisms*. Cambridge University Press, Swansea.

Monteith JL. 1981. Evaporation and surface temperature. *Quarterly Journal of the Royal Meteorological Society* 107(451): 1-27.

Monteith JL. 1985. Evaporation from land surfaces: progress in analysis and prediction since 1948. In *National conference on advances in evapotranspiration, Hyatt Regency Chicago, Ill. (USA), 16-17 Dec 1985*. American Society of Agricultural Engineers.

Moncreiff JB, Malhi Y, Leuning R. 1996. The propagation of errors in long-term measurements of land-atmosphere fluxes of carbon and water**.** *Global Change Biology* 2(2): 231-240.

Monteith JL. 1985. Does transpiration limit the growth of vegetation or vice versa.? *Journal of Hydrology*, 100(1-3): 57–68.

Moran MS, Rahman AF, Washburne JC, Goodrich DC, Weltz MA, Kustas WP. 1996. Combining the Penman-Monteith equation with measurements of surface temperature and reflectance to estimate evaporation rates of semiarid grassland. *Agricultural and Forest Meteorology* 80: 87-109.

Mu Q, Heinsch FA, Zhao M, Running SW. 2007. Development of a global evapotranspiration algorithm based on MODIS and global meteorology data. *Remote Sensing of Environment*111:519-536. 10.1016/j.rse.2007.04.015

Mu QZ, Zhao MS, Running SW. 2011. Improvements to a MODIS global terrestrial evapotranspiration algorithm. *Remote Sensing of Environment* 115: 1781-1800. 10.1016/j.rse.2011.02.019.

Műnch Z, Conrad JE, Gibson LA, Palmer AR, Hughes D. In press. Satellite earth observation as a tool to conceptualize hydrogeological fluxes in the Sandveld, South Africa. *Hydrogeology Journal*. In press.

Műnch Z, Gibson LA, Carstens M, Palmer AR. In press. Estimating evapotranspiration in a semi-arid, sparsely vegetated catchment using the SEBS model. *Water SA*. In press.

Myneni RB, Nemani RR, Running SW. 1997. Estimation of global leaf area index and absorbed par using radiative transfer models. *IEEE Transactions on Geoscience and Remote Sensing* 35(6): 1380-1393.

Myneni RB, Yang WZ, Nemani RR, Huete AR, Dickinson RE, Knyazikhin Y, *et al*. 2007. Large seasonal swings in leaf area of Amazon rainforests. *Proceedings of the National Academy of Sciences of the United States of America* 104(12): 4820-4823.

Nagler PL, Cleverly J, Glenn E, Lampkin D, Huete A, Wan Z. 2005. Predicting riparian evapotranspiration from MODIS vegetation indices and meteorological data. *Remote Sensing of Environment* 94: 17-30.

Nänni, UW. 1970. Trees, water and perspective. South African Forestry Journal 75: 9-17.

Nemani RR, Running SW. 1989. Testing a theoretical climate soil leaf-area hydrologic equilibrium of forests using satellite data and ecosystem simulation. *Agricultural and Forest Meteorology* 44(3-4): 245-260.

Nemani RR, Running SW. 1989. Estimation of regional surface-resistance to evapotranspiration from NDVI and thermal-IR AVHRR data. *Journal of Applied Meteorology* 28(4): 276-284.

Nishida K, Nemani RR, Glassy JM, Running SW. 2003. Development of an evapotranspiration index from aqua/MODIS for monitoring surface moisture status. IEEE *Transactions on Geoscience and Remote Sensing* 41(2): 493-501.

Nishida K, Nemani RR, Running SW, Glassy JM. 2003. An operational remote sensing algorithm of land surface evaporation. *Journal of Geophysical Research-Atmospheres* 108 (D9).

Norman JM, Kustas WP, Humes KS. 1995. Source approach for estimating soil and vegetation energy fluxes in observations of directional radiometric surface-temperature. *Agricultural and Forest Meteorology* 77(3-4): 263-293.

NWRS. 2004. *National Water Resources Strategy.* Pretoria: Department of Water Affairs.

Ooba M, Hirano T, Mogami JI, Hirata R, Fujinuma Y. 2006. Comparisons of gap-filling methods for carbon flux dataset: A combination of a genetic algorithm and an artificial neural network. *Ecological Modelling* 198: 473 - 486.

Oudin L, Hervieu F, Michel C, Perrin C, Andreassian V, Anctil F, *et al*. 2005. Which potential evapotranspiration input for a lumped rainfall-runoff model? Part 2 - Towards a simple and efficient potential evapotranspiration model for rainfall-runoff modelling. *Journal of Hydrology*303(1-4): 290-306.

Oudin L, Michel C, Anctil F. 2005. Which potential evapotranspiration input for a lumped rainfall-runoff model? Part 1 - Can rainfall-runoff models effectively handle detailed potential evapotranspiration inputs? *Journal of Hydrology*303(1-4): 275-289.

Palmer AR, Weideman CI. Exploring trends in evapotranspiration in the KNP: towards a water use efficiency model for rangeland production in semi-arid savannas. In: *Proceedings of the Proceedings of the IXth International Rangelands Congress*, 4-8 April 2011 2011. Rosario, Argentina, Vol. 1. IXth International Rangelands Congress, 248.

Palmer AR, Yunusa I. 2011. Biomass production and water use efficiency of arid rangelands in the Riemvasmaak Rural Area, Northern Cape, South Africa. *Journal of Arid Environments* 75: 1223-1227.

Palmer AR, Yunusa I. 2011. Biomass production, evapotranspiration and water use efficiency of arid rangelands in the Northern Cape, South Africa. *Journal of Arid Environments* 75: 1223-1227.

Penman HL. 1948. Natural evaporation from open water, bare soil and grass. *Proceedings of the Royal Society of London. Series A. Mathematical and Physical Sciences 193*(1032): 120-145.

Pollard S, du Toit D. 2008. Integrated water resource management in complex systems: How the catchment management strategies seek to achieve sustainability and equity in water resources in South Africa. *Water SA* 34(6): 671-679.

Price JC. 1990. Using spatial context in satellite data to infer regional scale evapotranspiration. *IEEE Transactions on Geoscience and Remote Sensing* 28: 940-948.

Priestley CHB, Taylor RJ. 1972: On the Assessment of Surface Heat Flux and Evaporation Using Large-Scale Parameters. *Monthly Weather Review*100: 81–92.

Privette JL, Myneni RB, Knyazikhin Y, Mukelabai M, Roberts G, Tian Y, Wang Y, Leblanc SG. 2002. Early spatial and temporal validation of MODIS LAI product in the Southern Africa Kalahari. *Remote Sensing of Environment* 83: 232-243.

Privette JL, Roy DP. 2005. Southern Africa as a remote sensing test bed: the SAFARI 2000 Special Issue overview. *International Journal of Remote Sensing* 26(19): 4141-4158.

Rahaman MM, Varis O. 2005. Integrated water resources management: evolution, prospects and future challenges. *Sustainability: Science, Practice & Policy*, 1(1), 15-21.

Ramakrishna RN, Keeling CD, Hashimoto H, Jolly WM, Piper SC, Tucker CJ, Myneni RB Running SW. Climate-Driven Increases in Global Terrestrial Net Primary Production from 1982 to 1999. *Science* 6 June 2003: 300: no. 5625:1560-1563.

Rana G, Katerji N. 2008. Direct and indirect methods to simulate the actual evapotranspiration of an irrigated overhead table grape vineyard under Mediterranean conditions. *Hydrological Processes* 22: 181-188.

Reich PB, Walters MB and Ellsworth DS. 1997. From tropics to tundra: Global convergence in plant functioning. *Proceedings of the National Academy of Sciences of the United States of America* 94 (25): 13730-13734.

Reich PB, Wright IJ, Cavender-Bares J, Craine JM, Oleksyn J, Westoby M, Walters MB. 2003. The evolution of plant functional variation: Traits, spectra, and strategies. *International Journal of Plant Sciences* 164(3): S143-S164.

Royappen M, Dye PJ, Schulze RE, Gush M. 2002. An analysis of catchment attributes and hydrological response characteristics in a range of small catchments. *Water Research Commission (WRC) Report*, (1193/1), 02.

Samani Z, Hargreaves GH. 1985. Data requirement for evapotranspiration estimation - discussion. *Journal of Irrigation and Drainage Engineering-Asce* 111(4): 410-412.

Savage MJ. 2009. Estimation of evaporation using a dual-beam surface layer scintillometer and component energy balance measurements. *Agricultural and Forest Meteorology*149501-517.

Savage MJ, Metelerkamp BR. 1997. Evaporation Measurement Above Vegetated Surfaces Using Micrometeorological Techniques: Water Research Commission.

Savage MJ, Everson CS, Odhiambo GO, Megistu MJ, Jarmain C. 2004. Theory and practice of evaporation measurement, with special focus on SLS as an operational tool for the estimation of spatially-averaged evaporation. *WRC Report* no. 1335/1/04. Water Research Commission, Pretoria.

Savage MJ, Odhiambo GO, Mengistu MG, Everson CS, Jarmain C. 2010. Measurement of grassland evaporation using a surface-layer scintillometer. *Water SA* 36: 1-8.

Scholes RJ, Gureja N, Giannecchinni M, Dovie D, Wilson BE, Davidson N, *et al*. 2001. The environment and vegetation of the flux measurement site near Skukuza, Kruger National Park. *Koedoe* 44: 73-83.

Schulze RE, Horan MJC, Schmidt EJ. 2000. Hydrological complexities in assigning rainfed sugarcane a 'Stream Flow Reduction Activity'. In *Proceedings of the Annual Congress–South African Sugar Technologists' Association* (No. 74, pp. 140-150).

Schulze RE, Kunz RP. 1995. Potential shifts in optimum growth areas of selected commercial tree species and subtropical crops in southern Africa due to global warming. *Journal of Biogeography* 22(4-5): 679-688.

Schulze RE, Lynch SD. 2007. Annual Precipitation. In: Schulze RE (ed), *South African Atlas of Climatology and Agrohydrology*, Pretoria: Water Research Commission.

Schulze RE, Hewitson BC, Barichievy KR, Tadross, MA, Kunz RP, Horan MJ, Lumsden TG. 2011. *Methodological Approaches to Assessing Eco-Hydrological Responses to Climate Change in South Africa.WRC Report* No. 1562/1/10 ISBN 978-1-4312-0050-4. Water Research Commission, Pretoria.

Schulze RE, Lynch SD. 2007. Annual Precipitation. In: Schulze RE(ed),*South African Atlas of Climatology and Agrohydrology*. Water Research Commission, Pretoria.

Scott DF, Lesch W. 1997. Streamflow responses to afforestation with Eucalyptus grandis and Pinus patula and to felling in the Mokobulaan experimental catchments, South Africa. *Journal of Hydrology* 199(3-4): 360-377.

Scott DF, Smith RE. 1997. Preliminary empirical models to predict reductions in total and lowflows resulting from afforestation. *Water SA* 23: 135-140.

Scott DF. 1999. Managing riparian zone vegetation to sustain streamflow: Results of paired catchment experiments in South Africa. *Canadian Journal of Forestry Research* 29: 1149 - 1157.

Scott DF, Prinsloo FW, Moses G, Mehlomakulu M, Simmers ADA. 2000. 'A re-analysis of the South African catchment afforestation experimental data'. Report 810/1/00, *CSIR Report* ENV-S-C 99088. Water Resources Commission, South Africa.

Shabanov NV, Huang D, Yang WZ, Tan B, Knyazikhin Y, Myneni RB, *et al*. 2005. Analysis and optimization of the MODIS leaf area index algorithm retrievals over broadleaf forests. *IEEE Transactions on Geoscience and Remote Sensing* 43(8): 1855-1865.

Shabanov NV, Huang D, Yang WZ, Tan B, Knyazikhin Y, Myneni RB, Ahl DE, Gower ST, Huete AR, Aragao L, Shimabukuro YE. 2005. Analysis and optimization of the MODIS leaf area index algorithm retrievals over broadleaf forests. *IEEE Transactions on Geoscience and Remote Sensing* 43: 1855-1865. 10.1109/tgrs.2005.852477.

Shabanov NV, Lo K, Gopal S, Myneni RB. 2005. Subpixel burn detection in Moderate Resolution Imaging Spectroradiometer 500-m data with ARTMAP neural networks. *Journal of Geophysical Research-Atmospheres* 110 (D3).

Shuttleworth WJ. 2007. Putting the 'vap' into evaporation. *Hydrology and Earth System Sciences*11:210-244.

Sinclair S, Pegram G. 2010. A comparison of ASCAT and modelled soil moisture over South Africa, using TOPKAPI in land surface mode. In *EGU General Assembly Conference Abstracts* (Vol. 12, p. 2743).

Stoy PC, Katul GG, Siqueira MBS, Juang JY, Novick KA, Uebelherr JM, Oren R. 2006. An evaluation of models for partitioning eddy covariance-measured net ecosystem exchange

into photosynthesis and respiration. *Agricultural and Forest Meteorology* 141: 2-18. 10.1016/j.agrformet.2006.09.001.

Su Z. 2002. The Surface Energy Balance System (SEBS) for estimation of turbulent heat fluxes. *Hydrology and Earth System Sciences* 6: 85-99.

Sverdrup HU. 1943. On the ratio between heat conduction from the sea surface and the heat used for evaporation. *Annals of the New York Academy of Sciences* 68: 81-88.

Swap RJ, Annegarn HJ, Otter L. 2002. Southern African regional science initiative (SAFARI 2000): Summary of science plan. *South African Journal of Science, 98*(3/4): 119-124.

Swinbank WC. 1951. The measurement of vertical transfer of heat and water vapour by eddies in the lower atmosphere. *Journal of Meteorology* 8: 135-145.

Thornthwaite CW. 1948. An approach toward a rational classification of climate. *Geographical review* 38(1): 55-94.

Tucker C. 1979. Red and infrared linear combinations for monitoring vegetation. *Remote Sensing of Environment* 8: 127−150.

Turc L. 1961. Evaluation de Besoins en Eau d'Irrigation, ET Potentielle. *Ann. Agron*. 12: 13-49.

Turpie JK, Marais C, Blignaut JN. 2008. The working for water programme: Evolution of a payments for ecosystem services mechanism that addresses both poverty and ecosystem service delivery in South Africa. *Ecological Economics* 65: 788-798. 10.1016/j.ecolecon.2007.12.024.

Tyree MT. 1997. The cohesion-tension theory of sap ascent: current controversies. *Journal of Experimental Botany* 48(10): 1753-1765.

Unland H, Arain A, Harlow C, Houser P, Garatuza-Payan J, Scott P. 1998. Evaporation from a riparian system from a semi-arid environment. *Hydrological Processes* 12:527-542.

Van der Merwe I. 1999. The Knysna and Tsitsikamma forests: their history, ecology and management. Department of Water Affairs and Forestry, Pretoria. 152 pp.

Van der Zel, DW. 1987. Hydrological implications of the changing role of forestry in a catchment context. In: *Proc. 3rd South African National Hydrological Symposium, Vol. 2*: 671-679. Hydrological Research Unit, Dept. of Geography, Rhodes University, Grahamstown, September.

Van der Zel DW. 1995. Accomplishment and dynamics of the South African Afforestation Permit System. *South African Forestry Journal* 172: 49-58.

Verstraeten WW, Veroustraete F, Feyen J. 2008. Assessment of evapotranspiration and soil moisture content across different scales of observation. *Sensors* 8:70-117. 10.3390/s8010070.

Villegas JC. 2008. Ecosystem water exchange and partitioning of evapotranspiration along vegetation gradients: Implications of projected dust-bowl climate in Arizona. School of Natural Resources, College of Agriculture and life Sciences; Department of Ecology and Evolutionary Biology, College of Science Institute for the Study of Planet Earth, University of Arizona.

Von Maltitz, G., Mucina, L., Geldenhuys, C., Lawes, M. J., Eeley, H., Adie, H., Vink D, Fleming G, Bailey C. Classification system for South African indigenous forests: an objective classification for the Department of Water Affairs and Forestry. *Pretoria: Council for Scientific and Industrial Research, Environmentek.*

Warburton ML, Schulze RE, Jewitt GPW. 2012. Hydrological impacts of land use change in three diverse South African catchments. *Journal of Hydrology* 414: 118-135.

Wilcox BP, Seyfried MS, Breshears DD. 2003. The water balance on rangelands. Pages 791 – 794.In: Stewart BA, Howell TA (eds), *Encyclopaedia of Water Science*. Marcel Dekker, New York.

Wilcox BP, Sorice MG, Young MH. 2011. Dryland Ecohydrology in the Anthropocene: Taking Stock of Human–Ecological Interactions. *Geography Compass* 5(3): 112-127.

Williams DG, Cable W, Hultine K, Hoedjes JCB, Yepez EA, Simonneaux V, Er-Raki S, Boulet G, De Bruin HAR, Chehbouni A, Hartogensis OK, Timouk F. 2004. Evapotranspiration components determined by stable isotope, sap flow and eddy covariance techniques. *Agricultural and Forest Meteorology* 125: 241-258.

Yang W, Shabanov NB, Huang D, Wang W, Dickinson RE, Nemani RR, Knyazikhin Y, Myneni RB. 2006. Analysis of leaf area index products from combination of MODIS Terra and Aqua data. *Remote Sensing of Environment* 104: 297-312.

Zeweldi DA, Gebremichael M, Wang J, Sammis T, Kleissl J, Miller D. 2009. Intercomparison of Sensible Heat Flux from Large Aperture Scintillometer and Eddy Covariance Methods: Field Experiment over a Homogeneous Semi-arid Region. *Boundary-LayerMeteorology* 135: 151–159.

Zhang P, Anderson B, Barlow M. 2004. Climate-related vegetation characteristics derived from Moderate Resolution Imaging Spectroradiometer (MODIS) leaf area index and normalized difference vegetation index. *Journal of Geophysical Research-Atmospheres*109. 10.1029/2004JD004720.